universität wien

DIPLOMARBEIT

Titel der Diplomarbeit

The molecular effects of fatty acid synthase inhibition on major gene regulatory pathways and their relationship to ovarian cancer growth control

angestrebter akademischer Grad

Magister/Magistra der Naturwissenschaften (Mag. rer.nat.)

Verfasserin / Verfasser:	Katharina Tomek
Matrikel-Nummer:	0203909
Studienrichtung /Studienzweig (lt. Studienblatt):	Molekularbiologie (A-490)
Betreuerin / Betreuer:	O. Univ.-Prof. DI. Dr. Wolfgang J. Schneider

Wien, im Juli 2009

Danksagung

Ich danke O. Univ.-Prof. DI. Dr. Wolfgang J. Schneider, der mir die Durchführung meiner Diplomarbeit an der Medizinischen Universität ermöglicht hat.

Mein ganz besonderer Dank gilt Hr. AO Univ.-Prof. Mag. Dr. Thomas W. Grunt nicht nur für seine hervorragende Betreuung, für die Themenstellung und Finanzierung, sondern auch für die zahlreichen und spannenden fachlichen Diskussionen.

Weiters danke ich Univ.-Prof. Dr. Heidrun Karlic und Dr. Franz Varga für ihre Unterstützung und ihre interessanten Anregungen.
Meiner Kollegin Renate Wagner danke ich herzlich für ihre Hilfe, Geduld und Unterstützung bei der Durchführung der Experimente und für das angenehme Arbeitsklima.

Außerdem möchte ich meinen Studienkolleginnen Caroline Brünner-Kubath und Victoria Saferding für ihre freundschaftliche Unterstützung während meiner Diplomarbeit danken.

Meinem Freund Michael danke ich für seine liebevolle Unterstützung während meiner gesamten Ausbildung.

Mein größter Dank gilt meinen Eltern, die mich immer dabei unterstützt haben, mir mein Studium zu ermöglichen.

Darüber hinaus danke ich all jenen, die mich nach meiner Ausbildung zur Biomedizinischen Analytikerin motiviert haben, das Studium der Molekularbiologie zu betreiben.

Abstract

Epithelial ovarian cancer is the fourth leading cause of cancer-related death in women and accounts for the highest mortality rate of all gynecological malignancies. In fact, the cure rates have remained unchanged over the last 20 years though radical surgery, radiation therapy, chemotherapy and targeted therapy have improved survival times. Thus, additional treatment options in ovarian cancer therapy are urgently needed. It is documented that fatty acid synthase (FASN) is overexpressed in more than 80% of ovarian carcinomas, whereas in normal cells FASN is mostly absent. Therefore, FASN represents a very promising molecular anticancer target. FASN has been identified as an independent prognostic factor for clinical outcome in ovarian cancer and increased expression of FASN in ovarian neoplasms predicts shorter survival. Natural and synthetic compounds have been described that inhibit FASN activity very efficiently. Moreover, inhibition of FASN causes growth arrest in breast cancer and delays disease progression of ovarian carcinomas in xenograft models. Up to date, a conclusive molecular explanation of the anti-proliferative and death-promoting effect of FASN inhibitors is still missing. This work is the first report about epigenetically modulating activity of FASN inhibition. Using the FASN inhibitor C75, we could show a demethylation of the hypermethylated death associated protein (DAP) kinase promoter region followed by enhanced DAP kinase mRNA transcription in the ovarian cancer cell line A2780. The expression of epigenetically active enzymes was also found to be modulated by the FASN blocking drug C75. We further pointed out several effects of FASN inhibition including enhanced ubiquitin-dependent protein degradation and downregulation of PI3K signaling molecules. Moreover, we could confirm anti-proliferative and apoptosis-inducing actions induced by FASN inhibition in Affimetrix microarray mRNA expression analyses.

Zusammenfassung

Epitheliales Ovarialkarzinom ist die vierthäufigste Todesursache bei Frauen aufgrund von Krebs und hat die höchste Mortalitätsrate von allen gynäkologischen Erkrankungen. In den letzten 20 Jahren blieb die Heilungsrate von Ovarialkarzinomen weitläufig unverändert, allerdings konnte der Überlebenszeitraum durch chirurgische Operation, Strahlentherapie, Chemotherapie und gezielter molekularen Therapie verlängert werden. Deshalb werden zusätzliche Behandlungsmethoden in der Ovarialkarzinom-Therapie dringend gebraucht. Das Enzym Fettsäuresynthase (FASN) wird in über 80% der Ovarialkarzinome über-exprimiert, wohingegen dieses Enzym in normalen Zellen meist gar nicht exprimiert wird. Aufgrund dieser Tatsache repräsentiert FASN ein vielversprechendes molekulares Ziel für eine Therapie gegen Krebs. FASN ist außerdem ein unabhängiger prognostischer Faktor für den klinischen Ausgang bei Ovarialkarzinomen und sagt einen kürzeren Überlebenszeitraum bei ovarialer Neoplasie voraus. Es wurden bereits einige natürliche und synthetische Substanzen beschrieben, die die FASN-Aktivität sehr effizient inhibieren. Darüber hinaus konnte gezeigt werden, dass die Inhibierung von FASN zu einem Wachstumsarrest von Mammakarzinomen führt und das Fortschreiten von Ovarialkarzinomen in Xenograft Modellen verzögert wird. Bis jetzt konnte man noch keine schlüssige molekulare Erklärung für die anti-proliferativen und Apoptose-induzierenden Effekte von FASN-Blockern finden. Diese Arbeit berichtet erstmalig über die epigenetisch modulierenden Aktivitäten der FASN-Inhibierung. Unter Verwendung des FASN-Inhibitors C75 konnte eine Demethylierung der hypermethylierten „death associated protein“ (DAPK) Promotor Region und eine anschließende vermehrte DAPK mRNA Transkription in der ovarialen Karziomzelllinie A2780 gezeigt werden. Darüber hinaus wurde in dieser Arbeit auch eine Modulierung der Expression von epigenetisch aktiven Enzymen durch FASN-Inhibierung beschrieben. Zudem wurden mehrere zusätzliche Effekte der FASN-Blockade herausgearbeitet, die unter anderem

Ubiquitin-abhängige Protein Degradation und Aktivitätshemmung der PI3K/AKT Signal Moleküle beinhalten. Abschließend konnten die anti-proliferativen und Apoptose-induzierenden Effekte der FASN-Inhibierung durch Affimetrix Microarray mRNA Expressionsanalyse bestätigt werden.

Table of contents

DANKSAGUNG ..... **III**

ABSTRACT ..... **V**

ZUSAMMENFASSUNG ..... **VI**

TABLE OF CONTENTS ..... **IX**

INDEX OF FIGURES ..... **XII**

INDEX OF TABLES ..... **XIV**

1 INTRODUCTION **1**

1.1 DEFINITIONS 1

1.2 INCIDENCE AND MORTALITY RATE OF OVARIAN CANCER 2

1.3 EPIDEMIOLOGY AND HIGH-RISK POPULATION OF OVARIAN CANCER 2

1.4 STAGING 3

1.5 TREATMENT OPTIONS IN OVARIAN CANCER 5

1.5.1 Surgery *5*

1.5.2 First-line Therapy *6*

1.5.3 Second-line Therapy *6*

1.5.4 Radiation Therapy *6*

1.5.5 Targeted Therapies *7*

1.6 FREQUENT MOLECULAR ABERRATIONS IN OVARIAN CANCER 8

1.6.1 Receptor Tyrosine Kinases *8*

1.6.2 Phosphatidylinositol 3-kinase (PI3K)/AKT/mTOR/p70S6K *9*

1.6.3 Fatty Acid Synthase (FASN) *11*

1.6.4 Cell cycle control at G1/S checkpoint *20*

1.6.5 Epigenetic gene silencing in cancer *22*

1.7 THE UBIQUITIN/PROTEASOME PATHWAY 24

2 MATERIALS AND METHODS **27**

2.1 CELL CULTURE AND CELL LINE 27

2.1.1 Maintenance of Cells *27*
2.1.2 Storage of Cells *28*
2.1.3 Used drugs *29*
2.2 GENE EXPRESSION ANALYSIS ON MRNA LEVEL 30
2.2.1 Treatment of Cells *30*
2.2.2 RNA Isolation *31*
2.2.3 RNA-Measurement *32*
2.2.4 cDNA Synthesis *35*
2.2.5 Real Time RT-Polymerase Chain Reaction (PCR) *35*
2.3 METHYLATION SPECIFIC REAL TIME RT-PCR 41
2.3.1 Treatment of Cells *41*
2.3.2 DNA Isolation *42*
2.3.3 Sodium Bisulfide Conversion *44*
2.3.4 Nested PCR – 1st Step *46*
2.3.5 Real Time PCR using SYBR Green – 2nd step of nested PCR *49*
2.4 WESTERN BLOTTING – PROTEIN ANALYSIS 55
2.4.1 Treatment of the Cells *55*
2.4.2 RIPA Lysis *56*
2.4.3 Protein Quantification *57*
2.4.4 SDS- Polyacryl Amide Gel Electrophoresis (PAGE) *58*
2.4.5 Electrotransfer *60*
2.4.6 Immunostaining of the Blot Membranes *61*
2.4.7 Stripping of Membranes *65*
2.4.8 Densitometry of the Protein Bands *65*
2.5 MRNA GENE EXPRESSION ARRAY 66
2.5.1 Treatment of Cells *68*
3 RESULTS 69
3.1 CHANGES IN MRNA LEVELS RESULTING FROM FASN-INHIBITION BY C75 OR FROM PI3K-INHIBITION BY LY294002 IN A2780 CELLS 69
3.1.1 Changes in mRNA expression of tumor suppressor genes resulting from FASN-inhibition by C75 or PI3K-inhibition by LY294002 in A2780 cells *69*

3.1.2 Changes in mRNA expression level of apoptosis associated genes resulting from FASN-inhibition by C75 or PI3K-inhibition by LY294002 in A2780 cells 75

3.1.3 Changes in mRNA expression level of epigenetically active enzymes resulting from FASN-inhibition by C75 or PI3K-inhibition by LY294002 in A2780 cells 77

3.2 CHANGES IN METHYLATION STATUS OF TUMOR SUPPRESSOR GENES RESULTING FROM FASN-INHIBITION BY C75 OR PI3K-INHIBITION BY LY294002 IN A2780 CELLS 82

3.2.1 The promoter of the $p15^{INK4b}$ tumor suppressor gene is not hypermethylated in A2780 cells 83

3.2.2 C75-mediated upregulation of DAPK mRNA correlates with demethylation of the hypermethylated gene promoter 84

3.3 THE FASN TARGETING DRUG C75 AFFECTS PROTEIN EXPRESSION AND ACTIVITY (PHOSPHORYLATION) OF PI3K/AKT EFFECTOR MOLECULES 86

3.3.1 Reduction of protein expression and phosphorylation of PI3K/AKT signaling molecules by the FASN inhibitor C75 86

3.3.2 Reduction of protein expression levels caused by FASN inhibition appears not to be due to translation inhibition by dephosphorylated 4eBP1 92

3.3.3 Reduction of protein expression caused by FASN inhibition appears to be due to enhanced protein degradation 93

3.3.4 Reduction of protein expression caused by FASN inhibition appears to be due to enhanced proteasomal protein degradation 95

3.4 CHANGES IN GENE EXPRESSION RESULTING FROM INHIBITION OF FASN 96

4 DISCUSSION 105

REFERENCES 117

CURRICULUM VITAE 133

Index of figures

Figure 1: Scheme of PI3K/AKT/mTOR/p70S6K signaling cascade 11
Figure 2: Warburg effect connected with fatty acid biosynthesis in cancer cells..... 13
Figure 3: Crosstalk between EGFR family members and FASN..... 16
Figure 4: Blocking sites of FASN inhibitors 18
Figure 5: Several molecular mechanisms of the tumoricidal Effects of FASN Inhibition 20
Figure 6: Mechanism of cyclin dependent kinase inhibitors 22
Figure 7: The Ubiquitin/Proteasome pathway 25
Figure 8: Chemical Structure of C75 29
Figure 9: Chemical structure of LY294002..... 30
Figure 10: Chemical Structure of Cycloheximide 30
Figure 11: Example for Qualitative Control of Isolated Total RNA by 1% Agarose Gel . 34
Figure 12: Schemata of Real Time RT-PCR using Gene Expression Assay. 38
Figure 13: Example of First Step PCR Product of $p15^{INK4b}$ Extern Primers..... 49
Figure 14: Basic Steps of Quantitative Real Time PCR Based on SYBR Green Intercalation..... 51
Figure 15: Example of a Melting Curve after SYBR Green Real Time PCR Amplification 54
Figure 16: Example of CT-Detection Curve Performing SYBR Green Real Time PCR Amplification 55
Figure 17: Assembly of Transfer Apparatus..... 61
Figure 18: Detection of Proteins by Chemoluminescence 62
Figure 19: Inhibition of FASN or PI3K increases mRNA expression of cyclin-dependent kinase inhibitor $p15^{INK4b}$. 71
Figure 20: Inhibition of FASN or PI3K decreases mRNA expression of cyclin-dependent kinase inhibitor $p16^{INK4b}$. 72
Figure 21: Inhibition of FASN or PI3K increases mRNA expression of the tumor suppressor gene CDH1. 73
Figure 22: Inhibition of FASN or PI3K increases mRNA expression of the tumor suppressor gene DAPK. 74

Figure 23: FASN inhibitor increases mRNA expression of death associated FAS more significantly than PI3K inhibitor. 76
Figure 24: FASN inhibition increases mRNA expression of MnSOD2 more significantly than PI3K inhibition. 77
Figure 25: Inhibition of FASN or PI3K decreases DNMT1 mRNA expression level after 24 hours of treatment. 79
Figure 26: Inhibition of FASN or PI3K increases DNMT3a mRNA expression. 80
Figure 27: Inhibition of FASN or PI3K decreases DNMT3b mRNA expression level. 81
Figure 28: Inhibition of FASN or PI3K increases mRNA expression of HDAC2. 82
Figure 29: Analysis of the methylation status of the $p15^{INK4b}$ promoter region. 84
Figure 30: Analysis of the methylation status of the DAPK promoter region using quantitative methylation-specific PCR (Q-MSP). 85
Figure 31: FASN inhibition reduces phosphorylation and expression of $p15^{INK4b}$, ERK1/2 and PI3K downstream signaling proteins. 88
Figure 32: PI3K inhibition by LY294002 is more effective in blocking the PI3K pathway than FASN inhibition. 91
Figure 33: FASN inhibition enhances protein degradation. 94
Figure 34: Fatty acid synthase and proteasome pathways crosstalk with each other. ... 96

Index of tables

Table 1: Mastermix for cDNA sythesis 35
Table 2: TaqMan Gene Expression Assay Probes used for Real Time RT-PCR 39
Table 3: PCR Mix for Real Time RT-PCR Containing TaqMan Gene Expression Assay Probes 39
Table 4: Cycling Conditions for Real Time RT-PCR using predeveloped TaqMan Gene Expression Assay Probes 40
Table 5: Conditions for Sodium Bisulfite Conversion 45
Table 6: Nucleotide Sequences of Extern Primers of $p15^{INK4b}$ 46
Table 7: Components for First Step PCR of p15-e 47
Table 8: Cyling Conditions for First Step PCR in MSP for Amplification of p15 external gene region 48
Table 9: Primer Sequences for SYBR Green Real Time RT-PCR 52
Table 10: Components for SYBR Green Real Time PCR Mix 53
Table 11: Cyling Conditions for SYBR Green Real Time PCR Amplification of $p15^{INK4b}$ methylated, $p15^{INK4b}$ unmethylated 53
Table 12: Cyling Conditions for SYBR Green Real Time PCR Amplification of DAP kinase methylated, and DAP kinase unmethylated 53
Table 13: Ingredients for RIPA Lysis Buffer 56
Table 14: RIPA+ Lysis Buffer 57
Table 15: Ingredients for 4 x Sample Buffer 58
Table 16: Preparation of 30% Acrylamide/Bis Solution 59
Table 17: Separating Gel. Preparation of 7,5% Polyacryl amide gel 59
Table 18: Stacking Gel. Preparation of 4% Polyacryl amide gel 60
Table 19: First Antibodies 64
Table 20: Secondary Antibodies 65
Table 21: Specifications of Affymetrix Human GeneChip Gene 1.0 ST Array 68
Table 22: mRNA gene expression array 104

1 Introduction

1.1 Definitions

The ovaries contain three kinds of tissue. First, epithelial cells which cover the ovary, second, germ cells which produce the oocyte inside the ovary, and third, stromal cells which produce most of the female hormones such as estrogen and progesterone. The tumors in the ovary are named for the kinds of cells the tumor started from. Therefore, there are three main types of ovarian tumors. The epithelial ovarian tumor is the most common type of ovarian tumors and can be divided into three sub-groups describing the malignancy of the tumor. The benign epithelial tumor does not spread whereas the epithelial ovarian tumors of low malignant potential (LMP tumors) only spreads slowly. This kind of epithelial ovarian tumor is also known as borderline tumor, which cells do not have cancerous morphology and mostly affects women at a younger age. Approximately nine out of ten ovarian carcinomas are epithelial ovarian cancers and the cell line A2780 that is used for several experiments in this work was also isolated from this kind of ovarian cancer. For the sake of completeness, it should be mentioned that also germ cell tumors such as teratoma, dysgerminoma, endodermal sinus tumor or choriocarcinoma can occur. Most of the germ line tumors are not cancerous. Stromal tumors can be either benign such as thecomas and fibromas or cancerous such as granulose cell tumor, granulose-theka tumors or sertoli-leydig cell tumors. More than fifty percent of the women suffering from stromal tumors are over fifty year old. Furthermore, some rare cancers show similar symptoms to epithelial ovarian cancer. These are the primary peritoneal carcinoma, which starts outside the ovaries and grows from the cells that line the pelvis and the abdomen and second the fallopian tube cancer which starts from the tube that carries the oocyte from the ovary to the

uterus. Moreover, ovarian cysts also show similar symptoms to epithelial ovarian cancer. Ovarian cysts collect fluid inside an ovary, which is often absorbed without any treatment (American Cancer Society, 2009).

1.2 Incidence and Mortality Rate of Ovarian Cancer

Epithelial ovarian cancer is the fourth leading cause of cancer-related death in women and accounts for the highest mortality rate of all gynecological malignancies (Brewer et al., 2003). Undisturbed growth of the tumor in the peritoneal cavity where the ovaries are localized without any symptoms often gives reasons for poor prognosis of epithelial ovarian carcinoma. Moreover, the detection of ovarian cancer at an early and curable state is very difficult due to the asymptomatic appearance of this disease (Cannistra et al., 2004). The overall prognosis of the 5-year survival is less than 30%, whereas 70% of these tumors are diagnosed with metastases. 90% of stage IA tumors and 70% of stage II tumors can be cured by current treatment actions, but the cure rate decreases below 30% for tumor stage III and IV (Brewer et al., 2003). In fact the cure rates have remained unchanged the last 20 years though radical surgery, radiation therapy, chemotherapy and targeted therapy have improved survival times (Brewer et al., 2003).

1.3 Epidemiology and High-Risk Population of Ovarian Cancer

Ovarian surface epithelial cells are normally quiescent but proliferate after ovulation to repair the epithelial wound caused by the release of an oocyte from a mature follicle. Growth factors and high estrogen may provide stimuli for proliferation and wound healing (Brewer et al., 2003). Thus, larger number of

ovulatory cycles caused by fertility drugs or early age at menarche and late age at menopause increase the risk of ovarian cancer. On the contrary, suppressed ovulation caused by pregnancy, breast feeding and birth control pill is associated with decreased risk of developing epithelial ovarian cancer. Moreover, BRCA1 mutation is linked to an approximately 40-60% risk of developing ovarian cancer and an 85% risk of developing breast cancer. Advanced age is another risk factor for developing epithelial ovarian cancer (Brewer et al., 2003).

1.4 Staging

Staging is the process of finding out how far the cancer has spread and influences the treatment. The TNM system is used to describe the cancer in terms of the extent of the tumor (T), whether or not it has spread to the nearby lymph nodes (N), and whether it has metastasized to organs farther away (M). When the TNM groups have been described, the information is combined and assigned to a number from 1 to 4 (American Cancer Society, 2009).

Tumors

Primary tumors (T) are classified according to the following categories:

T1: The tumor is limited to one or both ovaries.

T1a: The tumor is limited to one ovary. The capsule of the tumor is intact, there is no tumor on the ovarian surface, and there are no ovarian cancer cells in ascites or peritoneal lavage.

T1b: The tumor is limited to both ovaries. The capsule is intact, there is no tumor on the ovarian surface, and there are no ovarian cancer cells in ascites or peritoneal lavage.

T1c: The tumor is limited to one or both ovaries with any of the following: ruptured capsule, tumor on ovarian surface, or cancer cells in the ascites or peritoneal lavage.

T2: The tumor involves one or both ovaries and has spread into the pelvis.
T2a: The tumor has spread and/or attaches to the uterus and/or fallopian tubes. There are no ovarian cancer cells in ascites or peritoneal lavage.
T2b: The tumor has spread to other pelvic tissues. There are no cancer cells in ascites or peritoneal lavage.
T2c: The tumor has spread to pelvic tissues, with ovarian cancer cells in ascites or peritoneal lavage.
T3: The tumor involves one or both ovaries, with microscopically confirmed peritoneal metastasis outside the pelvis and/or metastasis to regional lymph node(s).
T3a: Microscopic peritoneal metastasis beyond the pelvis.
T3b: Macroscopic peritoneal metastasis beyond the pelvis, 2 cm or less in greatest dimension.
T3c: Peritoneal metastasis beyond the pelvis, more than 2 cm in greatest dimension.

Nodes
The regional lymph nodes (N) are classified according to the following categories:
N0: The regional lymph nodes contain no metastases.
N1: There is evidence of lymph node metastasis.

Metastasis
The state of metastasis (M) is classified according to the following categories:
M0: There are no distant metastases found.
M1: Distant metastases are present.

Stage Grouping
The four basic stage groupings within the TNM system:
Stage I: The cancer is contained within the ovaries

Stage Ia: T1a, N0, M0

Stage Ib: T1b, N0, M0

Stage Ic: T1c, N0, M0

Stage II: The cancer is in one or both ovaries and has spread to other organs in the pelvis such as the bladder, colon, rectum, or uterus

Stage IIa: T2a, N0, M0

Stage IIb: T2b, N0, M0

Stage IIc: T2c, N0, M0

Stage III: The cancer is in one or both ovaries and has spread to one or both of the following: the lining of the abdomen or the lymph nodes.

Stage IIIa: T3a, N0, M0

Stage IIIb: T3b, N0, M0

Stage IIIc: T3c, N0, M0, or T(any), N1, M0

Stage IV: This is the most advanced stage. The cancer has spread from one or both ovaries to distant organs, such as the liver or lungs, or there may be ovarian cancer cells in the fluid around the lungs.

Stage IV: T(any), N(any), M1

(American Cancer Society, 2009; Oncologychannel, 2009)

1.5 Treatment Options in Ovarian Cancer

1.5.1 Surgery

Surgery is usually performed to remove as much of the tumor tissue as possible. The tumor, lymph nodes in the abdomen, lymph nodes in the pelvis, abdominal fluids, uterus, both ovaries, both fallopian tubes and the omentum are also analyzed by a gynecologic oncologist to stage the cancer. Depending on the stage of the tumor the appropriate treatment is chosen (American Cancer Society, 2009).

1.5.2 First-line Therapy

Most patients suffering from advanced ovarian cancer are not curable by surgery alone. Therefore, chemotherapy represents an essential method of treatment. Ovarian cancers in general are seen as chemotherapy-sensitive tumors because approximately 75% of the patients response to an initial treatment with platinum-containing drugs cisplatin and carboplatin either used alone or in combination with the taxane-containing drug paclitaxel. The treatment with platin-combinations provides longer survival rates than without platin or platin monotherapy. However, in 80-85% of the patients the tumors become resistant. If the duration of remission is longer than 6 months the tumor is considered as platinum-sensitive and the same drugs are used in second-line therapy as in first-line therapy. 25% of these patients show response to this kind of second-line therapy. Patients who have a shorter duration of remission than 6 months after first-line therapy have very poor prognosis (Kelland et al., 2005).

1.5.3 Second-line Therapy

As many tumors become resistant to the drugs of the first-line therapy, doxorubicin, topotecan, hexamethylmelamine, gemcitabine or docetaxel several other drugs are used for the second-line therapy (Kelland et al., 2005).

1.5.4 Radiation Therapy

Radiation therapy used high energy x-rays to reduce ovarian cancer cells and to shrink the tumor in its size. This kind of treatment may be executed additionally and is only rarely used as the main treatment for ovarian cancer (American Cancer Society, 2009).

1.5.5 Targeted Therapies

Because of the resistance of many tumors to cytotoxic agents used in chemotherapy additional treatment options in ovarian cancer therapy are urgently needed.

1.5.5.1 Monoclonal Antibodies

There are several drugs that selectively recognize proteins or receptors of the ovarian tumor cells. For example, intraperitoneal administration of cisplatin- or radio-labelled monoclonal antibodies are currently exploited in clinical trials. The advantage of (radio-) immunotherapy is the possibility of regional administration and thereby limiting systemic side-effects. Furthermore, monoclonal antibodies targeting the ovarian carcinoma biomarker CA-125 are already tested (Kelland et al., 2005). Monoclonal antibodies binding to EGFR (cetuximab) or to the ErbB2 (trastuzumab, pertuzumab) are reported to improve ovarian cancer treatment only in combination with standard cytotoxic agents (docetaxel) and may be considered for clinical trials (Bijman et al., 2009).

1.5.5.2 Small Molecules

Several small molecules have been designed to inhibit cancer specific pathways. Therefore, agents targeting drug resistance mechanisms or drugs that disrupt the cancerous angiogenesis are being developed. Furthermore, tumor specific enhanced cell proliferation and survival pathways can be blocked by small molecules inhibiting phosphorylation and activation of responsible kinases. Concerning this strategy, agents targeting EGFR family members, K-Ras inhibitors and PI3K/Akt/mTOR inhibitors are already at clinical level (Kelland et al., 2005).

1.6 Frequent Molecular Aberrations in Ovarian Cancer

Proto-oncogenes and tumor suppressor genes play a critical role in regulation of proliferation and tumorigenesis. Activating mutations of proto-oncogenes promote transformation of normal cells into malignant ones. Furthermore, inactivated tumor suppressor genes, which normally inhibit cell division and promote cell death, cause loss of the negative control of the cell (Nielson et al., 2004).

1.6.1 Receptor Tyrosine Kinases

The epidermal growth factor receptor (EGFR) family consisting of EGFR, ErbB2, ErbB3 and ErbB4 is responsible for growth regulation and differentiation in response to ligand binding and heterodimer formation among EGFR family members. The receptors are located in the cell membrane and show high structural homology. Neuregulins 1-4 serve as ligands for ErbB3 and ErbB4, while epiregulin and ß-cellulin activate ErbB1 and ErbB4. While ErbB2 is lacking a known ligand, ErbB3 lacks a functional kinase domain. Ligand binding induces ErbB (hetero-) dimer formation, whereas one ErbB kinase domain activates its dimer-partner. This leads to autophosphorylation or transphosphorylation of tyrosine residues that causes interaction between the activated receptor and SH2 or adapter proteins, which promote further downstream signaling (Citri et al., 2006). Several ovarian carcinomas show abnormal expression and abnormal signaling through EGFR pathways that confer negative prognosis in malignancy (Graeff et al., 2008). EGFR is reported to be overexpressed in more than 55% of ovarian cancers (Lassus et al., 2006) and more than 35% harbour molecular aberrations in ErbB2 (Lassus et al., 2004). However, several clinical studies document that monotherapies with EGFR or ErbB2 inhibitors or antibodies are largely inefficient against ovarian cancer (Reibenwein et al., 2008).

1.6.2 Phosphatidylinositol 3-kinase (PI3K)/AKT/mTOR/p70S6K

It is reported that a proportion of ovarian carcinomas harbor molecular aberrations of PI3K and/or PTEN. Receptor tyrosine kinases activate PI3K that is involved in many cellular functions such as proliferation, differentiation, tumorigenesis, angiogenesis and anti-apoptosis. Amplification of PI3K is observed in approximately 40% of ovarian carcinoma cell lines and patient tumor samples (Shayesteh et al., 1999; Meng et al., 2006). PI3K can be activated by the ErbB receptor tyrosine kinase family or via insulin-like growth factor-I receptor, which can interact with ErbB receptors to integrate signals across distinct signaling pathways (Olayioye et al., 2000). The tumor suppressor gene Phosphatase and Tensin homolog (PTEN) is mutated especially in advanced ovarian carcinomas and decreased PTEN expression is associated with enhanced progression of the tumor. PTEN is a lipid phosphatase that counteracts PI3K by removing phosphate from the D3 position of the inositol ring of PIP3 (Datta et al., 1999). The best known downstream target of PI3K is the serine-threonine kinase AKT, which has three isoforms that share high structural homology. AKT is recruited to the plasma membrane and binds to PIP3 via the pleckstrin homology domain, becomes phosphorylated by PDK1 at Thr308 and finally by PDK2 at Ser473 (Stephens et al., 1998). AKT1 kinase activity is frequently enhanced in a proportion of ovarian carcinomas and several studies have established that AKT activation promotes tumor cell survival, cancer cell growth and invasiveness (Datta et al., 1999). Phosphorylation of AKT at Ser473 can also be driven by mammalian target of rapamycin (mTOR) associated with rapamycin-insensitive companion of mTOR (rictor) which is also named mTORC2 (Sarbassov et al., 2006). AKT directly phosphorylates tuberous sclerosis complex 2 (TSC2, tuberin) on multiple sites that abrogates the inhibitory effects of the TSC1-TSC2 complex on Rheb and mTOR (Huang et al., 2009). AKT can phosphorylate mTOR directly too (Manning et al., 2002). The mTOR signaling is also observed to be constitutively activated in several cancers

(Gao et al., 2004). The mTOR is phosphorylated by PI3K/AKT at Ser 2448. (Nave et al., 1999). In response to low energy levels or under hypoxic conditions the function of mTOR is blocked by tuberous sclerosis complex proteins TSC1 and TSC2 (Easton et al., 2006). The mTOR is a serine-threonine kinase that by substrate phosphorylation transmits activation from AKT to p70S6K and inactivates eukaryotic initiation factor 4E (eIF4E) inhibitor binding protein 1 (4eBP1) that normally blocks cap-dependent translation. Phosphorylation of 4eBP1 at Ser65 by mTOR results in release of eIF4E and activation of cap-dependent mRNA translation. The downstream effector protein p70S6K is a serine-threonine kinase. In total, two isoforms of S6K with 2 splice variants each have been identified: The cytoplasmatic p70S6K1 and p54S6K2 and the nuclear p85S6K1 and p60S6K2. Phosphorylation of p70S6K at Thr389 is closely related to its kinase activity (Pullen et al., 1997). The p70S6K1 is an important cascade molecule downstream of PI3K and AKT in tumor cell progression and proliferation (Meng et al., 2006; Gao et al., 2004) and ubiquitination-dependent degradation of p70S6K1 has recently been associated to the regulation of its steady-state level (Wang et al., 2008). Moreover, S6K1 is reported to be overexpressed or constitutively active in early stages of transformation in ovarian epithelium with BRCA1 mutations (Easton et al., 2006). The p70S6K phosphorylates the S6 protein of the 40S ribosomal subunit and is involved in translation control.

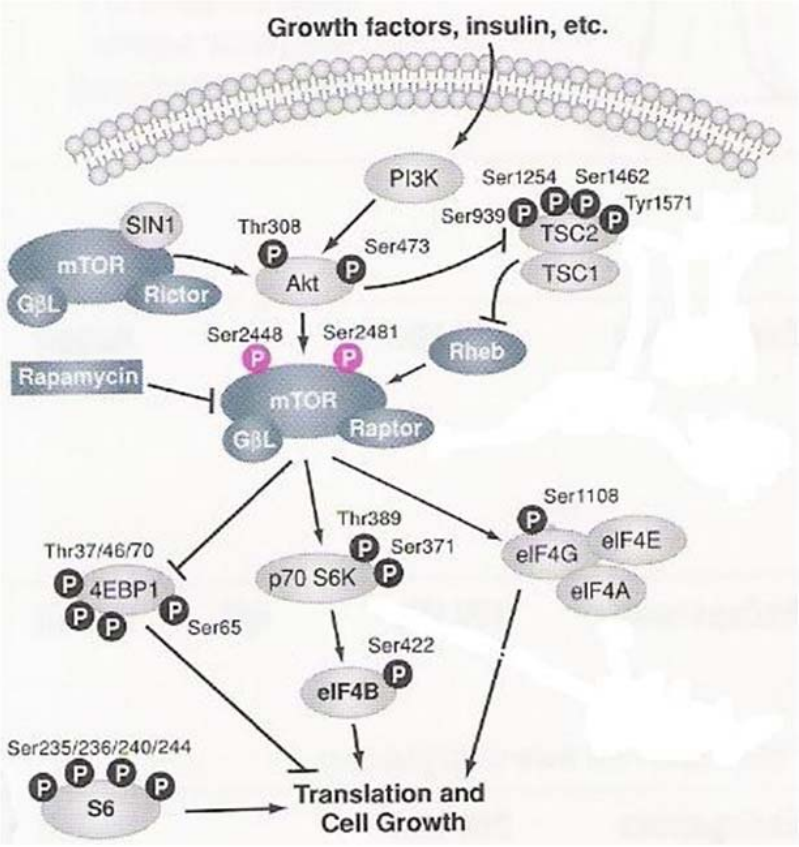

Figure 1: Scheme of PI3K/AKT/mTOR/p70S6K signaling cascade
Source: "Cell Signaling Technology Inc. , 2007-2008, Catalog and Technical Reference, p.125, mTOR" – with modifications

1.6.3 Fatty Acid Synthase (FASN)

It is documented that FASN protein is overexpressed in more than 80% of ovarian carcinomas (Alo et al., 2000). Furthermore, FASN has been identified as an independent prognostic factor for clinical outcome in ovarian cancer and increased expression of FASN in ovarian neoplasms predicts shorter survival (Graeff et al., 2008; Reibenwein et al., 2008; Gansler et al., 1997). Moreover, inhibition of FASN causes growth arrest in breast cancer and delays disease progression of ovarian carcinomas in xenograft models (Gansler et al., 1997; Pizer et al., 1996). Cancers usually reveal increased de novo lipogenesis as fatty acids are essential for all biological membranes and important for energy

metabolism. Normal cells usually prefer exogenously-derived fatty acids for the synthesis of new lipids. The biosynthesis of endogenously-synthesized fatty acids is catalyzed by the multifunctional, homodimeric enzyme fatty acid synthase (FASN) that is 250-270 kDa in size (Wakil et al., 2004). In normal conditions FASN converts excess carbohydrate into fatty acids that are then converted into triacylglycerols which can provide energy through ß-oxidation if needed. During ß-oxidation acyl-coenzymeA (CoA) is broken down to acetyl-CoA in the mitochondria of the cell. Acetyl-CoA is then the entry molecule for the citric acid cycle. The main product of FASN is a 16-carbon fatty acid, palmitate that is synthesized by using acetyl-CoA and malonyl-CoA as carbon donor and NADPH as reducing agent. Besides the exacerbated de novo biogenesis of fatty acids in cancer cells, high levels of carbon flux through aerobic glycolysis are hallmarks of tumors and provide them growth advantages. This rapid consume of glucose under aerobic conditions in tumor cells is named Warburg effect. In cancer cells there are many enzymes involved in metabolism of glucose to fatty acids (Figure 2).

1.6.3.1 Biosynthesis of endogenously-synthesized fatty acids

First, glucose is taken up via glucose transporters and converted to glucose-6-phosphate by hexokinase. Most of the glucose-6-phosphate is used for ATP generation by the glycolytic pathway. Therefore, pyruvate is converted to acetyl-CoA that enters the mitochondrian citric acid circle to generate ATP. Requisite citrate, which could not be fully oxidized is converted back into acetyl-CoA by ATP citrate lyase (ACLY). The rate limiting enzyme acetyl-CoA carboxylase (ACACA) carboxylates a proportion of acetyl-CoA into malonyl-CoA. FASN condensates acetyl-CoA and malonyl-CoA to the 16 carbon saturated fatty acid palmitate and is dependent on NADPH, which is used as the reducing agent in this reaction. NADPH can be acquired through the pentose phosphate pathway. Palmitate and other saturated long-chain fatty acids can be converted into more complex fatty acids that are then used for synthesis of phospholipids,

triglycerides, cholesterol esters or acetylated proteins. Under anaerobic conditions pyruvate can also be used for the production of lactate by lactate dehydrogenase (LDH). In this case accumulated lactate is secreted out of the cell (Menendez et al., 2007)

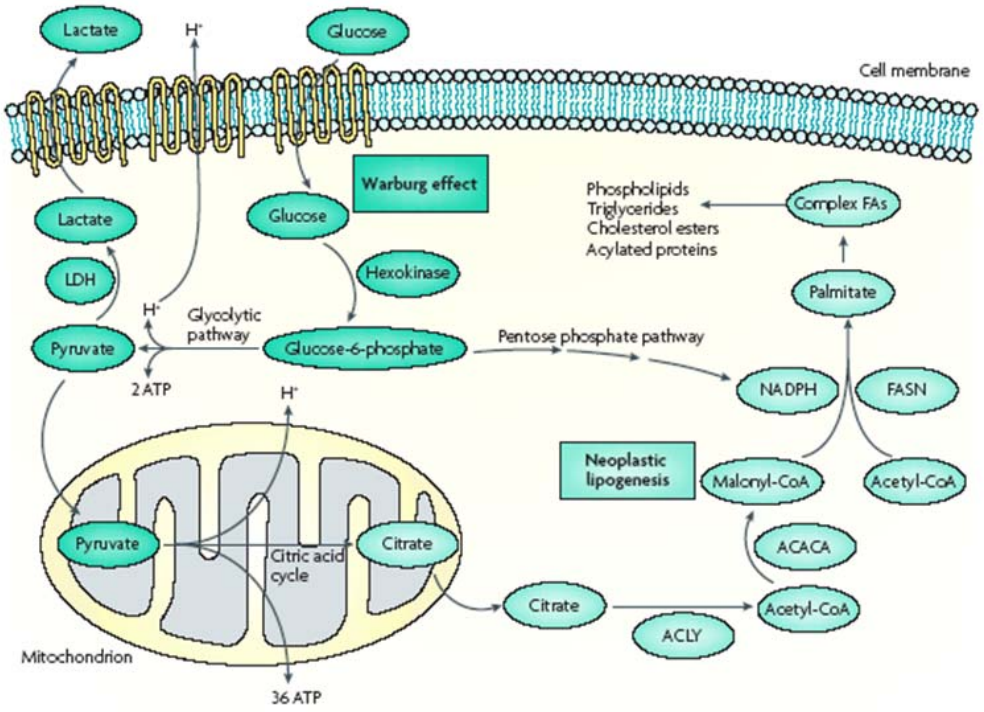

Figure 2: Warburg effect connected with fatty acid biosynthesis in cancer cells
Source: "Menendez, Lupu, Nature Reviews Cancer, 7, 763 (2007)"

1.6.3.2 Regulation of FASN expression in tumor cells

One of two main pathways to regulate tumor associated FASN expression in cells is to phosphorylate receptor tyrosine kinases such as EGFR or ErbB2 via growth factor dependent phosphorylation or growth factor independent autophosphorylation that triggers a downstream activation of PI3K/AKT. Steroid hormones such as estradiol, progestin and androgen, which can bind to their corresponding steroid hormone receptors also lead to a downstream activation. In tumor cells FASN induction is constitutively driven because of hyperactivation of these pathways due to overproduction of growth factors, loss of PTEN function

and amplification of PI3K. However, in normal adipocytes and hepatocytes FASN expression is regulated by carbohydrates, fatty acids and fasting. The expression of FASN is directly modulated by the helix-loop-helix leucine zipper transcription factor sterol regulatory element-binding protein 1c (SREBP1c) that binds to the promoter region of FASN. Inactive SREBP1c precursor protein (pSREBP1c) is anchored in the membrane of the endoplasmatic reticulum (ER) and can be released by its activating protein SCAP. When enough activating signals have entered the cell, the SCAP-pSREBP1c complex moves from the ER membrane to the Golgi apparatus membrane where pSREBP1c is then cleaved by proteases releasing the cytoplasmatic domain, which translocates into the nucleus and transcribes FASN (Menendez et al., 2007) (Figure 3).

The second pathway to achieve enhanced FASN expression in tumor cells takes place at a post-translational level. Normally, FASN protein level is modulated via ubiquitin-dependent proteasomal degradation. In prostate cancer cells, it has been observed that FASN interacts with the ubiquitin-specific protease named USP2 that removes ubiquitin from FASN and rescues FASN from proteasomal degradation (Graner et al., 2004) (Figure 3).

1.6.3.3 Crosstalk between EGFR family members and FASN

Phospholipids generated by FASN are integrated into membrane lipid rafts that localize membrane receptor tyrosine kinases such as the EGFR family members. Thus, formation of increased membrane lipid rafts by enhanced FASN activity initiates more signaling of receptor tyrosine kinases for proliferation and survival in tumor cells (Menendez et al., 3, 2005; Grunt et al., 2009) (Figure 3). Crosstalk between FASN and oncogenic PI3K/AKT pathway has been discussed in two recent puplications. Wang et al observed that in ovarian carcinoma cells AKT activation regulates FASN expression whereas FASN activity modulates AKT activation (Wang et al., 2005). Grunt et al also demonstrated that inhibition of FASN reduces EGFR and sensitizes ovarian carcinoma cells against ErbB targeting agents (Grunt 2009 BBRC). Moreover, several mechanisms are known

that regulate ErbB2 signaling by FASN. First, blocking of FASN leads to accumulation of its substrate malonyl-CoA, which enhances nuclear PEA3 that represses ErbB2 transcription (Menendez et al., 5, 2004). Second, FASN inhibition leads to an accumulation of NADPH. NADPH activates NADPH oxidase (NOX) that generates reactive oxygen species (ROS), which disables ErbB2 expression (Menendez et al., 2007) (Figure 3). Third, FASN blocking reduces synthesis of phospholipids integrated into the membrane lipid rafts. Therefore, ErbB2 receptors cannot be accommodated into the lipid raft aggregates and are recycled by endocytosis and lysosomal degradation (Nagy et al., 2002) (Figure 3). Fourth, activation of PI3K/AKT by FASN is reported to upregulate the transcription factor Sp1 (Jin et al., 2007). The protein Sp1 stimulates EGFR transcription via binding to the EGFR promoter which contains Sp1 motif (Liu et al., 1, 2005). Interestingly, FASN promoter also contains some Sp1 transcription factor binding sites (Roder et al., 1999). Thus, maybe FASN activates an autostimulatory loop by AKT that may increase both FASN and EGFR transcription (Figure 3). Fifth, a recent report indicates that hypoxia induces phosphorylation of AKT at Ser 473 which in turn activates SREBP1c to enhance FASN transcription (Furuta et al., 2008)

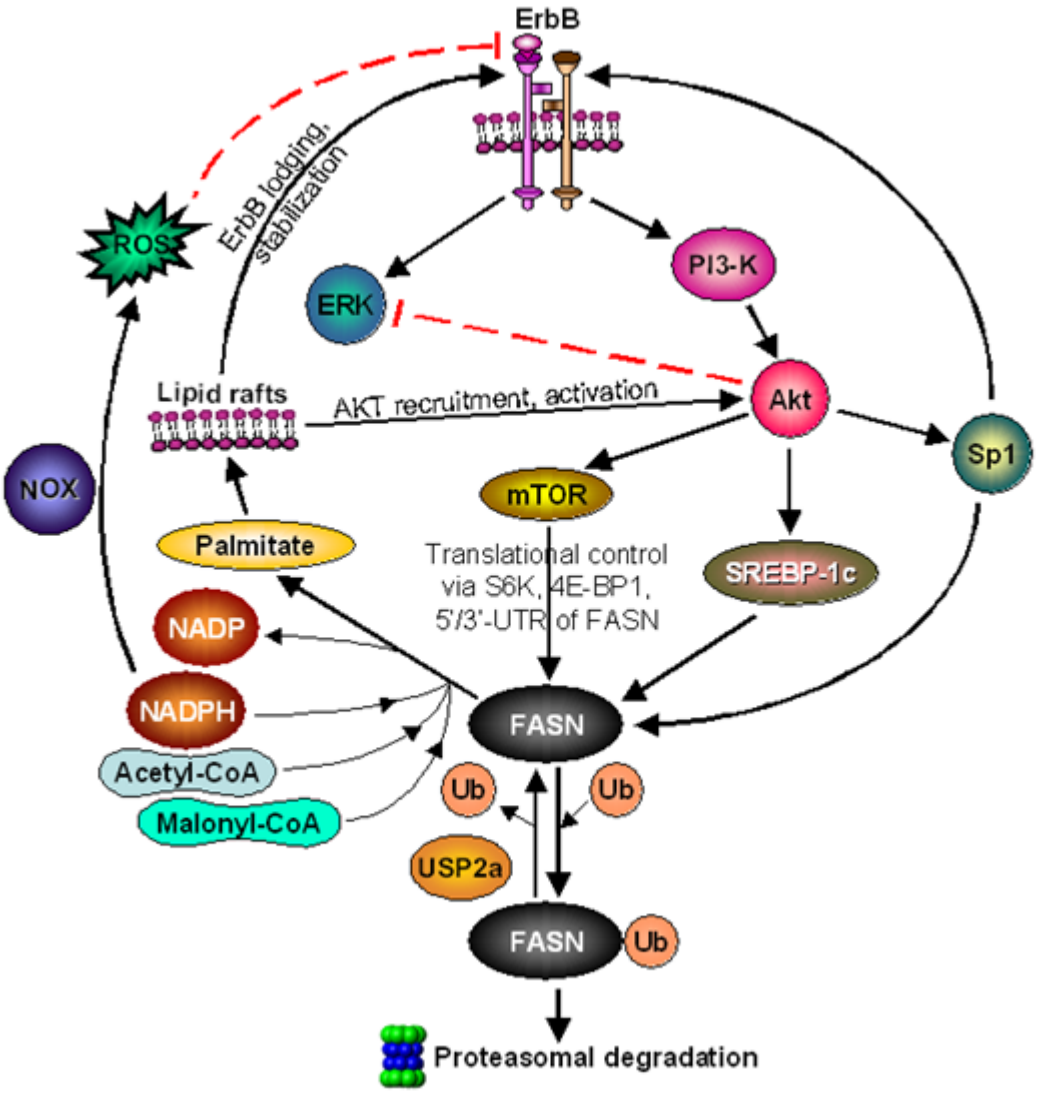

Figure 3: Crosstalk between EGFR family members and FASN
Source: "Grunt et al, BBRC, 2009"

1.6.3.4 FASN Inhibitors

As FASN expression is enhanced in more than 80% of ovarian carcinomas (Alo et al., 2000) it provides an attractive target for cancer therapy. That means that pharmacological FASN inhibitors selectively kill tumor cells and delay disease progression of ovarian carcinomas in xenograft models (Gansler et al., 1997; Pizer et al., 1996). The mammalian FASN is a multifunctional homodimeric

enzyme. Each of its two identical polypeptides includes seven catalytic domains: ß-ketoacyl synthase (KS) domain, malonyl/acetyltransferase (MAT) domain, dehydrase (DH) domain, enoyl reductase (ER) domain, ß-ketoacyl reductase (KR) domain, acyl carrier protein (ACP) domain and thioesterase (TE) domain (Wakil et al., 2004). Five well known drugs blocking FASN activity are as following: The FASN inhibitor cerulenin is a natural product isolated from Cephalosporium caerulens. It covalently binds to the KS domain of FASN thereby prohibiting the condensation between the fatty acid chain and acetyl or malonyl molecules. Cerulenin is chemically instable and possesses a reactive epoxy group which limits its clinical relevance (Lupu et al., 2006). Orlistat blocks the TE domain of FASN and thus prevents releasing of the end-product palmitate (Knowles et al., 2004). Furthermore, orlistat has a poor solubility, which excludes it as an anti-ovarian cancer drug (Menendez et al., 2, 2005). Triclosan inhibits the ER domain of FASN and accumulates unsaturated enoyl thioester intermediate (Liu et al., 2002). The well known green tea component epigallocatechin-3-gallate (EGCG) blocks the KS domain of FASN and naturally occurring polyphenols with similar chemical structures such as luteolin, quercetin or kaempferol also inhibit FASN activity by binding this domain (Brusselmans et al., 2005). In this report we used C75 for FASN inhibition in our experiments. C75 especially blocks the KS domain of FASN and resembles cerulenin without its reactive epoxy group that makes C75 chemically more stable. Structurally, C75 is a cell permeable α-methylene-γ-butyrolacetone which is less reactive than. In contrast to cerulenin, which only blocks the KS domain of FASN, C75 also inhibits ER and TE domain of FASN. Furthermore, C75 is a competitive inhibitor of acetyl-CoA, malonyl-CoA and NADPH. Besides the cytotoxic effects in cancer cells, C75 is also proposed as an anti-obesity agent. As C75 blocks activity of FASN its substrate malonyl-CoA accumulates in the cells that normally has an inhibitory effect on carnitine palmitoyl transferase 1 (CPT1). This usually regulates mitochondrial fatty acid ß-oxidation. As C75 also acts as a malonyl-CoA blocker, it can antagonize its effects on CPT1 and can drive ß-oxidation. A

second anti-obesity effect of C75 is the modulation of the metabolism in the hypothalamus, where it mediates appetite suppression via malonyl-CoA accumulation (Bentebibel et al., 2006). Patients suffering from cancer should not loose weight and adipose mass. Thus, novel designs of C75 have been synthesized, but explicit results concerning effects on CPT1 expression are still missing (Wang et al., 2009).

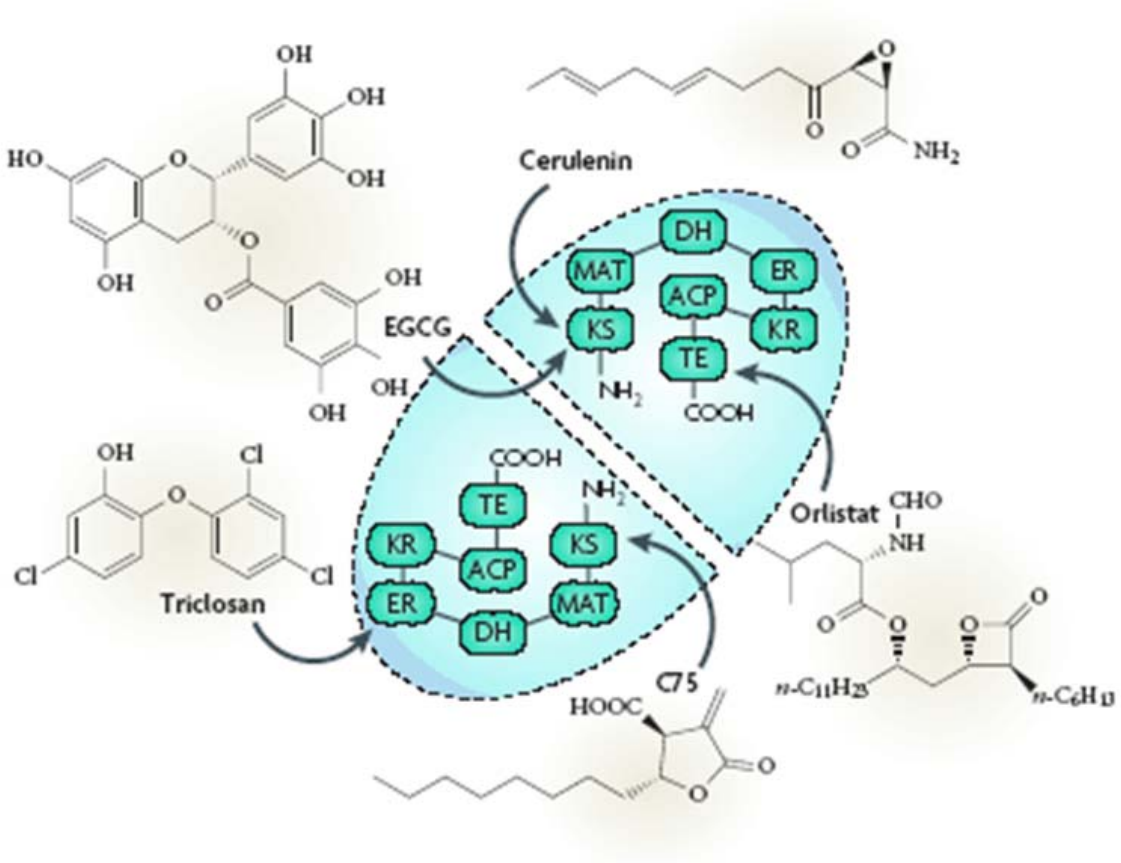

Figure 4: Blocking sites of FASN inhibitors
Source: "Menendez, Lupu, Nature Reviews Cancer, 7, 763 (2007)"

1.6.3.5 Cytotoxic Effects of FASN Inhibition in Cancer Cells

Inhibition of FASN causes growth arrest in breast cancer cells and delays disease progression of ovarian carcinomas in xenograft models (Gansler et al., 1997; Pizer et al., 1996). There are several mechanisms that can explain the cytotoxic effects due to FASN inhibition. Blockade of FASN activity leads to

accumulation of its substrate, malonyl-CoA, which is an inhibitor of CPT1 regulated ß-oxidation. Decreased ß-oxidation accretes ceramides that induce transcription of apoptotic genes such as DAP kinase, BNIP3 and TRAIL (Bandyopadhyay et al., 2006). FASN inhibition induces apoptosis in tumor cells lacking p53 rather than in cells with intact p53. Whereas blocking of FASN leads to growth arrest in cancer cells containing a functional p53 tumor suppressor gene, FASN inhibition leads to a genotoxic stress and apoptosis in p53 deficient cells (Menendez et al., 1, 2005). As FASN is responsible for synthesis of membrane phospholipids, an end product starvation in highly proliferating tumor cells induces apoptosis selectively in these cells (Rodriguez-Gonzalez et al., 2005). Furthermore, FASN inhibition modulates lipid raft formation and decreases correct localization and function of tyrosine kinase receptors in the membranes (Nagy et al., 2002). Moreover, it has been observed that downregulation of FASN leads to decreased AKT activity and to decreased anti-apoptotic signaling of this pathway (Wang et al., 2005). It is well known that FASN inhibition leads to cell cycle arrest in G1 by several mechanisms. During G1 and S phase the phospholipid biosynthesis is normally greatest to prepare the cell for following division. The blocking of the cell cycle by FASN inhibition is reported to be caused by cyclin-dependent kinase inhibitors such as p21 or p27, BRCA1, SKP2 and nuclear factor κB (NF κB) (Knowles et al., 2004; Bandyopadhyay et al., 2006; Menendez et al., 4, 2004). Furthermore, it is documented that transcription of cyclin-dependent kinase inhibitor $p15^{INK4b}$ mRNA is upregulated after mTOR and p70S6K inhibition (Heinonen et al., 2007). As mTOR and p70S6K are downstream of AKT, which is decreased after FASN blocking, we hypothesize that p15 transcription could be upregulated that way. The enhanced mRNA transcription of cyclin-dependent kinase inhibitor $p15^{INK4b}$ could also be due to increased activity of forkhead box O (FOXO) transcription factors. FOXOs are negatively regulated by AKT phosphorylation (Katayama et al., 2008) which is decreased by FASN inhibition. Thus, FASN inhibition may

lead to decreased AKT activity that could induce FOXO-dependent $p15^{INK4b}$ transcription, which may finally enhance G1 cell cycle arrest.

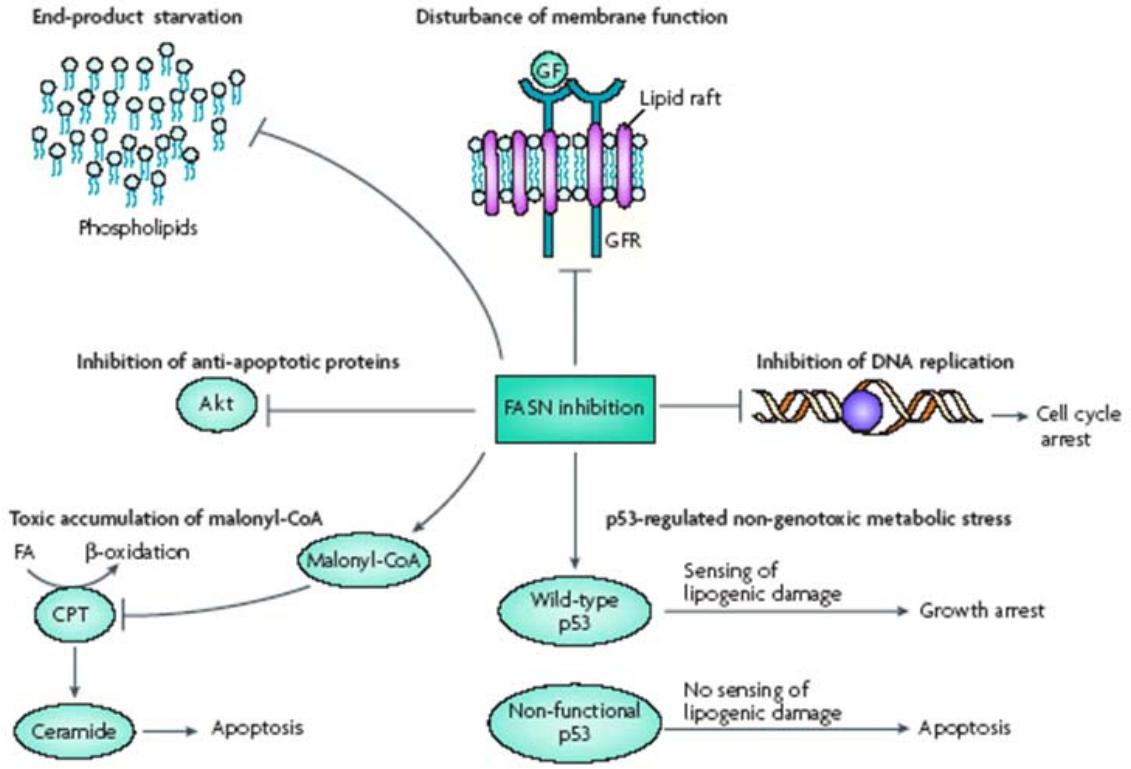

Figure 5: Several molecular mechanisms of the tumoricidal Effects of FASN Inhibition
Source: "Menendez, Lupu, Nature Reviews Cancer, 7, 763 (2007)"

1.6.4 Cell cycle control at G1/S checkpoint

Enhanced unscheduled proliferation in tumor cells frequently is caused by hyperactivation of cell-cycle cyclin-dependent kinases (Cdks) through amplification, mutation or overexpression of cyclins and frequent inactivation of Cdk inhibitors (Malumbres et al., 2001). In fact, alteration of Cdk inhibitors is a frequent event in several tumor types. The tumor suppressor proteins $p15^{INK4b}$ and $p16^{INK4a}$ are inhibitors of Cdks that prevent the cell from going through the G1-S phase transition.

Inactivation of $p15^{INK4b}$ and $p16^{INK4a}$ genes, which are lokalized on the band p21 of chromosome 9 has been detected in various human tumors and is thought to

be an important step in cancer development (Herman et al., 1996). Via polymerase chain reaction (PCR)-based analysis homozygous deletions of $p16^{INK4a}$ were detected in 7% ovarian carcinomas, while homozygous deletions of $p15^{INK4b}$ were detected in 33% ovarian carcinomas (Wong et al., 1997). Furthermore, it is well documented that more than 33% of ovarian carcinomas harbor $p15^{INK4b}$ methylation and more than 19% show $p16^{INK4a}$ methylation that is associated with transcriptional silencing of these tumor suppressor genes (Liu et al., 2, 2005; Rojas et al., 2009; Katsaros et al., 2004; Tam et al., 2007). The most common tumor suppressor gene p53 encodes a 53 kDa nuclear protein. 53% of patients suffering from ovarian cancer are reported to overexpress mutant p53 protein (Nielsen et al., 2004). The tumor suppressor p53 induces G1 cell cycle arrest following DNA damage. Besides, it regulates transcription, differentiation, senescence, genomic instability, apoptosis and survival as well as glucose metabolism, oxidative stress and angiogenesis. Normally the protein level of p53 is low due to its short half-life. Mutations in p53 lead to a more stable, but inactive protein that is resistant to degradation that results in accumulation of p53 in the nucleus. Currently, p53 alterations are the most common defects, which are identified in epithelial ovarian cancers (Darcy et al., 2008) and are also associated with poor prognosis (Nielsen et al., 2004). Ovarian cancers that show inhanced expression of p53 protein contain mutations in conserved regions of the p53 gene. These mutations are predominantly transitions, which suggests that they arise spontaneously rather than being caused by carcinogen exposure (Berchuck et al., 1994).

The tumor suppressors $p15^{INK4b}$ and $p16^{INK4a}$ are homologous inhibitors of the cyclin-dependent kinases CDK4 and CDK6 and control the commitment of eukaryotic cells to transit the gap1 (G1) phase and enter the DNA synthesis (S) phase. The binding of $p15^{INK4b}$ or $p16^{INK4a}$ to CDK4 and CDK6 induces an allosteric change which abrogates the association of these kinases to D-type cyclins (cyclin D1) forcing a kinase inactive state. In contrast, the tumor suppressor p21 binds CDK2/CyclinE complexes forming ternary structures (Kim

et al., 2006). It has been shown that p21 plays a major role in inducing p53-dependent G1 cell cycle arrest following DNA damage (Malumbres et al., 2003). Thus, phosphorylation of retinoblastoma (Rb) proteins is inhibited (Kim et al., 2006). Phosphorylation of Rb by CDK4/6 or CDK2 dissociates the repressor Rb from E2F transcription factor permitting transcription of S-phase promoting genes. Accordingly, $p15^{INK4b}$, $p16^{INK4a}$ or p21CIP1 maintains Rb in a hypophosphorylated state that promotes binding to E2F, which prevents G1 – S phase transition (Harbour et al., 2000).

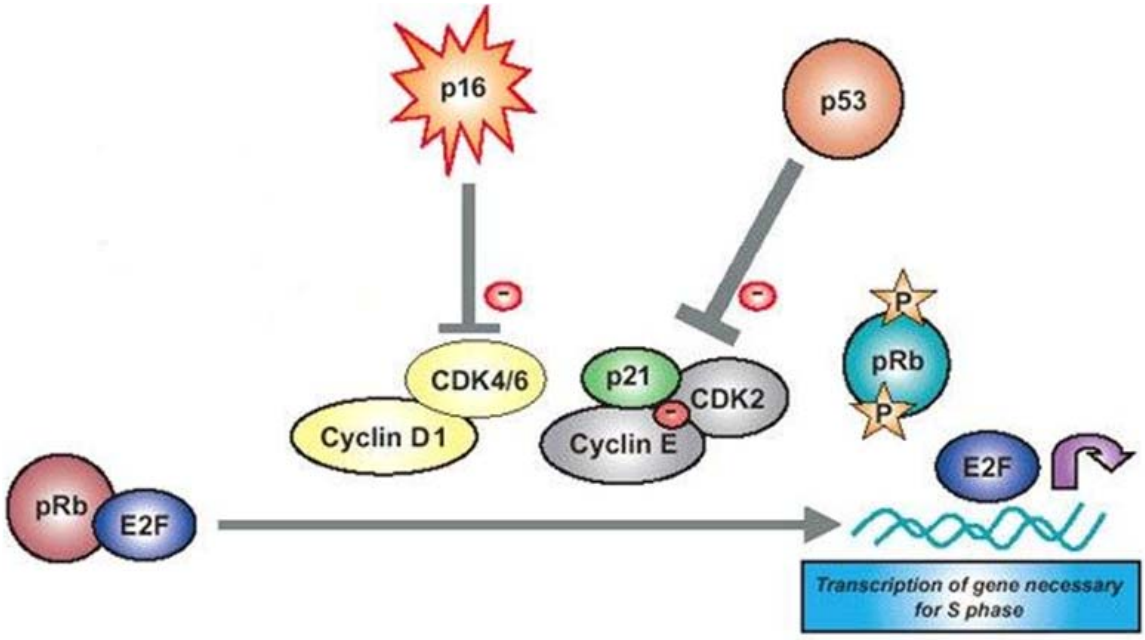

Figure 6: Mechanism of cyclin dependent kinase inhibitors
Source: "Cancer Control, 2004, Lee Motfitt ,Cancer Center and Research Institute, Inc." (http://www.medscape.com) – with modifications.

1.6.5 Epigenetic gene silencing in cancer

DNA methylation is a naturally occurring event in organisms in order to protect host DNA from digestion by restriction endonucleases, which are designed to eliminate foreign DNA. In higher eukaryotes DNA methylation is implicated in gene expression control during genetic imprinting, embryonic development, X-chromosomal silencing and cell cycle regulation (Costello et al., 2001).

Furthermore, it is well known that DNA hypermethylation is involved in cancer development (Stirzaker et al., 1997). During DNA methylation a methyl group is added to the fifth carbon position of the cytosine pyrimidine ring by DNA methyltransferase enzymes (DNMTs). Most DNA methylation modifications occur in 5´-CpG-3´dinucleotides. About 80 percent of all 5´-CpG-3´dinucleotides in human genomes are methylated. The remaining twenty percent unmethylated are located within promoter regions or in the first exons of genes (Adams et al., 1995). Many tumor suppressor genes are reported to be promoter hypermethylated. Aberrant methylation of CpG islands in promoter regions of $p15^{INK4b}$ (Herman et al., 1996) and $p16^{INK4a}$ (Katsaros et al., 2004) as well as gene methylation of DAP Kinase (Collins et al., 2006) and CDH1 (Rathi et al., 2002; Makerla et al., 2005) has been observed. Several types of tumors, including ovarian cancer, are known to have a hypermethylation phenotype (Esteller et al., 2001; Strathdee et al., 2001). It is shown that in a proportion of ovarian carcinomas aberrant promoter methylation of CDH1 gene (≤42%) is detected and that methylation status of CDH1 is closely associated with the decrease of E-Cadherin protein expression (Yuecheng et al., 2006). Especially, DAP kinase methylation is observed in 67% of patients with malignant ovarian carcinomas (Collins et al., 2006). Moreover, it is well documented that more than 33% of ovarian carcinomas harbor $p15^{INK4b}$ methylation and more than 19% show $p16^{INK4a}$ methylation.

As DNMT1 is reported to preference hemi-methylated substrates to maintain the methylation patterns following DNA replication, it accounts for basic methylation (Esteller et al., 2007). For example, DNMT1 methylates and silences multiple genes on the inactivated X chromosome of females (Collins et al., 2006). DNMT3a and DNMT3b are known to be responsible for de novo methylation. However, novel studies indicate that DNMT1, DNMT3a and DNMT3b posses all de novo and maintenance functions (Esteller et al., 2007). The conserved amino-terminal domains of the four core histones (H2A, H2B, H3 and H4) contain lysines that are acetylated by histone acetyltransferases (HATs) and

deacetylated by histone deacatylases (HDACs). Removal of acetyl groups from histone lysine tails by HDAC increases the ionic interactions between the positively charged histones and the negatively charged DNA resulting in a compact transcriptionally repressive chromatin state. Histone hypoacetylation is not always explained by HDAC hyperactivation but also can be due to decreased HAT activity caused by mutations or chromosomal translocations (Espada et al., 2004). Methyl-CpG binding proteins (MBDs) are associated to methylated DNA and HDAC-containing complexes to establish a transcriptionally inactive chromatin environment. Thus, hypermethylated CpG islands of silenced tumor-suppressor genes are characterized overall by histone methylation and histone hypoacetylation (Esteller et al., 2007).

1.7 The Ubiquitin/Proteasome pathway

The ubiquitin/proteasome pathway leads to specific degradation of several proteins with a low half-life period and is conserved from yeast to mammals in all eukaryotic cells. Proteins, which have not been properly fold, or cell cycle proteins, which have to be eliminated for purposes of regulation, but also for quantity control are targeted to be reduced by proteasomal degradation. Ubiquitin modification of proteins is ATP-dependent and occurs through sequential steps catalyzed by three classes of enzymes. The ubiquitin activating enzyme (E1) forms a thio-ester bond with ubiquitin. Therefore, the ubiquitin conjugating enzyme (E2) can join ubiquitin, a 76 amino acid polypeptide, at its carboxy-terminus to the lysine of target proteins through an isopeptide bond. Then, several ubiquitin ligase enzymes (E3) pass the ubiquitin to the substrate and provide specificity in modifying target proteins. To target a protein for proteasomal degradation multiple ubiquitination cycles are needed that result in a polyubiquitination chain. Monoubiquitination acts as a signal for intracellular trafficking, while polyubiquitination of proteins results in recruitment of the 26S

proteasome and degradation. The 26S proteasome is a 2,5MDa complex, multisubunit protein that recognizes, unfolds and degrades targeted proteins. The proteasome uses energy from ATP hydrolyses to unfold the targeted proteins and to translocate the polypeptide chain into the cylindrical core of the complex (Pickart et al., 2004). The specificity of proteasomal degradation is achieved by several types of E3, each of which can only modify a subset of proteins. Moreover, specificity is provided by post-translational modifications of the target proteins including phosphorylation. However, up to date a conclusive molecular mechanism for specific targeting of proteins for ubiquitin-dependent proteasomal degradation remains elusive. As ubiquitin-dependent degradation is often involved in cell cycle control and cell growth, proteasome inhibitors are currently under investigation as anti cancer drugs (Adams et al., 2004).

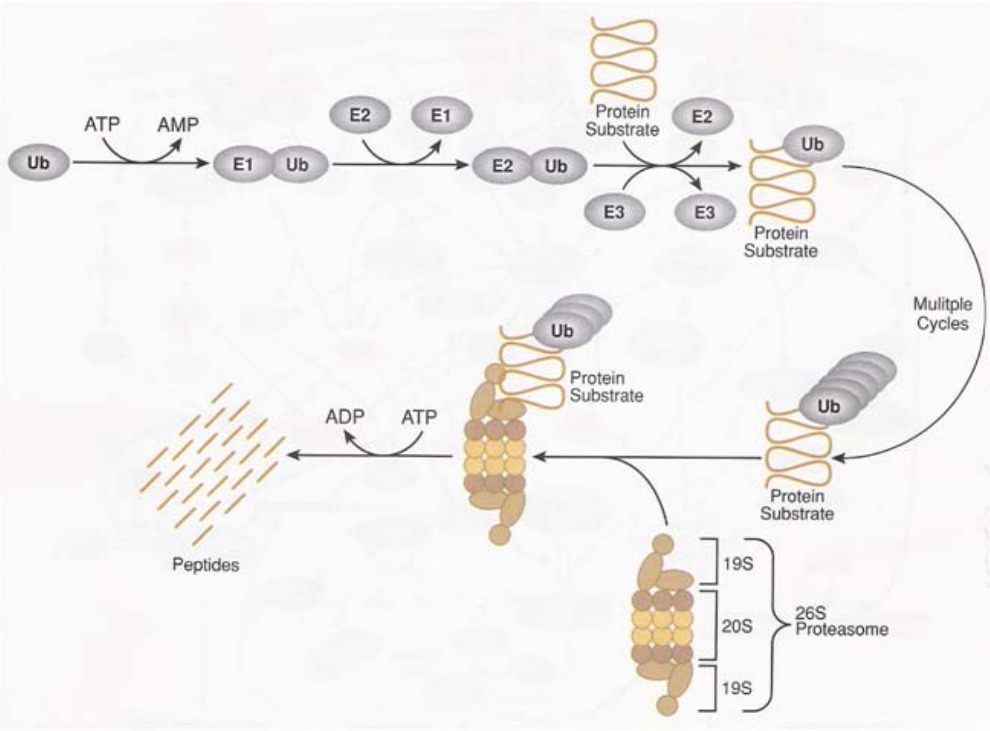

Figure 7: The Ubiquitin/Proteasome pathway

Source: "Cell Signaling Technology Inc., 2007-2008, Catalog and Technical Reference, p.402"

This work is the first report about the epigenetically modulating activity of FASN inhibition. We further pointed out several effects of FASN blocking including enhanced ubiquitin-dependent protein degradation and downregulation of PI3K signaling. Moreover, we could confirm anti-proliferative and apoptosis-inducing actions induced by FASN inhibition.

2 Materials and Methods

2.1 Cell culture and Cell line

In our experiments we used the human ovarian carcinoma cell line A2780, which was isolated from an untreated patient. The A2780 cell line was obtained from M. Krainer, Medical University of Vienna, in early passages. This epithelial cell line grows adherently and forms a monolayer. It is cultivated in RPMI1640 medium (Gibco, 32404-014) supplemented with 10% heat inactivated fetal calf serum (FCS) (Gibco, 10270-106), 100 U/ml Penicilline and 100mg/ml Streptomycine (PenStrep) (Gibco, 15140-148) and 2mM L-Glutamine (Gibco, 25030-032). After preparation of the culture medium, the medium always was sterile filtered by sterile bottle filter system with 0,2µm diameter. Moreover, all preparations with living cells were performed under sterile conditions in laminar air flow hood (HERAsafe).

2.1.1 Maintenance of Cells

The cell line A2780 was maintained at 37°C in a 5% carbon dioxide atmosphere with 95% relative humidity. The cell line was cultivated on 25cm^2 tissue culture flasks (Falcon, 353009) in 7ml of the medium containing 10% FCS, 100U/ml Penicilline, 100µg/ml Streptomycine and 2mM L-Glutamine. At a confluence of approximately 90%, cells were passaged. After removal of the culture medium the cells were washed with PBS Dulbecco´s (Gibco, 14190-094) and incubated with Trypsin/EDTA (Gibco, 25300-054) for 5 minutes at 37°C to detach them. Then the cells were resuspended in the RPMI1640 culture medium to obtain a single cell suspension and passaged at ratios from 1:15 to 1:20 corresponding to a density of about 1x10^6 cells in 7ml fresh culture medium. The fast growing

A2780 cells were passaged twice a week. Confluence, morphology and treatment effects were checked under light microscope.

2.1.2 Storage of Cells

To avoid long-term-effects, such as mutations, we used the cells for experiments only until passage 30. Therefore, we expanded the A2780 cells at a low passage and stored them at a density of $2x10^6$ cells/ml in liquid nitrogen. For freezing, the cells were washed with PBS Dulbecco´s and incubated with Trypsin/EDTA for 5 minutes at 37°C to detach them. Then the cells were resuspended in 5ml RPMI1640 culture medium, centrifuged at 1000rpm for 5minutes and again resuspended in only 3 ml culture medium to obtain a concentrated single cell suspension for counting. To select the intact cells, 20µl single cell suspension was incubated with 180µl 0,4% Trypanblue Solution (Sigma, T8154), whereas only the trypanblue solution excluding cells were counted in a counting chamber under the light microscope. The remaining 3ml cell suspension is then adjusted to $4x10^6$ cells/ml in culture medium before it is diluted 1:2 with culture medium supplemented with 20% dimethyl-sulfoxide (DMSO)(Sigma, D2650) to a final DMSO concentration of 10% and $2x10^6$ cells/ml. Before 1ml of the adjusted cell suspension was transferred into liquid nitrogen, the cells were slowly frozen in cryotubes (NUNC, 368632) in an isolating Styrofoam box at -80°C for 48 hours. In the end, the cells were stored in liquid nitrogen for years. For experiments, we quickly thawed the cells. For this purpose, we transferred the cryotube from liquid nitrogen directly into a beaker filled with ice before the vial was then thawed in a beaker containing warm water. Afterwards, the 1ml cell suspension was transferred into a 50ml falcon tube containing precooled 10ml culture medium and centrifuged at 1000rpm for 5minutes at 4°C. The cell pellet containing $2x10^6$ cells was resuspended with 1ml culture medium and sowed into a tissue culture flask. The cells were at least cultured 2 weeks to recover before they were used for experiments.

2.1.3 Used drugs

Cells were treated for the indicated times and drug concentrations.

The **FASN inhibitor C75** (Sigma, C5490) was dissolved in DMSO under sterile conditions and stored at -80°C. Further dilutions were made in culture medium. C75 is a small molecule inhibitor of the ketoacyl synthase domain (KS) of FASN, thus preventing the condensation reaction between the elongating fatty acid chain and successive acetyl or malonyl residues. C75 is a cerulenin-derived semi-synthetic FASN inhibitor lacking the reactive epoxy group of cerulenin. In contrast to cerulenin, C75 additionally inhibits enoyl reductase and thioesterase. Moreover, C75 is a competitive irreversible inhibitor of acetyl-CoA, malonyl-CoA, and NADPH (Price et al., 2001; Reninda et al., 2005). In mice, C75 treatment induces rapid and profound weight loss and loss of adipose mass by affecting food intake and energy expenditure. These side effects of C75 preclude its development as an anti-tumor agent. Nevertheless, C75 has been used as a leading compound for discovering the role of FASN in obesity and cancer (Wang et al., 2009; Menendez et al., 2007). Optimal effects of FASN inhibition were obtained with 7µg/ml concentration of C75 in A2780 cells (Grunt et al., 2009).

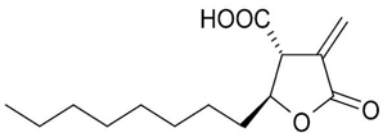

Figure 8: Chemical Structure of C75

The **PI3K inhibitor LY294002** (Calbiochem, 440202) was dissolved in DMSO under sterile conditions and stored at -80°C. Further dilutions were made in culture medium. LY294002 is a cell-permeable, potent, and specific phosphatidylinositol 3-kinase inhibitor that acts on the ATP-binding site of the enzyme. We used this inhibitor at a concentration of 40µM in A2780 cells.

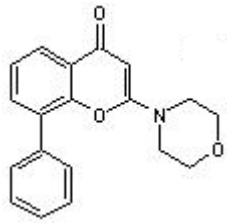

Figure 9: Chemical structure of LY294002

The **translation inhibitor Cycloheximide** (CHX) (Sigma, C1988-1G) was dissolved in DMSO under sterile conditions and stored at -80°C. Further dilutions were made in culture medium. Cycloheximide is an elongation inhibitor. It blocks the translation of messenger RNA on cytosolic, 80S ribosomes, but does not inhibit organelle protein synthesis (Obrig et al., 1971). The optimal translation inhibition of the analyzed proteins was obtained at a final concentration of 15µ/ml in A2780 cells.

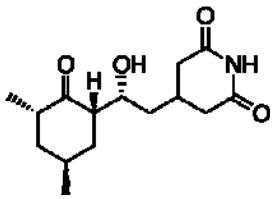

Figure 10: Chemical Structure of Cycloheximide

2.2 Gene expression analysis on mRNA level

2.2.1 Treatment of Cells

We plated 5,36x10^5 A2780 cells per tissue culture flask T25 (25cm^2 growth area) or 16,08x10^5 cells per tissue culture flask T75 (75cm^2 growth area). Cells were cultured in RPMI1640 supplemented with 5% FCS, 100U/ml Penicilline, 100µg/ml Streptomycine and 2mM L-Glutamine. We let them adhere over night before we started the treatment with 7µg/ml of C75 or 40µM LY294002 or the DMSO solvent control (0,0389% for C75 and 0,1% for LY294002). We exposed

the cells to the agents for indicated times at 37°C protected from light. Exactly 20minutes before homogenization we stimulated the cells with 100ng/ml epidermal growth factor (EGF) (Sigma, E9644). Then we checked the cell monolayer under the light microscope and noted confluence, morphology and apoptosis of the cells.

2.2.2 RNA Isolation

Homogenization

For following procedures we used autoclaved material and wore sterile gloves in order to avoid degradation of RNA by RNAses which are very stable. Furthermore, we worked in laminar air flow hood because of the toxicity of some used reagents. We poured off the media and carefully removed any residual amounts of media with a blue Gilson pipet tip. Afterwards, 3ml cold TRI Reagent (Molec. Res. Ctr., TR118) per T25 or T75 were added to the cells. The culture flask was stored horizontally for at least 5min at room temperature before the cell lysate was passed through a pipette for several times. The homogenate was then distributed into two 2ml Eppendorf tubes (Eppendorf, 0030.120.094).

RNA-Extraction

For RNA extraction of the homogenised cells cold 0.15ml BCP (1-bromo-3-chloropropane) (Molec. Res. Ctr., BP151) per sample containing 1.5ml TRI Reagent was added. Then each sample was vortexed for 15seconds and stored for 15min at room temperature before the probes were centrifuged at 12.500rpm for 15min at 4°C.

RNA-Precipitation

After centrifugation the sample was separated into two phases. The lower red organic phase and the white interphase contained DNA and proteins, whereas the upper colourless aqueous phase contained RNA. We carefully removed the

upper phase with a blue pipette tip avoiding the white interphase and transferred this volume to new 1,5ml Eppendorf tubes (0030120.086). 2ml Eppendorf tubes containing the interphase and lower phase were stored at -80°C for subsequent isolation of DNA for bisulfite conversion and following methylation specific PCR. For precipitation of RNA 1ml isopropanol (Sigma) was added to each sample, vortexed for 15seconds and stored on ice for further 30minutes. Then the probes were centrifuged at 12500rpm for 15minutes at 4°C to pellet the precipitated RNA of cells.

RNA-Wash

To gain pure RNA we carefully aspirated the supernatant with a self-drawn Pasteur pipette connected to a water-jet vacuum pump and added 1.5ml 75% EtOH per sample (Merck). After vortexing the pellet became visible and depending on the size of the pellet we could later adjust solubilization volume.

RNA-Solubilization

We carefully aspirated the EtOH supernatant with a self-drawn Pasteur pipette connected to a water-jet vacuum pump and air-dried the RNA pellets at room temperature until the white pellets became translucent. According to the pellet size RNA was dissolved in sterile Aqua bidest by passing the solution several times through a yellow pipette tip. As we obtained 2 Eppendorf tubes per experimental sample we pooled the adequate samples and stored them on ice for further analysis or for long term storage at -80°C.

2.2.3 RNA-Measurement

Qualitative RNA control

We checked the quality of the isolated RNA by 1% agarose-gel electrophoresis (‘check gel’). Therefore, we used a small electrophoresis unit with 15-slot comb and prepared 250ml running buffer containing 1xTAE (Sigma, T9650). For 1%

agarose gel we added 0,3g Saekem Agarose (Sigma) to 30ml 1xTAE, boiled the solution in a microwave until it became translucent, added 3µl 10 000 x GelRed nucleic acid gel staining solution (Biotium, BIB 41003) and poured the agarose gel containing 1xGelRed into the electrophoresis chamber. We then removed comb and restraining bars from the chamber after gel had polymerized after 30minutes. 250ml of previously prepared 1xTAE running buffer was spilled into the electrophoresis chamber unit. Before RNA samples were loaded into the slots, each 0,5µl RNA sample was supplemented with 12µl Aqua Bidest and 3µl of 5xgel loading buffer (Sigma, G2526).

The gel ran at constantly 70V for 40min. The isolated RNA could be detected by intercalated GelRed which was seen as bands at a different size. The gel was photographed with the Herolab Easy Gel Documentation System using adequate settings. When RNA quality was high there could be seen two predominant bands of small 18S rRNA (~2kb) and large 28S rRNA (~5kb). Sometimes additionally bulk mRNA (1 – 2kb), smear mRNA (2 – 7kb) and discrete bands of high molecular weight RNA (7-15kb) could be seen (Figure 11). When RNA was degraded during isolation a smear band containing spliced RNAs of all sizes could be observed instead of two predominand bands.

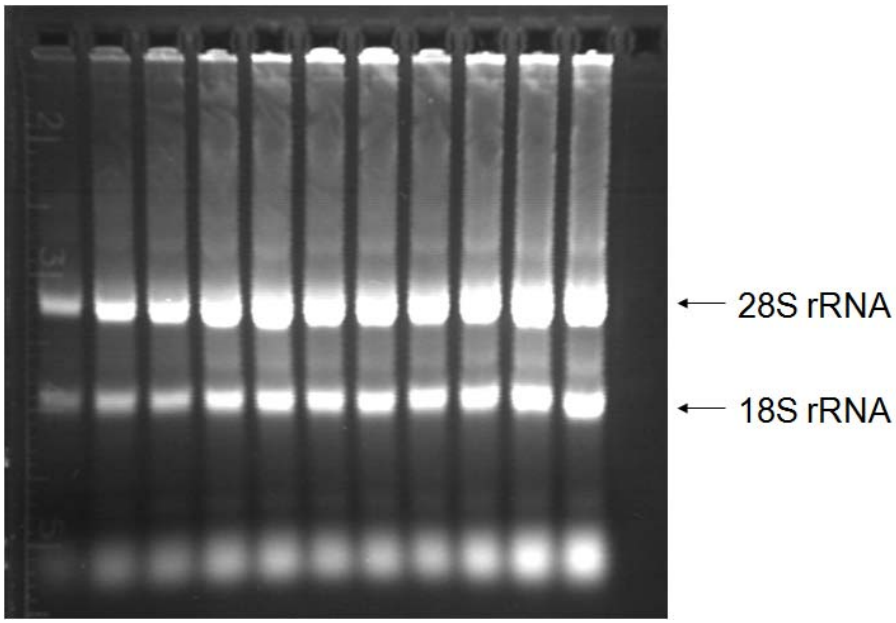

Figure 11: Example for Qualitative Control of Isolated Total RNA by 1% Agarose Gel

Quantitative RNA measurement

For adjusting RNA to a concentration of 0,2µg/µl for further cDNA conversion, we measured RNA quantity by a spectrophotometer (Eppendorf). Therefore RNA samples were placed on ice, mixed softly and diluted 1:250 in Aqua Bidest in adequate cuvettes. The optical densities of the probes were measured against that of Aqua Bidest at 260nm and 280nm wavelength. The quantity of RNA was calculated via multiplication of OD260 value by 40, which gave the amount of RNA in µg/µl. Furthermore we calculated the absorption ratio between OD260/OD280, which predicates the purity of the RNA from extraction reagents and should be between 1,7 and 2,2. If the ratio was less than 1,7, there was protein contamination in the sample, if the ratio was greater than 2,2, RNA degradation had occurred. Finally, the probes were adjusted to 0,2µg/µl RNA per sample with Aqua Bidest.

2.2.4 cDNA Synthesis

For Real Time PCR we used cDNA as a template because Taq Polymerase in PCR was DNA dependent. Therefore, we converted an aliquot of isolated mRNA into cDNA by reverse transcription using random hexamer primers. For reverse transcription of mRNA following mix was prepared in an Eppendorf tube (amounts per sample):

5xBuffer containing 50mM TrisHCL, 75mM KCl, 3mM Mg_2Cl_2 pH8,3 supplemented with Reverse Transcriptase (Invitrogen, 28025-013)	4µl
DTT supplemented with Reverse Transcriptase (Invitrogen, 28025-013)	2µl
nuclease free Bovine Serum Albumin (VWR, 11940.01) dissolved in DEPC water (VWR, 39798.03) to a final concentration of 2,9mg/ml	1µl
Protector RNAse inhibitor 40U/µl (Roche, 03335399001)	0,315µl
dNTP Set 25µM each (Amersham, 27-2035-01)	0,8µl
Random Hexamer Primers 100µM (Amersham, 27-2166-01)	1µl
MLV Reverse Transcriptase 200U/µl (Invitrogen, 28025-013)	1µl
Aqua Bidest	0,185µl

Table 1: Mastermix for cDNA sythesis

10µl (2µg) of adjusted RNA was added to Eppendorf tube containing 10,3µl of Mastermix, well mixed and incubated on a thermoblock at 37°C for 60minutes. Finally, the produced cDNA solution was stored at -80°C.

2.2.5 Real Time RT-Polymerase Chain Reaction (PCR)

Standard PCR is used to amplify a specific region of DNA, in order to produce enough DNA for detection. In general, every PCR is composed of the following 3 steps:

1. Denaturation: the DNA double strands are melted through heat (95°C).
2. Annealing: primers attach to the complementary sequences of the DNA template.
3. Synthesis and Elongation: primers are extended by DNA polymerase and the complimentary strand is synthesized starting at the 3´end of the annealed primers.

Standard PCR only gives qualitative information about a certain gene. That was the reason why we used quantitative Real Time RT-PCR for gene expression analysis.

Real Time RT-PCR using Gene Specific Probes and Primers

All PCRs were set up in laminar air flow hood whereas the UV-light in laminar air flow hood was turned on 20min before starting to avoid contamination. Furthermore, gloves, racks and Aqua Bidest were also exposed to UV-light before use. We performed Real Time RT-PCR using reagents of Applied Biosystems (ABI).

In this system Real Time RT-PCR is based on the concept of 5´nuclease activity of the DNA Polymerase (AmpliTaq DNA Polymerase), which cleaves the probe containing covalently linked reporter dye at its 5´end and a quencher dye at the 3´end oligonucleotide. The basic steps are presented in Figure 12:

1. When the probe is intact, the proximity of the reporter to the quencher results in suppression of the reporter fluorescence, primarily by Förster energy transfer.
2. After denaturation primers and probe hybridize to the complementary sequence of single stranded cDNA only if the gene if interest is present.
3. The probe which consists of an oligonucleotide with a 5´ reporter dye and a 3´quencher dye specifically targets the region between the forward and the reverse primer.

4. The 5´ to 3´ nuclease activity of the DNA polymerase cleaves the probe between reporter and quencher dye.
5. Cleavage of the probe separates the reporter dye from the quencher dye which results in increased fluorescence of the reporter. Probe fragments are displaced from the target and polymerization of the strand continues. Accumulation of PCR products is detected directly by monitoring the increase in fluorescence of the reporter dye.

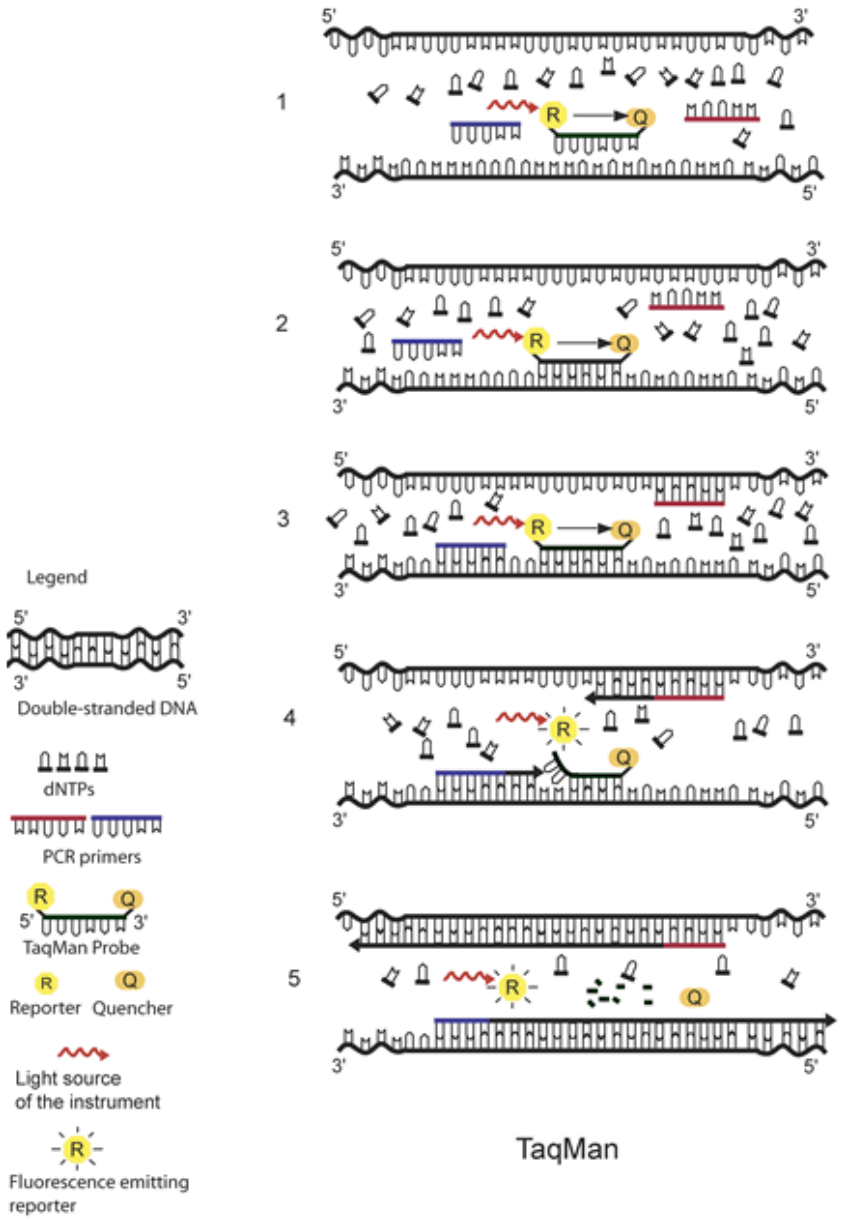

Figure 12: Schemata of Real Time RT-PCR using Gene Expression Assay.
Source: "da Silva A, Pieniazek N, Latest Advances and Trends in PCR-based Diagnostic Methods, Dionisio D (editor), Textbook-Atlas of Intestinal Infections in AIDS. Springer; 2003. p. 397-412"

In our experiments we used TaqMan Universal PCR Mastermix (ABI, 4324018) containing DNA polymerase, dNTPs with dUTP and optimized buffer components with gene specific primers and probes from Applied Biosystems

(TaqMan gene expression assay). The gene specific sequences of primers and probes are under corporate secret but several appropriately designed primers and probes were available. The supplemented thermal stable Taq DNA Polymerase has 5´ to 3´ nuclease activity but it lacks 3´ to 5´ exonuclease activity. We used following TaqMan gene expression assays:

$p15^{INK4b}$, CDKN2b (ABI, TaqMan Gene Expression Assay) hs_00793225_m1
$p16^{INK4a}$ CDKN2a (ABI, TaqMan Gene Expression Assay) hs_99999189_m1
HDAC2 (ABI, TaqMan Gene Expression Assay) hs_00231032_m1
DNMT1 (ABI, TaqMan Gene Expression Assay) hs_00945899_m1
DNMT3a (ABI, TaqMan Gene Expression Assay) hs_00602456_m1
DNMT3b (ABI, TaqMan Gene Expression Assay) hs_00171876_m1
DAP kinase (ABI, TaqMan Gene Expression Assay) hs_00234489_m1
E-Cadherin, CDH1 (ABI, TaqMan Gene Expression Assay)hs_01013959_m1
Aktin beta (ABI, TaqMan Gene Expression Assay) ACT 4352935E
GAPDH (ABI, TaqMan Gene Expression Assay) 00266705_g1

Table 2: TaqMan Gene Expression Assay Probes used for Real Time RT-PCR

All used TaqMan gene expression assay probes were FAM or VIC (Actin beta) labeled. According to the manufacture´s protocol we prepared the Real Time RT-PCR Mix as following (amounts per sample):

TaqMan Universal PCR Mastermix 2x (ABI, 4324018)	12,5µl
TaqMan Gene Expression Assay 20x (ABI, according to gene)	1,25µl
Aqua Bidest	10,25µl

Table 3: PCR Mix for Real Time RT-PCR Containing TaqMan Gene Expression Assay Probes

Finally, 1µl (~100ng) of cDNA was added to 24µl of PCR mix into a 96 well optical reaction plate (ABI, 30103781) and spinned down in a centrifuge before it was put into a thermocycler with sequence detection system (ABI 7000). We prepared triplicates for every sample and solvent controls. Every run was set with probes for the genes of interest, negative controls containing no cDNA, and at least one house keeping gene. Thermal cycling conditions for all used primers and probes were as following:

Activation of DNA Polymerase	95°C	10min	Hold
Denaturation	95°C	15min	40 Cycles
Annealing/Extension	60°C	1min	

Table 4: Cycling Conditions for Real Time RT-PCR using predeveloped TaqMan Gene Expression Assay Probes

Analysis and Calculation of Gene Expression

Analyzing the data from TaqMan Gene expression assays firstly requires to view the amplification plot and to set the baseline and threshold values according to the manufacture´s protocol. The threshold value was set in an area in which a significant increase of signal was first detected. The CT number represent the number of cycles which had to be run until the first adequate fluorescent signal could be detected for this probe. Therefore, the higher the CT number of a sample was, the lower was its gene expression level. GAPDH (p15, p16, HDAC2, DNMT1, DNMT3a, DNMT3b, CDH1, FAS, SOD2 and DAP kinase of C75-treated cells and p15, p16, HDAC2, DNMT1, DNMT3a, DNMT3b, FAS, SOD2, DAP kinase of LY294002-treated cells) or beta actin (CDH1 of LY294002-treated cells) was used as endogenous control. Gene expression was calculated by relating the CT values of control samples, which have been set at 1, to those of C75 or LY294002 treated cells. Means of triplicate determinations, mean standard deviations and Student´s TTESTs were calculated in Excel.

2.3 Methylation Specific Real Time RT-PCR

The most common technique to detect methylated DNA is to convert unmethylated cytosines into uracils whereas methylated cytosines remain unchanged during sodium bisulfite conversion. Therefore, sodium bisulfite is used to convert unmethylated cytosines to uracils, which are recognized as thymine by Taq polymerase, while 5´-methylcytosines remain unaltered. The converted DNA is then amplified by appropriate primers for methylated and unmethylated converted DNA sequences. So the individual steps in methylation specific PCR are as following:

1. DNA isolation of cells
2. Sodium bisulfite conversion of DNA
3. PCR using primers for methylated DNA or unmethylated, converted DNA
4. Detection of PCR products

In our experiments we performed a quantitative Real Time PCR for detection of the bisulfite-converted DNA using SYBR Green dye molecules which intercalate into double stranded DNA.

2.3.1 Treatment of Cells

We plated $5{,}36 \times 10^5$ A2780 cells per tissue culture flask T25 ($25 cm^2$ growth area) or $16{,}08 \times 10^5$ cells per tissue culture flask T75 ($75 cm^2$ growth area). Cells were cultured in RPMI1640 supplemented with 5% FCS, 100U/ml Penicilline, 100µg/ml Streptomycine and 2mM L-Glutamine. We let them adhere over night before we started the treatment with 7µg/ml of C75 or 40µM LY294002 or the DMSO solvent control (0,0389% for C75 and 0,1% for LY294002). We exposed the cells to the agents for indicated times at 37°C protected from light. Exactly 20minutes before homogenization we stimulated the cells with 100ng/ml

epidermal growth factor (EGF) (Sigma, E9644). Then we checked the cell monolayer under the light microscope and noted confluence, morphology and apoptosis of the cells.

2.3.2 DNA Isolation

Homogenization

For following procedures we used autoclaved material and wore sterile gloves in order to avoid degradation of DNA by DNAses which are very stable. Furthermore, we worked in laminar air flow hood because of the toxicity of some used reagents. We poured off the media and carefully removed any residual amounts of media with a blue Gilson pipet tip. Afterwards, 3ml cold TRI Reagent (Molec. Res. Ctr., TR118) per T25 or T75 were added to the cells. The flask was stored horizontally for at least 5min at room temperature before the cell lysate was passed through a pipette for several times. The homogenate was then distributed into two 2ml Eppendorf tubes (Eppendorf, 0030.120.094).

DNA-Extraction

For DNA extraction of the homogenised cells cold 0.15ml BCP (1-bromo-3-chloropropane) (Molec. Res. Ctr., BP151) per sample containing 1.5ml TRI Reagent was added. Then each sample was vortexed for 15seconds and stored for 15min at room temperature before the probes were spun down at 12.500rpm for 15min at 4°C.

DNA-Precipitation

After centrifugation the sample was separated into two phases. The lower red organic phase and the white interphase contained DNA and proteins, whereas the upper colourless aqueous phase contained RNA. We carefully removed the upper phase containing RNA with a blue pipette tip avoiding the white interphase, transferred this volume to new 1,5ml Eppendorf tubes (0030120.086)

and stored them at -80°C for subsequent cDNA sythesis. Any residual aqueous phase was carefully removed which is important for the quality of the isolated DNA. Then 450µl pure ethanol was added to each 2ml Eppendorf tube containing DNA in the interphase and lower phase. Tubes were mixed via inversion and stored for 3 minutes at room temperature. Afterwards, the samples were centrifuged at 2000rpm for 5min at 4°C.

DNA Wash

The phenol-ethanol supernatant was carefully aspirated with a self-drawn Pasteur pipette connected to a water-jet vacuum pump. For the first wash, 1,5ml of 0,1M Soduim Citrate (Natriumcitrat tribasisch Dihydrat, Sigma-Aldrich, S4641-25G) in 10% ethanol was added to the DNA pellet of each sample and inverted for several times during storage for 30 minutes at room temperature. After the first wash the samples were spun down at 2000rpm for 5 minutes at room temperature. Then the supernatant was carefully aspirated with a self-drawn Pasteur pipette connected to a water-jet vacuum pump. For the second wash, again 1,5ml of 0.1M Sodium Citrate in 10% ethanol was added per sample, the tubes were stored for 30 minutes at room temperature, mixed periodically, centrifuged, and finally the supernatant was aspirated. Very large pellets (>200ug) were washed a third time with 0,1M Sodium Citrate in 10% ethanol. After washing the DNA pellet with Sodium Citrate, the pellet was washed with 2ml of 75% ethanol and stored at room temperature for 10 minutes. During this time the tubes were mixed and inverted for several times. Afterwards, the tubes were spun down at 2000rpm for 5 minutes at room temperature and the DNA pellets became visibly white.

DNA Solubilization

For DNA solubilization, we first aspirated the ethanol supernatant with a self-drawn Pasteur pipette connected to a water-jet vacuum pump and air dried the DNA pellet for 3 minutes at room temperature. Then, the DNA pellet was

dissolved in ~20µl TE buffer solution (810mM TrisHCl; 1mM Disodium EDTA; pH8; Sigma, 93283-100ML) by slowly passing the solution through a pipette tip. The high molecular weight DNA increases the viscosity of the DNA solution and made it difficult to pool the two corresponding samples to a final volume of ~40µl.

DNA-Measurement

The quantity of DNA was measured by spectrophotometry (wave length 260/280nm) on an Eppendorf photometer. The DNA samples were diluted and mixed 1:500 in Aqua Bidest and the photometer automatically calculated concentration and purity (260/280 ratio) of the DNA samples related to the Aqua bidest. Finally, the DNA samples were diluted in TE buffer up to a concentration of 20ng/µl and could be stored at -80°C.

2.3.3 Sodium Bisulfide Conversion

The most common technique to detect methylated DNA is to convert unmethylated cytosines into uracils whereas methylated cytosines remain unchanged during sodium bisulfite conversion. In our experiments we used the EZ DNA Methylation-Direct Kit (Zymo Research, D5020) in which DNA denaturation and bisulfite conversion processes were combined into a single step and desulfonation reaction and DNA clean-up was included. For every experiment we included a universal unmethylated human genomic DNA (Chemicon, S7822) as negative control and performed bisulfite conversion following the manufacture´s instructions:

Sodium Bisulfite Conversion

At the beginning, the light sensitive conversion reagent solution was freshly prepared by adding 790µl solubilization buffer and 300µl dilution buffer to the conversion reagent. This freshly prepared conversion reagent solution was mixed for 10 minutes before 160µl of reaction buffer was added and mixed for

one additional minute. Then, 400ng of sample or control DNA was added to 130µl of conversion reagent solution to a final volume of 150µl into an Eppendorf 0,2ml PCR-tube that was mixed and spin down. The PCR tubes (Applied Biosystems, N801-0540) were placed into the thermal iCycler (Biorad) to be converted at following temperatures:

98°C	8min
64°C	210min
4°C	hold

Table 5: Conditions for Sodium Bisulfite Conversion

After conversion of the DNA samples, the samples were load into a column in which 600µl of binding buffer had been added. The columns were placed into a collection tube, inverted and spun down at full speed for 30 seconds. The flow through was discarded while the column containing the stacked DNA was washed with 100µl wash buffer that was prepared by adding 24ml pure ethanol to 6ml wash buffer concentrate. The column was centrifuged again at high speed for 30 seconds.

Desulfonation

After washing, the converted DNA was desulfonated by adding 200µl desulfonation buffer to each column, incubation for 20minutes at room temperature and centrifugation at high speed for 30 seconds. Then, each column containing DNA was washed twice with 200µl wash buffer and spun down at high speed for 30 seconds.

Elution

For elution of the DNA, the columns were placed into fresh 1,5ml Eppendorf tubes, eluted by 12µl elution buffer and centrifuged at high speed for 30 seconds.

It was very important to proceeding immediate with further PCR to make the modified DNA stable for long term storage.

2.3.4 Nested PCR – 1st Step

The methylation status of the promoter region for $p15^{INK4b}$ tumor suppressor gene was determined by the method of MSP further modified as a nested two-step approach in order to increase the sensitivity. For determining the methylation status of DAP kinase promoter region, MSP was performed without first step PCR amplification. The first step of nested PCR for $p15^{INK4b}$ was carried out with primer sets (forward and reverse) which were flanking the CpG-rich promoter regions of the $p15^{INK4b}$ gene. These extern primers ("p15-e") did not discriminate between methylated and unmethylated nucleotides following sodium bisulfide conversion.

P15-e-fw: 5´-GAYGTYGGTTTTTTGGTTTAGTTGA-3´ (VBC Genomics, HPLC-purified)
P15-e-rev: 5´-AACRCAACCRAACTCAAAACC-3´ (VBC Genomics, HPLC-purified)

Table 6: Nucleotide Sequences of Extern Primers of $p15^{INK4b}$

The first step PCR for $p15^{INK4b}$ was performed using 3µl (~100ng) of sodium bisulfite converted DNA and PCR Core Kit (Roche, 11578553001) containing 10x buffer (100mM TrisHCl, 500mM KCl, pH8,3) , MgCl (25mM), dNTPs (10mM each), and Taq DNA Polymerase (250U; 5U/µl). The first step PCR Master Mix was prepared according to the manufacture´s protocol:

Components	Stock Conc.	Final Conc.	Volume (for 1 rxn)
A.bid.	-	-	31,5µl
DNTP-Mix	10mM	200µM	1µl
10x PCR Buffer	10x (100mMTrisHCl, 500mM KCl; pH8,3)	1x (10mM TrisHCl, 50mM KCl)	5µl
Primer Mix	25µM p15-e-fw 25µM p15-e-rev	500nM fw 500nM rev	1µl
MgCl	25mM	4mM	8µl
TaqDNAPolymerase	5U/ul	2,5U	0,5µl
DNA (Bisulfite converted)	~33ng/ul	~100ng	3µl
		Total Volume	50µl

Table 7: Components for First Step PCR of p15-e

The components of the PCR mix were added in the following order:

Master Mix1 (amounts per sample):

11,75µl	Aqua Bidest
1µl	dNTPs
1µl	Primermix (fw+rev)

We put 13,75µl Master Mix1 into each 0,2ml Eppendorf PCR reaction tube before we added 3µl (~120ng) converted DNA or A. bid.

Master Mix2 (amounts per sample):

19,75µl	Aqua Bidest
5µl	10x PCR Buffer
8µl	MgCl
0,5µl	DNA-Polymerase

Accordingly, we put 33,25µl Master Mix2 into each 0,2ml Eppendorf PCR reaction tube, resuspended the components with components of Master Mix1 via resuspension and placed the tubes into the icycler (Biorad). We performed the first step PCR according to the following cycle profile:

HotStarTaq Activation	95°C	10min	
Denaturation	95°C	30sec	40 Cycles
Annealing	56°C	30sec	
Elongation	72°C	30sec	
Final Elongation	72°C	8min	
Holding	4°C	Hold	

Table 8: Cyling Conditions for First Step PCR in MSP for Amplification of p15 external gene region

2% Agarose Gel

The PCR-product of the p15 external region was 139bp in size. To detect the amplified DNA products we performed an agarose gel electrophoresis.

Therefore, we used electrophoresis unit with 10-slot comb and prepared 750ml running buffer containing 1xTAE (Sigma, T9650). For 2% agarose gel we added 2g Saekem Agarose (Sigma) to 100ml 1xTAE, boiled the solution in the microwave until it became translucent, added 10µl of 10 000xGelRed nucleic acid gel staining solution (Biotium, BIB 41003) and poured the agarose gel containing 1xGelRed into the electrophoresis chamber. After 40min gel had polymerized and we then removed comb and restraining bars from the chamber.

750ml of previously prepared 1xTAE running buffer was spilled into the electrophoresis chamber unit. Before DNA samples were loaded into the slots, each 25µl DNA sample was supplemented with 5µl of 5xgel loading buffer (Sigma, G2526). Furthermore, 1µl (1µg) 100bp-DNA –ladder (Promega, G176A) supplemented with 24µ Aqua Bidest and 5µl 5 x gel loading buffer was loaded into the first slot as size control. The gel ran at constantly 70V for 40min. The PCR products could be detected by intercalated GelRed which was seen as a band at 139bp. The gel was photographed with the Herolab Easy Gel Documentation System using adequate settings. PCR products of first step PCR were diluted 1:50 with Aqua Bidest and subjected to the second step of MSP.

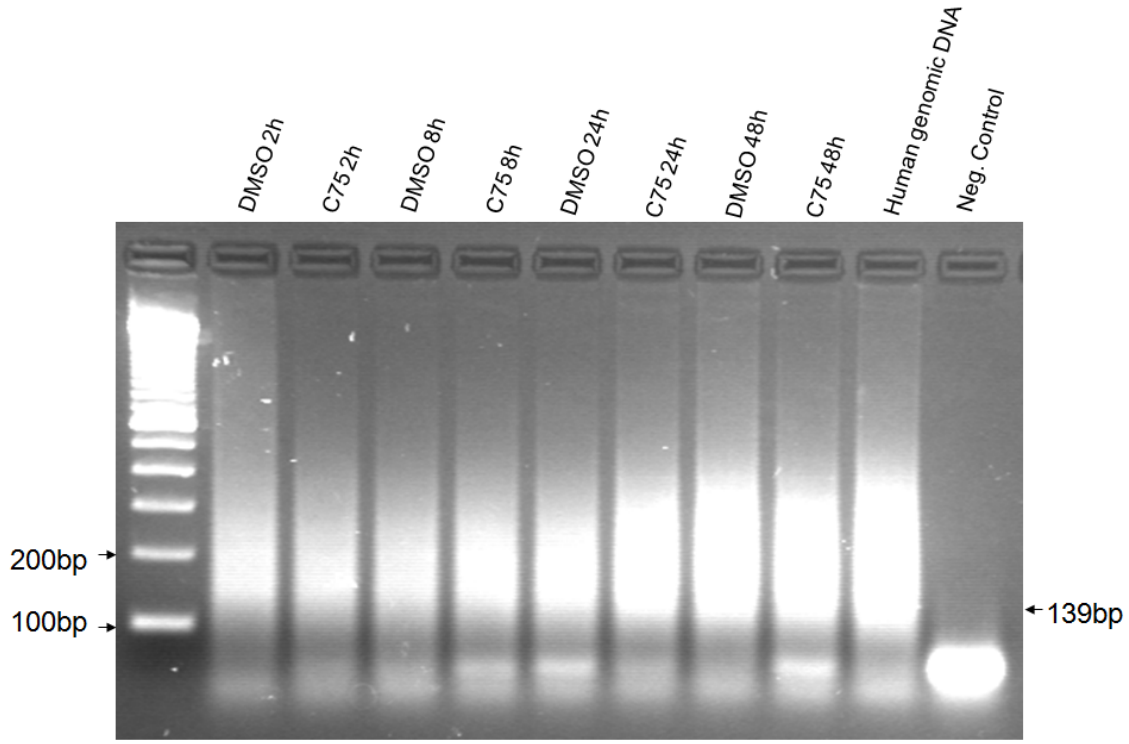

Figure 13: Example of First Step PCR Product of p15^{INK4b} Extern Primers

2.3.5 Real Time PCR using SYBR Green – 2nd step of nested PCR

Another method to perform quantitative Real Time PCR without predisigned TaqMan probes and primers is to use SYBR Green detection system. SYBR Green intercalates into the DNA double helix (Zipper et al., 2004). In solution,

unbound SYBR Green exhibits very little fluorescence which is greatly enhanced upon DNA-binding. Thus, during PCR cycles, the increase in SYBR Green fluorescence at 530nm wavelength is directly proportional to the amount of generated double-strand-DNA. The basic steps are presented in Figure 14:

1. The reaction mix contains optimized buffer, DNA, nucleotides, SYBR Green dye, and the primers complementary to the gene of interest. The unbound dye molecules weakly fluoresce and produce a minimal background fluorescence signal which is subtracted during computer analysis.
2. At 95°C the double-stranded DNA denaturize into two single-stranded DNA strands
3. When annealing temperature is achieved primers hybridize to the complementary sequences of the single stranded DNA only if the gene of interest is present. After annealing of the primers, a few SYBR Green molecules can intercalate to the double-stranded DNA.
4. Emission of fluorescence is increased during elongation.
5. More and more SYBR Green dye molecules can bind to the newly synthesized DNA. The fluorescence is increasing continuously. The measurement of the fluorescence is performed at the end of the elongation step of every PCR cycle to monitor the increasing amount of amplified DNA.
6. During the following denaturation step of the next PCR cycle the SYBR Green molecules are released and the fluorescence signal of the dye falls.

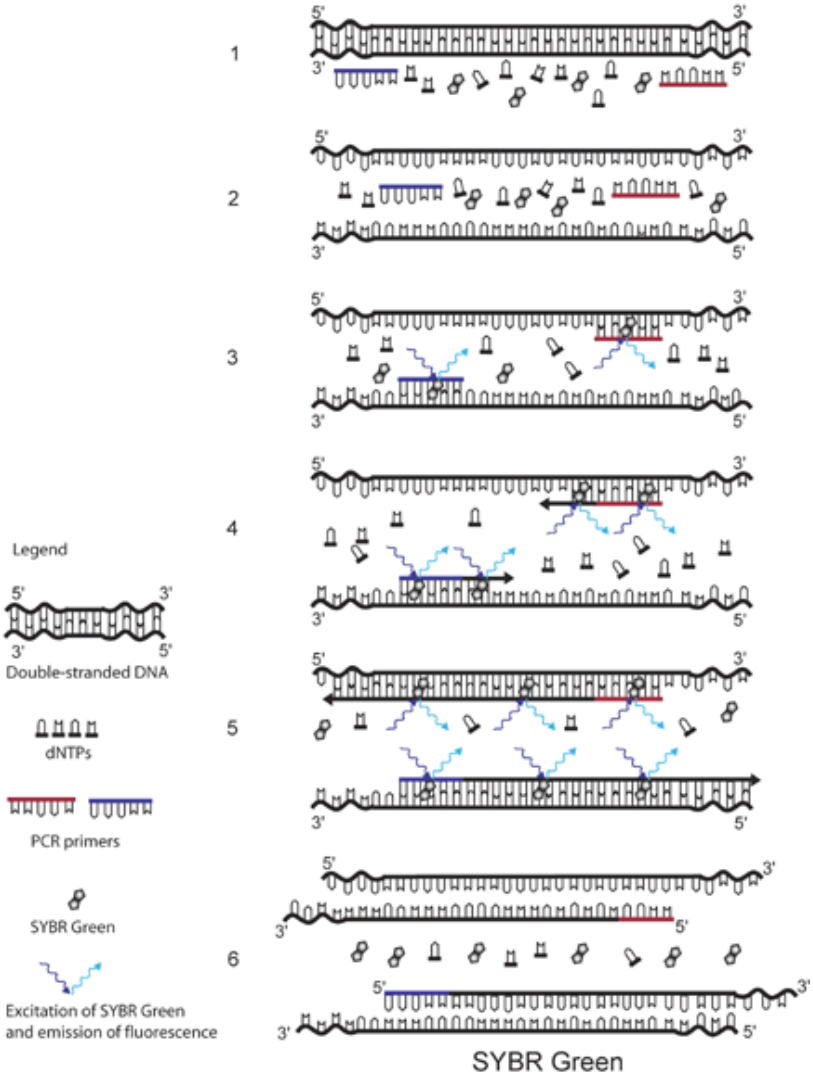

Figure 14: Basic Steps of Quantitative Real Time PCR Based on SYBR Green Intercalation

For quantitative methylation specific PCR we used primers which were synthesized by GenExpress and reagents from FastStart SYBR Green Master (Roche, 04673484001). The FastStart SYBR Green Master contained the FastStart Taq DNA Polymerase for hot start PCR which improved specificity and sensitivity of the PCR by minimizing the formation of non-specific products (Birch et al., 1996), dNTPs and an optimized buffer system.

The MSP contained primer sets for internal p15 unmethylated (p15-IU) or p15 internal methylated (p15-IM) and DAP kinase internal unmethylated (DAPK-IU) or DAP kinase internal methylated (DAPK-IM) sequences that were designed to recognize bisulfite-induced modifications of unmethylated cytosines. Adequate sequences were taken from House et al., 2003 and Collins et al., 2006:

Name/Symbol	Sequence	Product Size
DAPK-IM fw	5´-GGATAGTCGGATCGAGTTAACGTC-3´	98bp
DAPK-IM rev	5´-CCCTCCCAAACGCCGA-3´	
DAPK-IU fw	5´-GGAGGATAGTTGGATTGAGTTAATGTT-3´	106bp
DAPK-IU rev	5´-CAAATCCCTCCCAAACACCAA-3´	
P15-IM fw	5´-GGTTTTTTATTTTGTTAGAGCGAGGC-3´	68bp
P15-IM rev	5´-TAACCGCAAAATACGAACGCG-3´	
P15-IU fw	5´-GGTTGGTTTTTTATTTTGTTAGAGTGAGGT-3´	80bp
P15-IU rev	5´-AACCACTCTAACCACAAAATACAAACACA-3´	

Table 9: Primer Sequences for SYBR Green Real Time RT-PCR

We prepared the PCR Mix for Real Time PCR containing SYBR Green as following:

Components	Stock Conc.	Final Conc.	Volume (for 1 rxn)
SYBR Green Master	2x	1x	12,5µl
PrimerMix (for U **or** M)	10µM rev 10µM fw	300nM rev 300nM fw	0,75µl
Diluted DNA (1:50 from 1st step PCR for p15 or 1:20 from Bisulfite Conversion for DAP kinase)		~100ng (p15) ~10ng (DAPK)	11,75µl

		Total Volume	25µl

Table 10: Components for SYBR Green Real Time PCR Mix

Finally, 11,75µl (~100ng for p15 or ~10ng for DAP kinase) of DNA template was added to 13,75µl of PCR mix into Eppendorf PCR reaction tubes and put into a thermocycler with sequence detection system (Corbett RotorGene Real Time Thermoanalyzer). We prepared triplicates for every sample and for controls. Every run was performed with primer sets complementary to methylated and conversed sequences of p15 or DAP kinase, negative controls containing no template to detect potential primer duplexes, and unmethylated human genomic DNA control. Thermal cycling conditions for all used primers and probes were as following:

Activation of Hot StartTaq DNA Polymerase	95°C	10min	Hold
Denaturation	95°C	30sec	50 Cycles
Annealing	58°C	30sec	
Elongation	72°C	30sec	
Final Elongation	72°C	5min	Hold

Table 11: Cyling Conditions for SYBR Green Real Time PCR Amplification of $p15^{INK4b}$ methylated, $p15^{INK4b}$ unmethylated

Activation of Hot StartTaq DNA Polymerase	95°C	10min	Hold
Denaturation	95°C	30sec	50 Cycles
Annealing	60°C	60sec	
Elongation	72°C	60sec	
Final Elongation	72°C	5min	Hold

Table 12: Cyling Conditions for SYBR Green Real Time PCR Amplification of DAP kinase methylated, and DAP kinase unmethylated

Analysis and Calculation of Gene Expression

After the fiftieth cycle, a melting curve analyses was added to exclude detections of unspecific products. Sometimes the forward and the reverse primer built duplexes which were also detected by intercalation of SYBR Green leading to false positive values. During melting curve analysis, the thermo cycler accomplished a dissociation protocol that went through increasing temperatures and showed the melting temperature of the products. Normally, primer duplexes had a lower dissociation temperature as PCR products. Thus, identified samples containing unspecific primer duplexes were excluded from calculations.

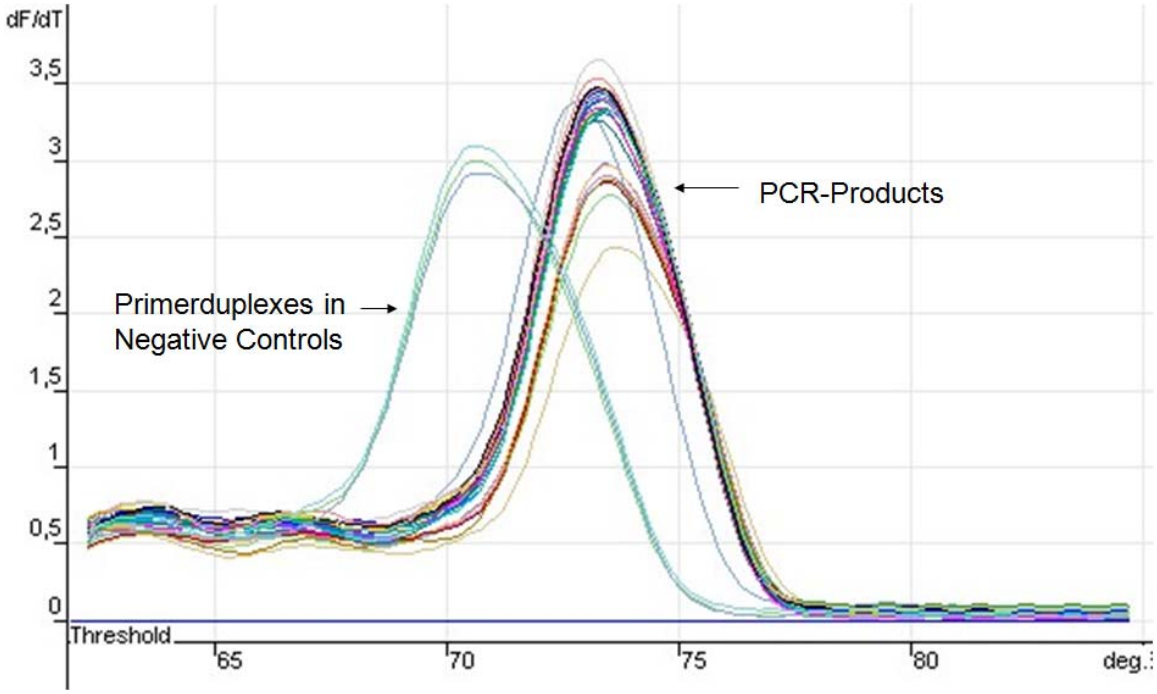

Figure 15: Example of a Melting Curve after SYBR Green Real Time PCR Amplification

Analyzing the data from SYBR Green Real Time PCR firstly requires to view the amplification plot and to set the baseline and threshold values according to the manufacture´s protocol. The threshold value was set in an area in which a significant increase of signal was first detected.

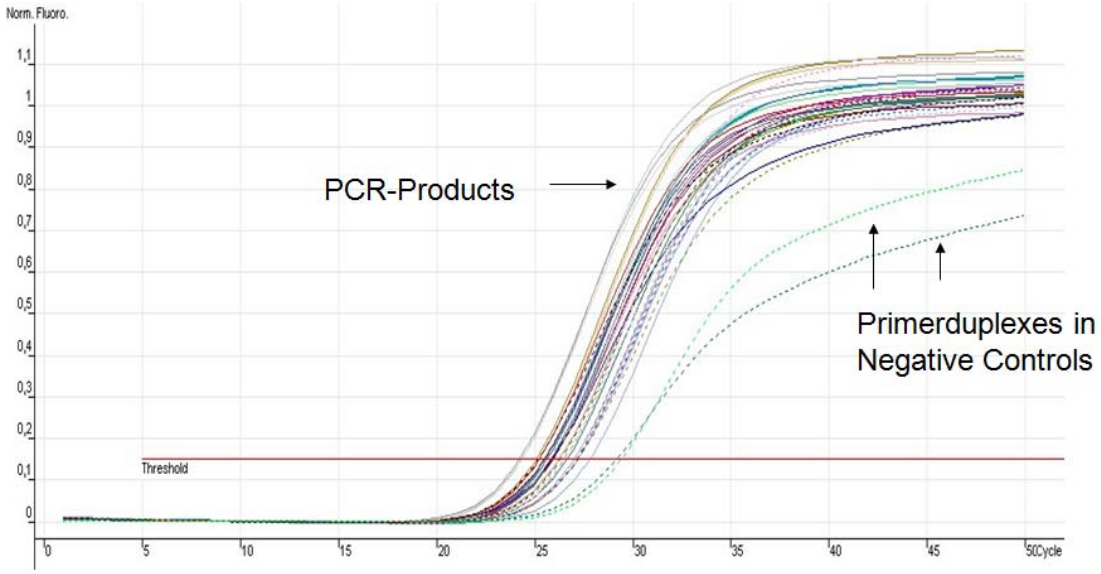

Figure 16: Example of CT-Detection Curve Performing SYBR Green Real Time PCR Amplification

Methylated gene expression was related to unmethylated gene expression. Methylation status of a gene was calculated by relating the CT values of control samples, which have been set at 1, to those of C75 or LY294002 treated cells. Unmethylated human genomic DNA was related to the solvent controls that have been set to 1. Means of triplicate determinations, mean standard deviations and Student´s TTESTs were calculated in Excel.

2.4 Western blotting – Protein Analysis

2.4.1 Treatment of the Cells

We plated $6x10^5$ A2780 cells per 60mm cell culture dish (Corning, NY, 430166). Cells were cultured in RPMI1640 supplemented with 5% FCS, 100U/ml Penicilline, 100µg/ml Streptomycine and 2mM L-Glutamine. We let them adhere over night before we started the treatment with 7µg/ml of C75, 40µM LY294002, 15µg/ml Cycloheximide, the combination of 7µg/ml C75 with 15µg/ml

Cycloheximide (CHX), or the DMSO solvent control (0,0389% for C75 and 0,1% for LY294002 and 0,0539% for CHX+C75). We exposed the cells to the agents for indicated times at 37°C protected from light. Exactly 20minutes before homogenization we stimulated the cells with 100ng/ml epidermal growth factor (EGF) (Sigma, E9644). Then we checked the cell monolayer under the light microscope and noted confluence, morphology and apoptosis of the cells.

2.4.2 RIPA Lysis

Before lysis, media was removed and the monolayer was washed twice with cold PBS Dulbecco´s (Gibco, 14190-094). The remaining PBS was carefully removed with a yellow pipet tip. Cells were lysed in 80µl of freshly prepared RIPA+ lysis buffer (as described in Table 13 and Table 14) which was added per 60mm dish (1 confluent 60mm dish gives ~150 µg protein).

Reagent	MW	Stock Concentration	Volume	Final Concentration
NaCl	58.44	5M	3ml	150mM
Tris pH 7.4	121.14	1M	5ml	50mM
DOC (Na-deoxycholate)	414.6	10%	5ml	0.5%
EGTA	380.4	50mM	4ml	2mM
EDTA, pH 7.4	372.2	50mM	10ml	5mM
NaF	41.99	500mM	6ml	30mM
ß-Glycerophosph.pH7.2	216	400mM	10ml	40mM
Tetrasodium pyrophosph.	446.06	100mM	10ml	10mM
Benzamidine	156.6	30mM	10ml	3mM
Nonidet P-40		pure	1ml	1%

Table 13: Ingredients for RIPA Lysis Buffer

The buffer was adjusted to pH 7,4, filled up with Aqua dest to 95ml and stored at 4°C. RIPA+ was freshly prepared before use.

Reagent	Volume
RIPA	1,90ml
200mM Na-Orthovanadate	20µl
25 x Complete stock solution (Protease Inhibitor Cocktail)	80µl

Table 14: RIPA+ Lysis Buffer

After adding 80 µl RIPA+, cells were left on ice for 5min and detached with a sterile scrapper. Then the lysates were transferred to an Eppendorf tube, vortexed for several times while incubating on ice and centrifuged for 30min at 12.500rpm at 4°C. The pellet was discarded and the supernatant was saved at -20°C for the protein assay.

2.4.3 Protein Quantification

We determined the protein concentration of each sample by BioRad Protein Assay Kit II (BioRad, 500-0112). This assay was performed in 96 well plates. First, a 10mg/ml BSA protein standard was produced by dissolving 10mg bovine serum albumine in 1ml Aqua dest. This protein standard was serially diluted 1:2 with RIPA+ to obtain 5, 2.5, 1.25, 0.625, 0.3125, 0.15625 µg/µl protein standards. All protein standards were set up in a 96 well plate. RIPA+ was used as a blank control. We added triplicates of 5µl per well RIPA+, 5µl per well increasing protein standard concentrations or 5µl per well of protein sample into the plate. Reagent A' of the Protein Assay Kit II was freshly prepared by adding 1ml Reagent A (BioRad, 5000113) to 20µl Reagent S (BioRad, 5000115). Afterwards, 20µl Reagent A' per well and 200µl Reagent B (BioRad, 5000114) per well were added to the probes and standards. After an incubation time of

20min the absorbtion was measured at 655/450 nm in the microplate reader (spectrophotometer Bio-Rad). The standard curve and protein concentrations were calculated using Excel. The protein samples were diluted to a concentration of 1,33 µg/µl with RIPA+ (3 parts) before 1 part of 4x sample buffer (Table 15) was added. The samples were adjusted to a final concentration of 1µg/µl in 1x sample buffer and stored at -20°C.

Reagent	MW	Stock	Volume	Final concentration
Glycerol	92.09	pure	5 ml	50%
Tris-HCl, pH 6.8	121.14	1M	1.25 ml	125mM
SDS		20%	2,00 ml	4%
Bromophenol blue		1%	1,25 ml	0,125%
Beta-mercaptoethanol (added just before use)		pure	0.5ml	5%

Table 15: Ingredients for 4 x Sample Buffer

2.4.4 SDS- Polyacryl Amide Gel Electrophoresis (PAGE)

In our experiments we analyzed proteins which were very different in size. The biggest protein was mTOR with 289kDa and the smallest protein was p15 with 15kDa. Therefore we used gradient gels (Laborpartner, ID531s) to be able to detect a greater range of proteins on one gel. Nevertheless, we also poured 7,5% SDS gels to detect proteins which were 40kDa to 90kDa in size. Thus, glass plates (Biorad, 1653308), spacers and gasket (Biorad, 1652904) were cleaned and assembled according to Bio-Rad instructions. Then, the 7,5% polyacryl amide separating gel was prepared (Table 16, Table 17 and Table 18).

Reagent	Volume
40% Acrylamid (BioRad, 1610140)	11,1 ml
2% Bis Solution (BioRad, 1610142)	3 ml
Aqua bidest.	0,9 ml
Total volume of 30 % A/B	15 ml

Table 16: Preparation of 30% Acrylamide/Bis Solution

Reagent	Volume
30% A/B (Table 16)	5 ml
Aqua dest.	9,7 ml
1,5M Tris 8,8 (BioRad, 1610798)	5 ml
10% SDS (BioRad, 1610418)	200µl
10% APS (BioRad, 1610700)	100µl
Temed pur (BioRad, 1610800)	10µl

Table 17: Separating Gel. Preparation of 7,5% Polyacryl amide gel

The glass plates were filled with ~5ml separating gel (Table 17) and carefully overlayed with some Aqua bidest to remove any air bubbles. After 40 minutes the polyacryl amide was polymerized, Aqua bidest. was poured off and the comb was inserted. Then, the 4% polyacryl amide stacking gel solution was prepared (Table 18) and added to the very top of the separating gel. After ~30minutes the stacking gel was polymerized and combs were removed.

Reagent	Volume
30% A/B (Table 16)	1,673ml
Aqua bidest.	7,47ml

0,5M Tris 6,8 (BoiRad, 1610799)	3,15 ml
10% SDS (BioRad, 1610418)	125µl
10% APS (BioRad, 1610700)	125µl
Temed pur (BioRad, 1610800)	12,5µl

Table 18: Stacking Gel. Preparation of 4% Polyacryl amide gel

The purchased plates including the gels or the self poured gels were inserted in the gel holder cassette (BioRad, 1703931) and the electrophoresis apparatus before 1x running buffer containing 25mM Tris, 192mM Glycine, and 0,1% SDS in Aqua bidest was added. First, the inner reservoir was filled with running buffer and checked for leak tightness before the outer reservoir was also filled with 1 x running buffer. Protein samples were boiled for 10 min at 95°C for denaturation. Then 20µg protein per sample was loaded into each slot. 1,5 µl of the molecular weight marker (Magic Mark XP from Invitrogen, LC5602) was loaded into the first lane of each gel without being boiled. The gel was run constantly at 100 Volt for ~2 hours. After electrophoresis, the gel was subjected to Western blotting.

2.4.5 Electrotransfer

The separated proteins were transferred from the polyacryl amid gel onto a polyvinylidenedifluoride (PVDF) membrane (NEF, 153196). The precooled transfer buffer containing 150mM Glycine, 50mM Tris pH8,3, 0,05% sodium dodecylsulfate (SDS), and 20% Methanol was pured into the transfer chamber and a stirring rod was put inside to prevent heating during transfer. The membrane which was marked with a pen was shortly soaked in pure methanol before the blotting sandwich was assembled as shown in Figure 17. Scotch brites and filter papers were also soaked in transfer buffer. Air bubbles were removed by rolling a pipet fragment over the blotting sandwich. The electrotransfer was performed at constant 290mA overnight at 4°C in a cold room.

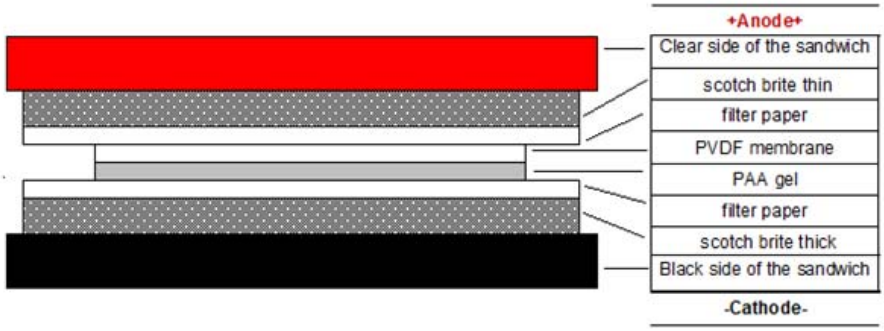

Figure 17: Assembly of Transfer Apparatus

2.4.6 Immunostaining of the Blot Membranes

The principle steps in immunostaining of western blots:

1. Blocking of unspecific binding sides on the membrane
2. Specific binding of the first antibody to the protein of interest.
3. Binding of the horseradish peroxidise (HRP) conjugated secondary antibody to the first antibody
4. Detection of proteins via HRP with enhanced chemiluminescense (Figure 18).

Between the individual steps many washing steps are performed.

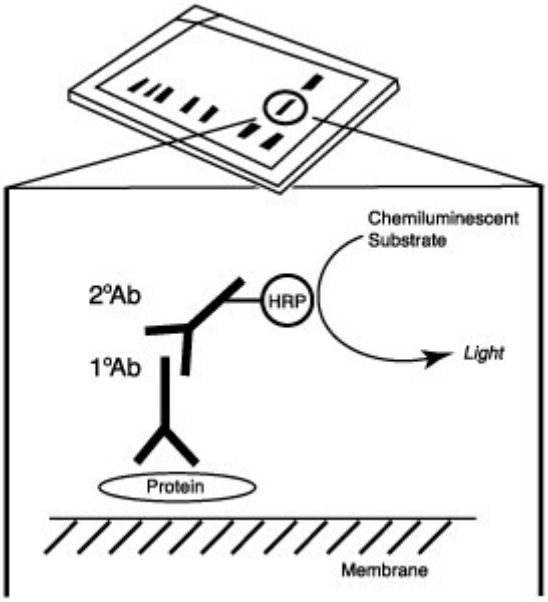

Figure 18: Detection of Proteins by Chemoluminescence

After disassembly of the transfer sandwich, the membrane was cut into the size of the gel by a razer blade. The first step in immunostaining was to block unspecific binding sides of the membrane. Therefore we prepared a blocking solution. The blocking solution contained 4% bovine serum albumin (BSA)(Fluka, 05480) in 1 x Tris Buffer Saline (BioRad, 1706435, containing 0,1M Tris pH7,5, 0,5M NaCl, Aqua dest) (TBS) supplemented with 0,1% Tween20 (BioRad, 1706531) (TBS-T) and 4% heat inactivated fetal calf serum (Gibco, 10270-106). The membrane was incubated in 10ml blocking solution for 1hour at room temperature while shaking.

During three washing steps in TBS-T each for 5minutes on the shaker at room temperature the first antibody solution was prepared. The first antibody solution consisted of 1 x TBS-T with 1% BSA and 0,05% Sodiumazide to make the antibody solution stable for longer storage. The specific first antibody binding the protein of interest was diluted 1:1000 (Table 19) with the first antibody solution and was incubated to the membrane at room temperature for 2 hours or over night at 4°C. After incubation, the membrane was washed twice for 5 minutes

and twice for 10 minutes in 1 x TBS-T on the shaker at room temperature to remove unspecific bindings of the first antibody. Then, the secondary antibody solution was prepared. The secondary antibody solution contained of 1 x TBS-T with 1% BSA in which an HRP conjugated antibody (Table 20) was diluted 1:15000. This solution was freshly prepared before use and was incubated to the membrane for 1 hour at room temperature on the shaker. Afterwards, the membrane was washed twice for 5 minutes and twice for 10 minutes in 1 x TBS at room temperature on the shaker. For detection by enhanced chemiluminescence (ECL) the membrane was incubated with a mixture of 2ml Detection solution1 and 2ml Detection solution 2 (Pierce, 32106) which reacted with the horseradish peroxidise (HRP) conjugated to the secondary antibody. The protein of interest was then detected by exposing the membrane to an x-ray film (Hyperfilm ECL high performance chemiluminescence film, Amersham, RPN3103K) in the dark room. Every membrane was incubated at least with beta actin or tubulin as loading control.

1st Antibody	Dilution	Feature	Company	Cat. No	Size of target protein
mTOR	1:1000	rabbit polyclonal IgG	Cell Signaling	2972	289kDa
phospho-mTOR (Ser2448)	1:1000	rabbit polyclonal IgG	Cell Signaling	2971	289kDa
p70 S6 Kinase	1:1000	rabbit polyclonal IgG	Cell Signaling	9202	70, 85kDa
phospho-p70 S6 Kinase (Thr421/Ser424)	1:1000	rabbit polyclonal IgG	Cell Signaling	9204	70, 85kDA

phospho-p70 S6 Kinase (Thr389)	1:1000	rabbit polyclonal IgG	Cell Signaling	9205	70, 85kDa
AKT1/2/3	1:1000	rabbit polyclonal IgG	Cell Signaling	9272	60kDa
phospho-AKT(Ser473)	1:1000	rabbit polyclonal IgG	Cell Signaling	9271	60kDa
P15 INK4B	1:1000	rabbit polyclonal IgG	Cell Signaling	4822	15kDa
4E-BP1	1:1000	rabbit polyclonal IgG	Cell Signaling	9452	15-20kDa
phospho-4E-BP1 (Ser65)	1:1000	rabbit polyclonal IgG	Cell Signaling	9451	15-20kDa
ERK1/2	1:1000	rabbit polyclonal IgG	Cell Signaling	9102	42/44kDa
phospho-ERK1/2 (Thr202/Tyr204)	1:1000	rabbit polyclonal IgG	Cell Signaling	9101	42/44kDa
Ubiquitin (P4D1)	1:1000	mouse monoclonal IgG	Cell Signaling	3936	
Alpha/beta Tubulin	1:1000	rabbit polyclonal IgG	Cell Signaling	2148	55kDa
beta Actin	1:600	goat polyclonal IgG	Santa Cruz Biotechnology	sc-1616	43kDa

Table 19: First Antibodies

2nd Antibody	**Dilution**	**Feature**	**Company**	**Cat. No**
Donkey-anti-rabbit	1:15000	horseradish peroxidase (HRP) linked	Promega	V795A

Donkey-anti goat	1:15000	horseradish peroxidase (HRP) linked	Santa Cruz Biotechnology	sc2020
Chicken-anti-mouse	1:15000	horseradish peroxidase (HRP) linked	Santa Cruz Biotechnology	sc2954

Table 20: Secondary Antibodies

2.4.7 Stripping of Membranes

After detection of a protein of interest it is possible to detach all antibodies from the protein and to incubate the blot with another antibody. Therefore we prepared a 1 x stripping solution containing 62,5mM Tris pH6,7 and 2%SDS and added 200µl ß-mercaptoethanol to 20ml of stripping solution. The blot was stripped for 20min at 50°C in a water-bath with frequent shaking. After stripping the membrane, the blot was washed 5 times for 5 minutes in TBS-T at room temperature on the shaker and blocked in blocking solution containing 4% FBS for 1 hour.

2.4.8 Densitometry of the Protein Bands

For quantification of the protein expression levels we performed densitometry using HeroLab software. Protein levels were estimated by relating the band of the specific antibody to that of beta actin. The antibody/actin ratios of treated samples were compared to those of vehicle-treated controls which have been set at 1 and the results were expressed in fold changes.

2.5 mRNA Gene Expression Array

For gene expression profiling we used Affymetrix Human GeneChip Gene 1.0 ST Array System. This array interrogates the most up-to-date content of well-annotated 28.869 genes with 764.885 distinct probes and was performed at Kompetenzzentrum für Fluoreszente Bioanalytik (KFB) in Heidelberg. They offer a complete solution for gene expression analysis that includes whole transcript sense target labeling, control reagents fluidics, scanning instrumentation and analysis. The Human Gene 1.0 ST Array uses a perfect match-only design with probes that hybridize to sense targets. The gene expression level of multiple probes on different exons is summarized into an expression value representing all transcripts from the same gene. Background is estimated using a set of ~17.000 generic background probes and several standard poly-A controls and hybridization controls are represented on the array to allow troubleshooting.
In fact, array analysis became a powerful approach for comparing RNA populations of treated and untreated cell cultures. The main steps performing an expression array involve:

1. Isolation of RNA from the cells to be compared (performed by ourselves)
2. Conversion of RNA to biotin-labeled cDNA by Reverse Transcription
3. Hybridization of each labeled cDNA sample to a separate Chip
4. Removal of unhybridized cDNA
5. Staining of hybridized cDNA with a streptavidin-phycoerythrin conjugate
6. Visualization with an array scanner and comparing the quantitative data from various samples

The typical Affimetrix is a glass slide array that is produced using special methods which allow the nucleotides to be synthesized directly on the Chip substrate. For validation we additionally performed Real Time RT-PCR of several genes of interest.

Correlation analysis was also performed by KFB according to the manufacture´s protocol. To simplify the interpretation of the data, the correlation values were evaluated by Pearson´s Correlation or Spearman Rank Correlation, whereas they summarized the detection of the signal for each probe set to the median probe set signal of one gene. They normalized gene expression and generated relative Log Expression Signals (KFB, Affymetrix, data sheet).

Array Format	169
Feature Size	5µm
Total Number of Distinct Probes	764.885
Oligonucleotide Probe Length	25-mer probes
Required Orientation of Labeled Targets to be Hybridized to the Array	Sense
Gene-level Probe Sets with Ensembl Support	28.132
Gene-level Probe Sets with Putative Full-length Transcript Support (GenBank and RefSeq)	19.734
Estimated number of Genes	28.869
Number of Probes per Gene (Resolution)	~26
Genome Assembly	March 2006 (USC Hg 18; NCBI build36)
RefSeq NM Transcripts	November 3, 2006
GenBank putative full-length transcripts	November 3, 2006
Positive Controls (constitutively expressed genes)	1.195 putative exon-level probe sets from putative constitutive genes

Negative Controls	2.904 putative intron-level probe sets from putative constitutive genes
Hybridization Controls	bioB, bioC, bioD, cre
Background Probes	Antigenomic Set
Poly-A Controls	dap, lys, phe, thr
Recommended Amount of Starting Material	100ng
Acceptable Range of Input Amount	100ng-1µg

Table 21: Specifications of Affymetrix Human GeneChip Gene 1.0 ST Array

Our results only show an excerpt from the Affymetrix Human GeneChip Gene 1.0 ST Array data. The genes were functional classified and revealed extensive changes in metabolism, cell survival, proliferation, transcription and degradation as a consequence of FASN inhibition.

2.5.1 Treatment of Cells

We plated 5,36x10^5 A2780 cells per tissue culture flask T25 (25cm^2 growth area) or 16,08x10^5 cells per tissue culture flask T75 (75cm^2 growth area). Cells were cultured in RPMI1640 supplemented with 5% FCS, 100U/ml Penicilline, 100µg/ml Streptomycine and 2mM L-Glutamine. We let them adhere over night before we started the treatment with 7µg/ml of C75 or 0,0389%DMSO solvent control. Cells were exposed to the agents for 48hours at 37°C protected from light. Exactly 20minutes before homogenization we stimulated the cells with 100ng/ml epidermal growth factor (EGF) (Sigma, E9644). Then we checked the cell monolayer under the light microscope and noted confluence, morphology and apoptosis of the cells. RNA was isolated from the cells (see chapter 2.2.2) and qualitative and quantitative controls were performed as described in chapter 2.2.3. 100ng RNA was sent to KFB for Affymatrix Human GeneChip Gene 1.0 ST Array analysis as described above.

3 Results

3.1 Changes in mRNA levels resulting from FASN-inhibition by C75 or from PI3K-inhibition by LY294002 in A2780 cells

Up to date, a conclusive molecular explanation of the anti-proliferative and death promoting effects of FASN-inhibitors is still missing. In particular, the relationship between the FASN biochemical pathway and the epigenetic regulation of tumor suppressor genes is completely unexplored. First of all, we examined the mRNA expression levels of several tumor suppressor genes, apoptosis-related genes and epigenetically active enzymes in the ovarian cancer cell line A2780, which has been treated with the specific FASN-inhibitor C75 (7µg/ml) or the specific PI3K inhibitor LY294002 (40µM). Several types of tumors, including ovarian cancer, are known to have a hypermethylation phenotype (Esteller et al., 2001; Strathdee et al., 2001). Therefore, we examined the gene expression status of some tumor suppressor genes, which have already been reported to be promoter hypermethylated.

3.1.1 Changes in mRNA expression of tumor suppressor genes resulting from FASN-inhibition by C75 or PI3K-inhibition by LY294002 in A2780 cells

The ovarian cancer cell line A2780 expresses high levels of FASN and its cell growth is sensitive to inhibition of FASN by C75. Growth data by Grunt et al. showed that best inhibition by C75 was achieved when A2780 had been treated with a concentration of 7µg/ml C75 (Grunt et al., 2009).Treatment times of 2,8 (data not shown), 24, 48,72 hours were chosen to capture early and late gene

changes associated with the block of cell cycle progression and the advent of apoptosis occurring in response to inhibition of FASN by C75. Results were examined in three biological experiments. The mRNA expression was normalized to ß-actin or glyceraldehyde-3-phosphate dehydrogenase (GAPDH) and compared to the solvent control of C75 for every time point. Correspondingly, cells were exposed to 40µM LY294002 for the same time periods and mRNA expression was analyzed as described for C75.

3.1.1.1 C75 and LY294002 increase $p15^{INK4b}$ mRNA expression level in A2780 cells

In A2780, C75 significantly enhances mRNA expression level of $p15^{INK4b}$ in three replicates. Inactivation of FASN elevates the transcript level of $p15^{INK4b}$ 5,6-fold after 24 hours of exposure to 7µg/ml C75, 6,8-fold after 48 hours of exposure and 7,9-fold after 72 hours of exposure. This indicates that treatment of A2780 cells with 7µg/ml C75 induces a time-dependent elevation of the gene expression level of this inhibitor of cyclin-dependent kinases that prevents the cell from going through the G1-S phase transition (Figure 19). However, our data suggest that this effect is more pronounced on the mRNA than on the protein level and actually cannot have further implication on the cell cycle as the protein level of p15 is even reduced in C75-treated A2780 (Figure 31, later time points).
Since FASN-inhibition has been reported to block the PI3K/AKT pathway (Grunt et al., 2009) we also used LY294002 in a concentration of 40µM as a PI3K inhibitor in A2780 to compare the changes on several tumor suppressor genes.
LY294002 exerts similar effects on $p15^{INK4b}$ mRNA expression in A2780 as compared to C75. Both compounds augment the gene expression level of this cyclin-dependent kinases inhibitor while C75 seems to be more effective in promoting $p15^{INK4b}$ mRNA expression. C75-treated cells show a maximum of 7,9-fold stimulation in $p15^{INK4b}$ mRNA expression after 72 hours of treatment and LY294002-treated cells reveal a maximal 5.5-fold increase in $p15^{INK4b}$ transcript level after 72 hours of exposure (Figure 19). As already seen in C75-treated

cells, LY294002 incubated cells also show an increase in mRNA expression of $p15^{INK4b}$ but no change in $p15^{INK4b}$ protein level (Figure 32). Therefore both substances do not seem to block the cell cycle in A2780 cells by the cyclin-dependent kinase inhibitor $p15^{INK4b}$ though a significant increase in its mRNA expression is observed (Figure 19).

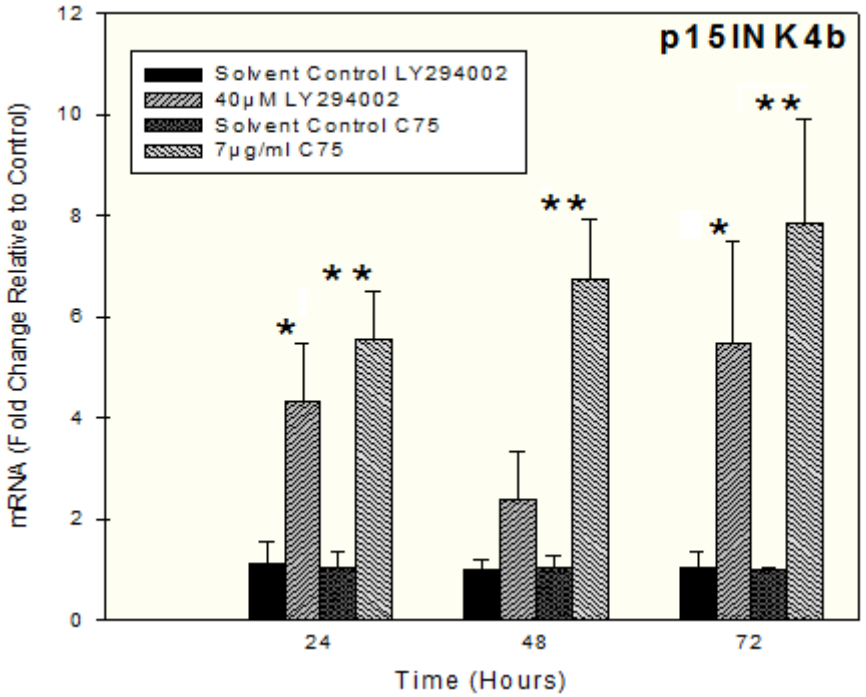

Figure 19: Inhibition of FASN or PI3K increases mRNA expression of cyclin-dependent kinase inhibitor $p15^{INK4b}$.

Quantitative Real Time RT-PCR was done on A2780 cells. Cells were treated with 7µg/ml C75 or 40µM LY294002 for 24, 48, or 72 hours. mRNA expression was determined relative to vehicle-treated controls ("solvent control"). Statistical significance between inhibitor- and vehicle-treated solvent controls was determined by two-tailed Student´s t-test, * indicates significant difference at p<0,05, ** indicates significant difference at p<0,01, and * indicates significant difference at p<0,001.**

3.1.1.2 C75 and LY294002 decrease $p16^{INK4a}$ mRNA expression level in A2780 cells

Neither FASN inhibition by C75 nor blocking of PI3K by LY294002 enhance the mRNA expression level of $p16^{INK4a}$ in A2780 after 24 hours of treatment. Instead, they rather decrease the $p16^{INK4a}$ mRNA level. Strongest down-regulation to 0,4-fold is seen after 72 hours of treatment with LY204002 and a 0,6-fold change appeared after 72 hours of incubation with C75 (Figure 20). This suggests that in A2780 the cyclin dependent kinase inhibitor $p16^{INK4a}$ is not responsible for cell cycle blockade in G1 caused by FASN or PI3K inhibition.

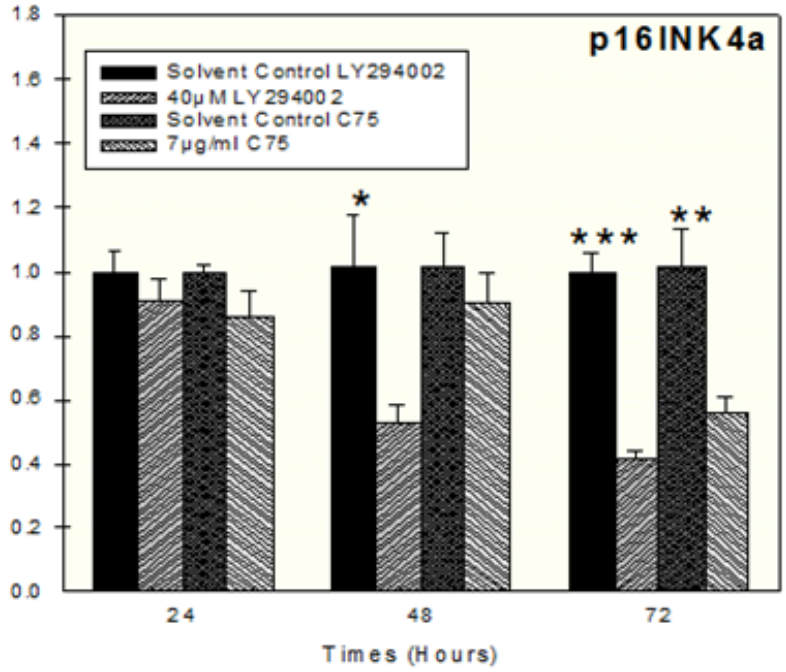

Figure 20: Inhibition of FASN or PI3K decreases mRNA expression of cyclin-dependent kinase inhibitor $p16^{INK4b}$.

Quantitative Real Time RT-PCR was done on A2780 cells. Cells were treated with 7µg/ml C75 or 40µM LY294002 for 24, 48, or 72 hours. mRNA expression was determined relative to vehicle-treated controls ("solvent control"). Statistical significance between inhibitor- and vehicle-treated solvent controls was determined by two-tailed Student´s t-test, * indicates significant difference at p<0,05, ** indicates significant difference at p<0,01, and * indicates significant difference at p<0,001.**

3.1.1.3 C75 and LY294002 increase E-Cadherin mRNA expression level in A2780

After 24 hours of treatment, the E-Cadherin mRNA expression level is not significantly modulated by C75 nor by LY294002. However, at later time points both compounds significantly elevate the CDH1 gene expression level in A2780 cells (Figure 21). LY294002 upregulates E-Cadherin mRNA 7,2-fold after 48 hours of treatment, which increases further to 10,2-fold after 72 hours of incubation (Figure 21).

C75 shows similar, but less pronounced effects. After 48 and 72 hours of treatment the gene expression level of E-Cadherin increases 4,2-fold and 4,4-fold, respectively (Figure 21). These results indicate that both compounds can modulate the adhesion specificity. This effect may be utilized in anticancer strategies by specific molecular targeting of invasion and metastasis processes in ovarian cancer.

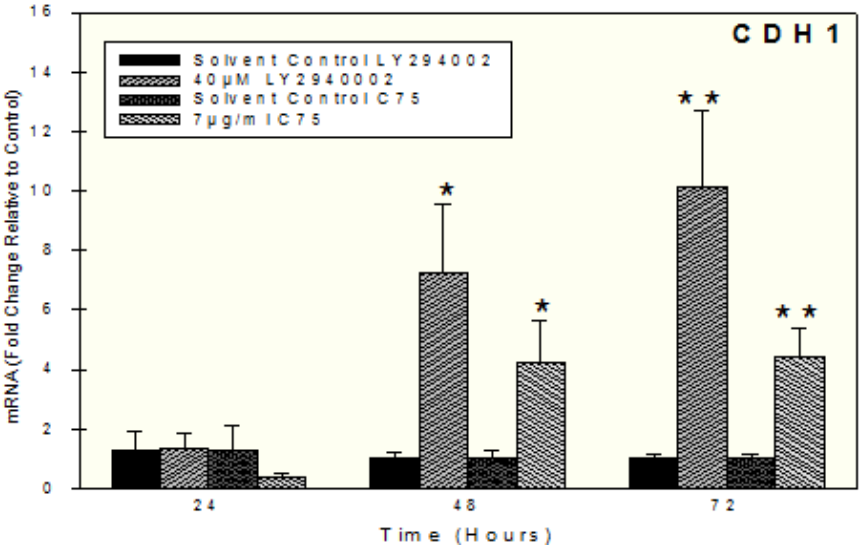

Figure 21: Inhibition of FASN or PI3K increases mRNA expression of the tumor suppressor gene CDH1.

Quantitative Real Time RT-PCR was done on A2780 cells. Cells were treated with 7µg/ml C75 or 40µM LY294002 for 24, 48, or 72 hours. mRNA expression was determined relative to vehicle-treated controls ("solvent control"). Statistical significance between inhibitor- and vehicle-treated solvent controls was determined by two-tailed Student´s t-test, *

indicates significant difference at p<0,05, ** indicates significant difference at p<0,01, and * indicates significant difference at p<0,001.**

3.1.1.4 C75 and LY294002 increase Death Associated Protein Kinase (DAPK, DAP-2) mRNA expression level in A2780 cells

In A2780 the DAPK mRNA expression level is markedly enhanced in a time dependent manner by LY294002 as well as by C75 (Figure 22). Cells incubated with LY294002 for 24 hours show 3,4-fold increase in gene expression level and after 48 hours of treatment with LY294002 the DAP-2 mRNA transcription is stimulated 3,8-fold. The most significant augmentation can be seen after 72 hours of incubation with LY294002 when the gene expression level of DAPK is elevated 6,3-fold. In C75 treated cells the mRNA level of DAPK is increased 2-fold after 24 hours, 5,9-fold after 48 hours and peaks at 6,7-fold after 72 hours of exposure (Figure 22).

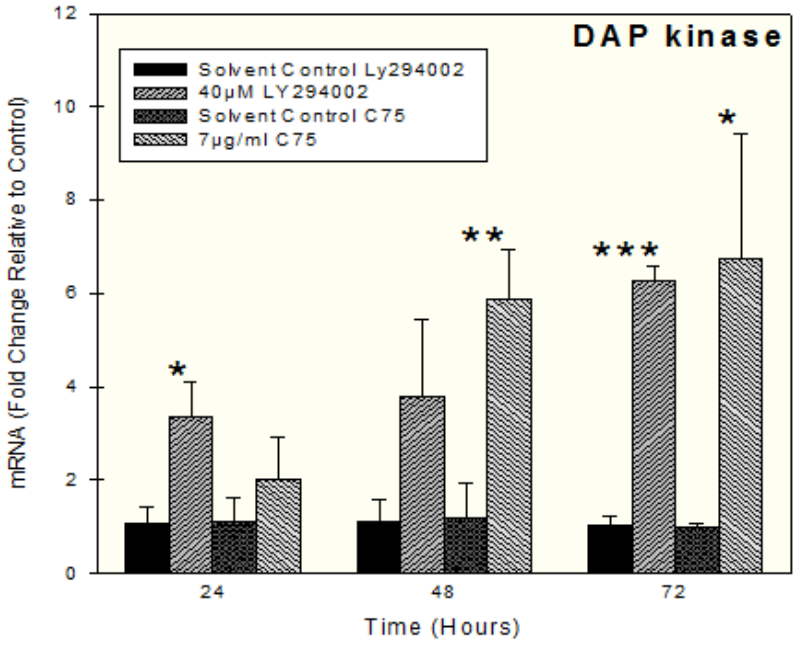

Figure 22: Inhibition of FASN or PI3K increases mRNA expression of the tumor suppressor gene DAPK.

Quantitative Real Time RT-PCR was done on A2780 cells. Cells were treated with 7µg/ml C75 or 40µM LY294002 for 24, 48, or 72 hours. mRNA expression was determined relative

to vehicle-treated controls ("solvent control"). Statistical significance between inhibitor- and vehicle-treated solvent controls was determined by two-tailed Student´s t-test, * indicates significant difference at p<0,05, ** indicates significant difference at p<0,01, and * indicates significant difference at p<0,001.**

3.1.2 Changes in mRNA expression level of apoptosis associated genes resulting from FASN-inhibition by C75 or PI3K-inhibition by LY294002 in A2780 cells

3.1.2.1 C75 and LY294002 increase FAS mRNA expression level in A2780 cells

While LY294002 upregulates FAS mRNA in A2780 only moderately to a maximum of 2,3-fold normalized to LY294002 solvent control after 72 hours of treatment, C75 significantly enhances FAS mRNA expression in a time dependent manner up to 97,9-fold after 72 hours of treatment. Even at earlier time points of C75 treatment the FAS gene expression is strongly augmented, 7,9-fold after 24 hours and 12,5-fold after 48 hours of C75 incubation (Figure 23). This suggests that FASN blockade stimulates not only stress associated apoptosis (Knowles et al., 2008) and mitochondrial associated apoptosis (Kawai et al., 1999), but, in contrast to LY294002, it foremost triggers TNF-α-dependent apoptosis process.

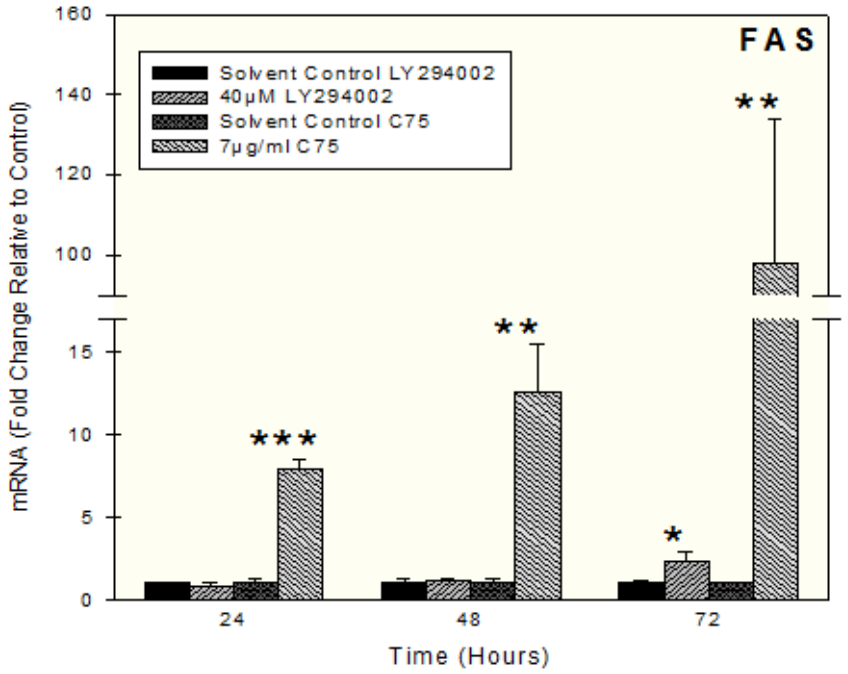

Figure 23: FASN inhibitor increases mRNA expression of death associated FAS more significantly than PI3K inhibitor.

Quantitative Real Time RT-PCR was done on A2780 cells. Cells were treated with 7µg/ml C75 or 40µM LY294002 for 24, 48, or 72 hours. mRNA expression was determined relative to vehicle-treated controls ("solvent control"). Statistical significance between inhibitor- and vehicle-treated solvent controls was determined by two-tailed Student´s t-test, * indicates significant difference at p<0,05, ** indicates significant difference at p<0,01, and * indicates significant difference at p<0,001.**

3.1.2.2 C75 and LY294002 increase manganese Superoxid Dismutase (MnSOD, SOD2) mRNA expression level in A2780 cells

LY294002 enhances SOD2 gene expression in A2780 only marginally after 24 and 48 hours treatment (1,4 and 1,3-fold, respectively). After 72 hours of incubation with LY294002, SOD2 gene expression was elevated 2-fold. On the contrary, C75-treated A2780 reveal rapid and strong upregulation of SOD2 mRNA. At 24 hours of C75 treatment no modulation is seen, whereas at 48 hours a significant 2-fold increase and at 72 hours a 2,7-fold change is observed (Figure 24).

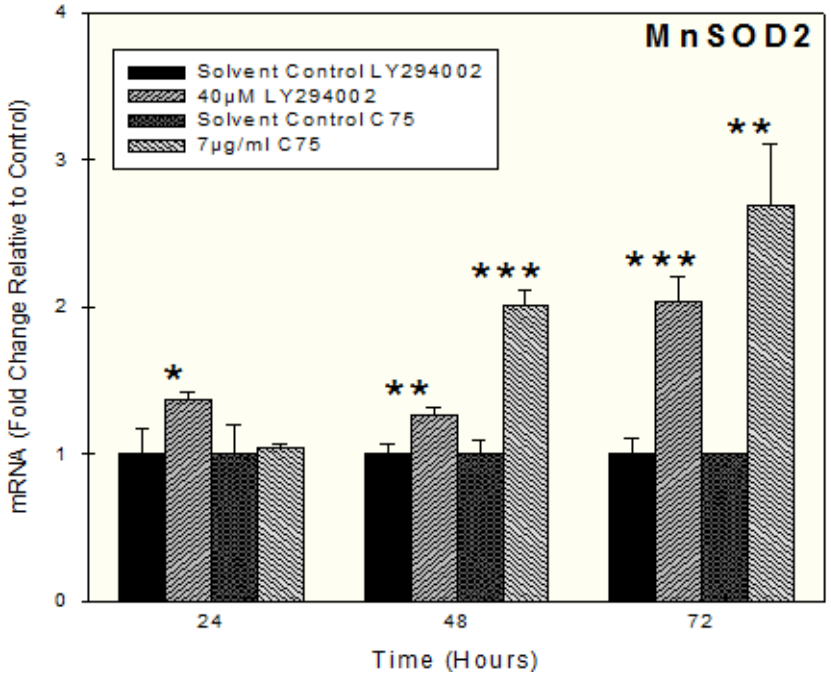

Figure 24: FASN inhibition increases mRNA expression of MnSOD2 more significantly than PI3K inhibition.

Quantitative Real Time RT-PCR was done on A2780 cells. Cells were treated with 7µg/ml C75 or 40µM LY294002 for 24, 48, or 72 hours. mRNA expression was determined relative to vehicle-treated controls ("solvent control"). Statistical significance between inhibitor- and vehicle-treated solvent controls was determined by two-tailed Student´s t-test, * indicates significant difference at p<0,05, ** indicates significant difference at p<0,01, and * indicates significant difference at p<0,001.**

3.1.3 Changes in mRNA expression level of epigenetically active enzymes resulting from FASN-inhibition by C75 or PI3K-inhibition by LY294002 in A2780 cells

Hypermethylated CpG islands of silenced tumor-suppressor genes are characterized overall by histone hypoacetylation and histone methylation (Esteller et al. 2007). We hypothesized that demethylation by C75 could be responsible for transcription stimulation of some tumor suppressor genes as many of them have already been reported to be promoter hypermethylated.

Aberrant methylation of CpG islands in promoter regions of $p15^{INK4b}$ (Herman et al., 1996) and $p16^{INK4a}$ (Katsaros et al., 2004) as well as gene methylation of DAPK (Collins et al., 2006) and CDH1 (Rathi et al., 2002; Makerla et al., 2005) have been observed. After having demonstrated that FASN inhibition upregulates the transcript levels of p15, E-Cadherin, DAPK, SOD2 and FAS in the ovarian carcinoma cell line A2780 we examined the effects of FASN targeting on the expression of epigenetically active enzymes and found some inhibitor-dependent regulations of these enzymes arguing for a possible epigenetic mechanism of action of this FASN blocking drug. Modulation of epigenetically active enzymes is expected to occur before transcriptional changes of affected tumor suppressor genes become evident. Therefore, examination of C75-effects on mRNA expression of epigenetically active enzymes was focused on earlier time points of C75 treatment.

3.1.3.1 C75 and LY294002 decrease DNA-methyltransferase 1 (DNMT1) mRNA expression level after 24 hours of treatment

At 24 hours, C75 inhibits DNMT1 mRNA expression 0,4-fold, whereas LY294002 exerts a weaker effect repressing DNMT1 mRNA 0,7-fold relative to solvent control. At later time points, C75 fails to down-regulate DNMT1, whereas LY294002 even enhances DNMT1 mRNA (Figure 25). Although DNMT1 is known as a basic DNMT it has been reported to be also involved in de novo methylation (Esteller et al., 2007). Our data thus indicate that FASN inhibition by C75 reduces transcription of this potent methylating enzyme hours before mRNA expression of some of the potentially hypermethylated tumor suppressor genes such as E-Cadherin and DAPK is increased.

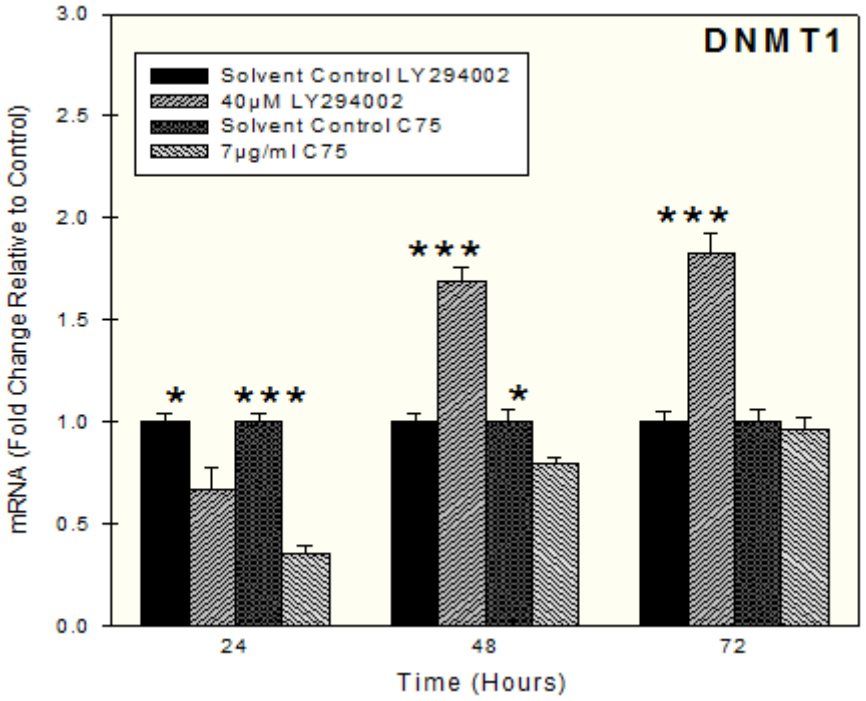

Figure 25: Inhibition of FASN or PI3K decreases DNMT1 mRNA expression level after 24 hours of treatment.

Quantitative Real Time RT-PCR was done on A2780 cells. Cells were treated with 7µg/ml C75 or 40µM LY294002 for 24, 48, or 72 hours. mRNA expression was determined relative to vehicle-treated controls ("solvent control"). Statistical significance between inhibitor- and vehicle-treated solvent controls was determined by two-tailed Student´s t-test, * indicates significant difference at p<0,05, ** indicates significant difference at p<0,01, and * indicates significant difference at p<0,001.**

3.1.3.2 C75 and LY294002 increase DNMT3a mRNA expression level in A2780 cells

We also examined the effects of C75 and LY294002 on DNMT3a mRNA level. Both compounds augment DNMT3a mRNA at 24, 48 and 72 hours of exposure (Figure 26). The modulation of tumor suppressor gene mRNA expression levels gives us just very indecisive information about methylating activities since the entire epigenetic machinery not only targets these genes. Therefore, DNMT3a probably targets at other genes that do not exert tumor suppressor functions.

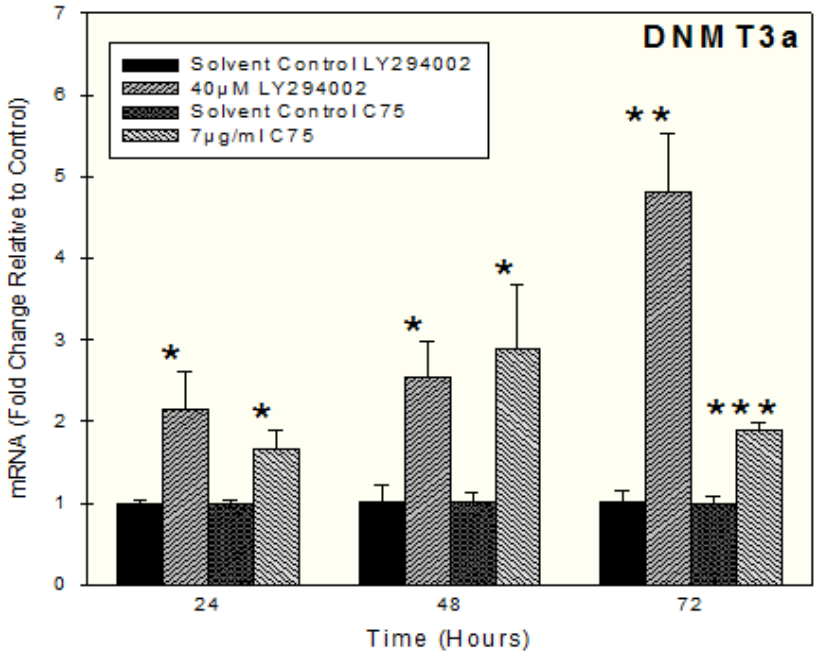

Figure 26: Inhibition of FASN or PI3K increases DNMT3a mRNA expression.
Quantitative Real Time RT-PCR was done on A2780 cells. Cells were treated with 7µg/ml C75 or 40µM LY294002 for 24, 48, or 72 hours. mRNA expression was determined relative to vehicle-treated controls ("solvent control"). Statistical significance between inhibitor- and vehicle-treated solvent controls was determined by two-tailed Student´s t-test, * indicates significant difference at p<0,05, ** indicates significant difference at p<0,01, and * indicates significant difference at p<0,001.**

3.1.3.3 C75 and LY294002 decrease DNMT3b mRNA expression level in A2780 cells

DNMT3a mRNA is down-regulated neither by LY294002 nor by C75 in A2780. Nevertheless, both agents decrease DNMT3b transcripts at 24 and 48 hours, and C75 at 72 hours as well (Figure 27). Thus, our data on DNMT1 and DNMT3b suggest that pharmacological FASN blockade exerts inhibiting effects on the methylation machinery, whereas the activity of PI3K inhibition is less consistent.

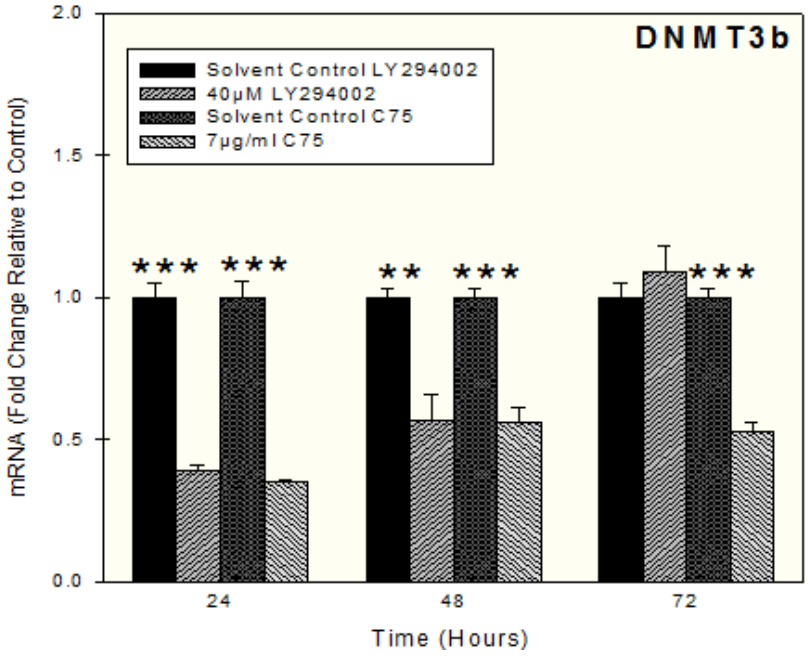

Figure 27: Inhibition of FASN or PI3K decreases DNMT3b mRNA expression level. Quantitative Real Time RT-PCR was done on A2780 cells. Cells were treated with 7µg/ml C75 or 40µM LY294002 for 24, 48, or 72 hours. mRNA expression was determined relative to vehicle-treated controls ("solvent control"). Statistical significance between inhibitor- and vehicle-treated solvent controls was determined by two-tailed Student´s t-test, * indicates significant difference at p<0,05, ** indicates significant difference at p<0,01, and * indicates significant difference at p<0,001.**

3.1.3.4 C75 and LY294002 do not down-regulate histone deacetylase 2 (HDAC2) mRNA in A2780 cells

After 24 hours of exposure to LY294002 or to C75 HDAC2 mRNA remains essentially unaffected. Moreover, at later time points, LY294002 and C75 rather up-regulate HDAC2 than reducing it (Figure 28). Histone deacetylases are known to repress transcription of methylated DNA of many tumor suppressor genes. The effects of C75 and LY294002 on the epigenetic machinery of A2780 cells thus remain controversial. Moreover, the epigenetic regulation does not act very specifically. Thus many genes can be targeted and it is still not clear how genes are chosen for methylation silencing.

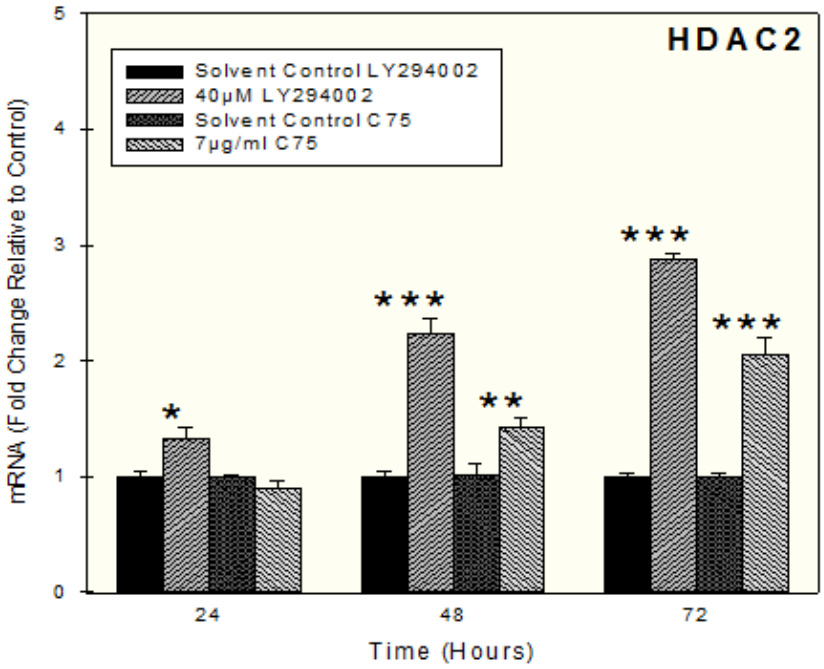

Figure 28: Inhibition of FASN or PI3K increases mRNA expression of HDAC2.
Quantitative Real Time RT-PCR was done on A2780 cells. Cells were treated with 7µg/ml C75 or 40µM LY294002 for 24, 48, or 72 hours. mRNA expression was determined relative to vehicle-treated controls ("solvent control"). Statistical significance between inhibitor- and vehicle-treated solvent controls was determined by two-tailed Student´s t-test, * indicates significant difference at p<0,05, ** indicates significant difference at p<0,01, and * indicates significant difference at p<0,001.**

3.2 Changes in methylation status of tumor suppressor genes resulting from FASN-inhibition by C75 or PI3K-inhibition by LY294002 in A2780 cells

After having demonstrated that both FASN and PI3K inhibition increase the mRNA expression levels of $p15^{INK4b}$ and DAPK, which both are reported to be promoter hypermethylated in ovarian cancer (Collins et al., 2007; Liu et al., 1, 2005), we examined the methylation status of these two genes after C75 or LY294002 treatment using methylation-specific PCR. A control sample

containing semi-methylated genomic DNA from healthy tissue was also included in the analyses.

3.2.1 The promoter of the $p15^{INK4b}$ tumor suppressor gene is not hypermethylated in A2780 cells

The genomic DNA control which should not exhibit hypermethylation in any tumor suppressor gene reveals higher methylation of $p15^{INK4b}$ than treated or untreated A2780 at any time point. This indicates that the ovarian carcinoma cell line A2780 does not feature a hypermethylation status in the promoter region of $p15^{INK4b}$ (Figure 29). After having demonstrated that there is no hypermethylation of the $p15^{INK4b}$ gene promoter region in A2780, no further demethylation can obviously be achieved with C75 or with LY294002 (Figure 29).

Although a hypermethylated phenotype in ovarian cancer has often been reported (Collins et al., 2007; Liu et al., 1, 2005) we could not show this methylation status for the promoter of $p15^{INK4b}$ in the A2780 cell line. This indicates that upregulation of $p15^{INK4b}$ mRNA expression must occur via mechanisms that are not related to gene promoter demethylation.

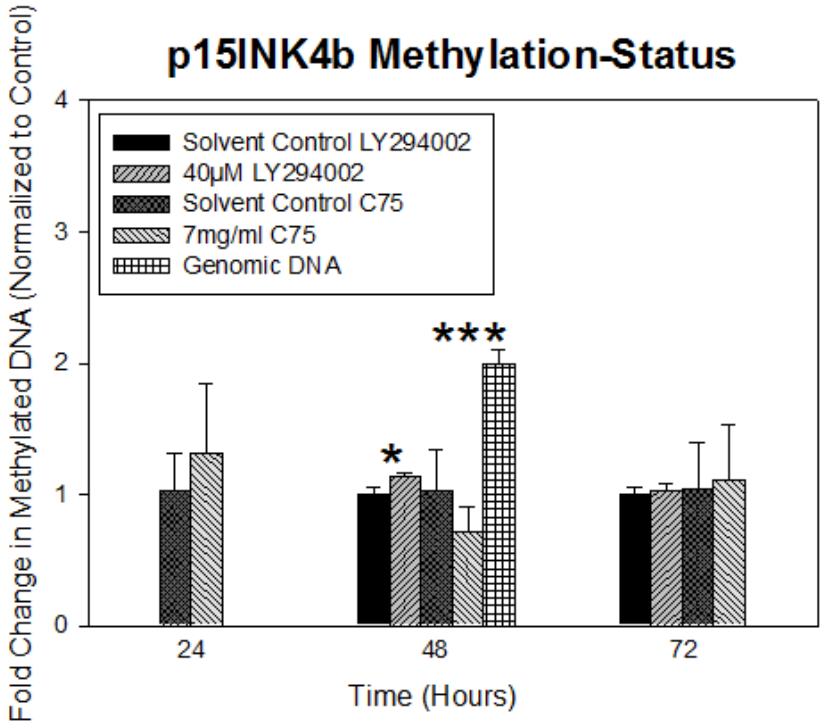

Figure 29: Analysis of the methylation status of the p15^{INK4b} promoter region.
As demonstrated by quantitative methylation-specific PCR (Q-MSP) no promoter hypermethylation of p15^{INK4b} was observed in A2780. Cells were treated with 7µg/ml C75 or 40µM LY294002 for 24, 48, or 72 hours. Methylation status was determined relative to vehicle-treated controls ("solvent control"). Statistical significance between inhibitor- and vehicle-treated solvent controls was determined by two-tailed Student´s t-test, * indicates significant difference at p<0,05, ** indicates significant difference at p<0,01, and * indicates significant difference at p<0,001.**

3.2.2 C75-mediated upregulation of DAPK mRNA correlates with demethylation of the hypermethylated gene promoter

Our results show that the methylation status of the DAPK promoter region in untreated A2780 cells is five times higher when compared to the methylation level found in a genomic DNA control sample. Treatment of A2780 with C75 time-dependently decreases methylation of the DAPK promoter. As soon as 2 hours after addition of C75 the methylation level of DAPK decreases by 50% when compared to solvent control. C75-mediated DAPK demethylation proceeds

to reach normal levels after 48 hours. At 72 hours the promoter is almost completely demethylated (Figure 30). This suggests that FASN blockade by C75 modulates expression of this tumor suppressor gene by epigenetic mechanisms. This provides another molecular explanation for the observed anti-proliferative and death promoting effects of FASN-inhibitors. Importantly, until now the relationship between FASN biochemical pathways and epigenetic regulation of tumor suppressor genes has been completely unexplored. Therefore, this is the first report demonstrating molecular links between FASN-mediated lipogenesis and epigenetic modulation of tumor suppressor gene expression in (cancer) cells.

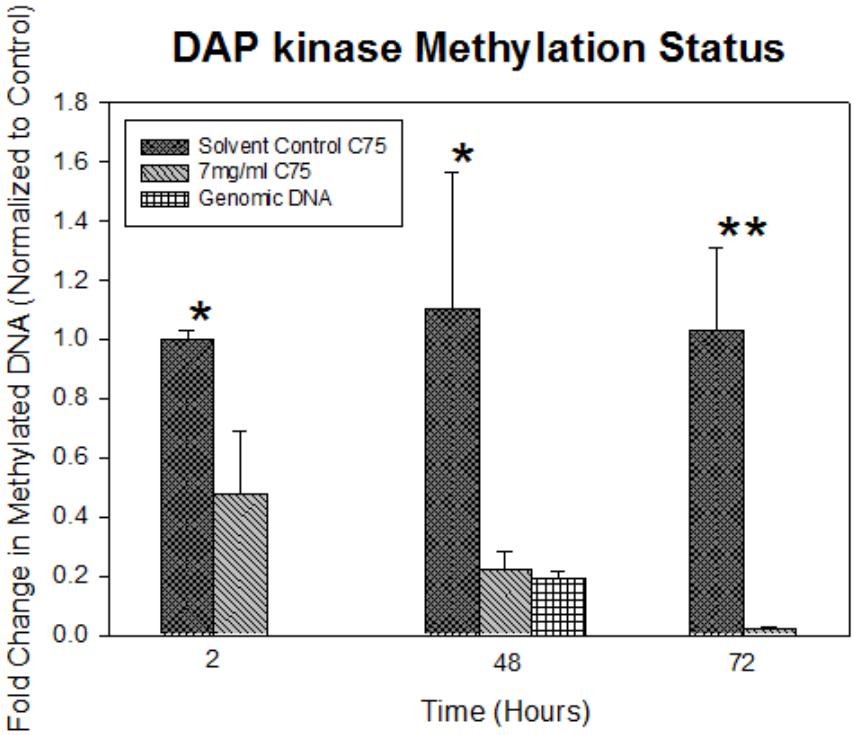

Figure 30: Analysis of the methylation status of the DAPK promoter region using quantitative methylation-specific PCR (Q-MSP).

A2780 cells were treated with 7µg/ml C75 for 2, 48, or 72 hours. Methylation status was determined relative to vehicle-treated controls ("solvent control"). Statistical significance between inhibitor- and vehicle-treated solvent controls was determined by two-tailed Student´s t-test, * indicates significant difference at p<0,05, ** indicates significant difference at p<0,01, and * indicates significant difference at p<0,001.**

3.3 The FASN targeting drug C75 affects protein expression and activity (phosphorylation) of PI3K/AKT effector molecules

The expression of cyclin-dependent kinase inhibitors (CDKIs) is reported to be regulated at least in part by the PI3K/AKT signaling pathway (Gao et al., 2004; Katayama et al., 2008). After having demonstrated that FASN inhibition increases mRNA expression of the CDKI $p15^{INK4b}$ in A2780 without inducing demethylation of the corresponding promoter we therefore examined the effects of C75 on the protein expression and activation (phosphorylation) of PI3K/AKT signaling molecules. Modulation of the PI3K/AKT pathway by FASN inhibition in ovarian carcinoma cell lines has already been observed (Grunt et al., 2009; Wang et al., 2005) and the PI3K activity is known to be required for ovarian cancer cell proliferation and G1 cell cycle progression (Gao et al., 2004; Katayama et al., 2008). Thus, we treated A2780 with the FASN inhibitor C75 followed by immunoblot analysis of AKT, phospho-AKT, mTOR, phospho-mTOR, p70S6K, phospho-p70S6K, 4eBP1, phospho-4eBP1, ERK1/2 and phospho-ERK1/2 to examine the molecular interaction between FASN, PI3K/AKT signaling, and the CDKI $p15^{INK4b}$.

3.3.1 Reduction of protein expression and phosphorylation of PI3K/AKT signaling molecules by the FASN inhibitor C75

At first, we examined the p15 protein level in A2780 after treatment with C75. Unexpectedly, we were unable to detect an increase of p15 protein level, which would correspond to our mRNA expression data, rather we obtained a slight decrease of $p15^{INK4b}$ upon C75 exposure indicating that $p15^{INK4b}$ is (post-) translationally modulated by C75 (Figure 31A). Either $p15^{INK4b}$ mRNA translation is affected or $p15^{INK4b}$ protein is post-translationally destabilized. Importantly, this data, which is conflicting with our observation that C75 stimulates $p15^{INK4b}$ mRNA

expression, indicates that this CDKI is not responsible for the G1 arrest caused by FASN blockade (Knowles et al., 2004).

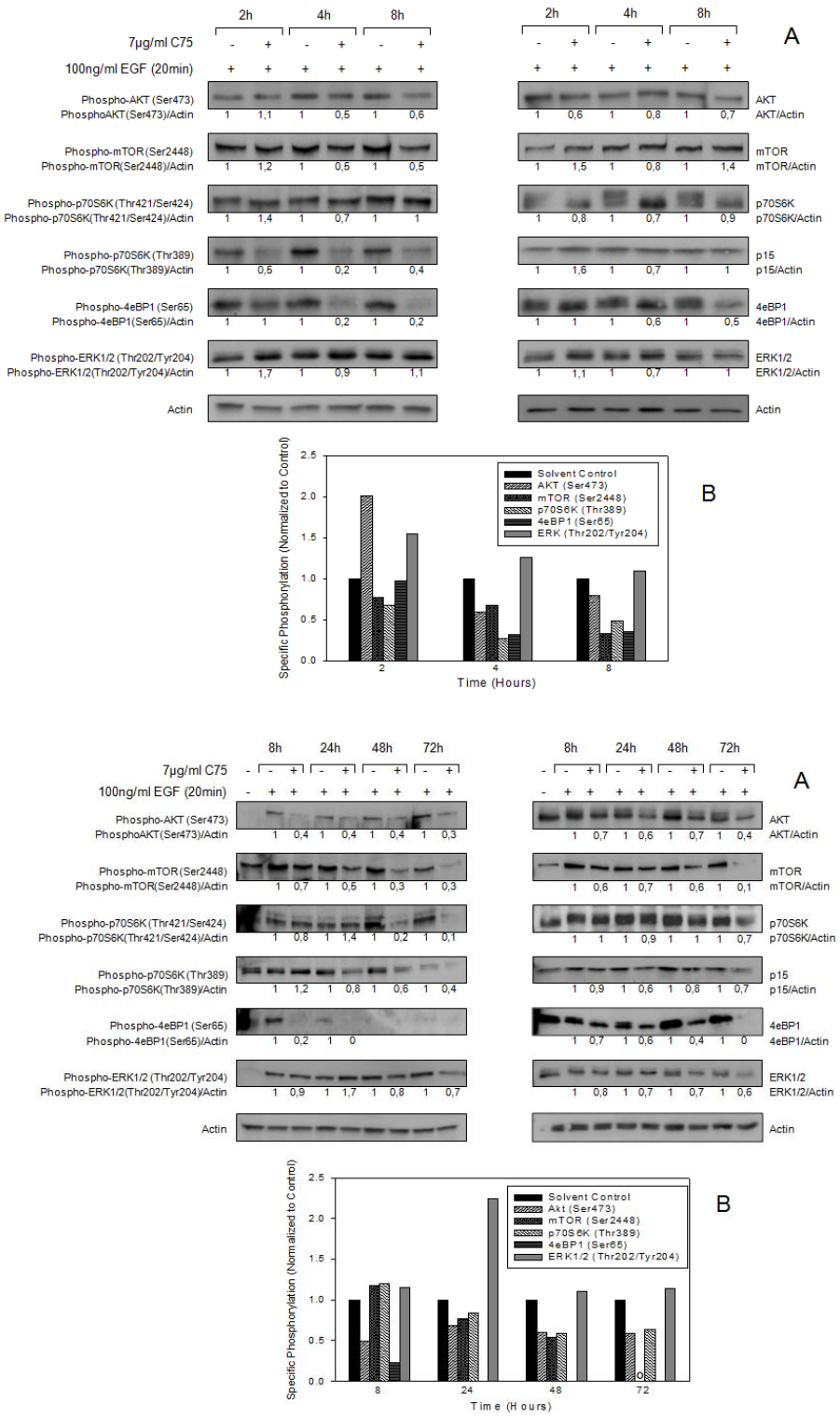

Figure 31: FASN inhibition reduces phosphorylation and expression of p15^{INK4b}, ERK1/2 and PI3K downstream signaling proteins.

A, A2780 cells were treated with vehicle (0,0389% DMSO) or C75 (7µg/ml) for the indicated times. Except from one untreated sample in Figure 31, all cells were stimulated for 20 minutes with 100ng/ml EGF. Cell lysates were collected as described in Materials and Methods for immunoblot analysis with specific antibodies for AKT, phospho-AKT (Ser473), mTOR, phospho-mTOR(Ser2448), p70S6K, phospho-p70S6K (Thr389 or Thr421/Ser424), $p15^{INK4b}$, 4eBP1, phospho-4eBP1 (Ser65), ERK1/2, phospho-ERK1/2 (Thr202/Tyr204), and ß-actin. Experiments were quantified using Herolab Software by measuring the optical density of the band specific for the respective protein of interest relative to that of ß-actin. Values of treated samples were then related to those of solvent control samples. B, specific phosphorylation level of each protein was quantified using the Herolab Software by relating the phospho-protein/ß-actin ratio to the corresponding protein/ß-actin ratio. The resulting value for the solvent control was arbitrarily set at 1 for each time point and the value for the corresponding C75-treated cells was related to it. Due to bad quality of the blot it was not possible to calculate the 72 hours time point for specific phosphorylation of mTOR.

Nevertheless, C75 downregulates expression and phosphorylation of signal effector proteins of the PI3K/AKT pathway such as AKT, mTOR, p70S6K and 4eBP1 in A2780 cells (Figure 31A, B). Interestingly, C75 pre-treatment inhibits AKT, mTOR, p70S6K and 4eBP1 phosphorylation elicited by EGF (100ng/ml) and simultaneously decreases the corresponding protein levels. In contrast, phospho-ERK1/2 levels slightly increase upon C75 treatment (Figure 31B), even though total ERK1/2 protein expression slightly declines at later time points of exposure (Figure 31A). Enhancement of ERK1/2 phosphorylation is also observed in LY294002 treated A2780 (Figure 32B). Unlike FASN inhibition by C75, the PI3K inhibitor LY294002 does not markedly lower the expression levels of several PI3K/AKT signaling proteins (Figure 31A, Figure 32A). Nevertheless, both drugs efficiently lower phosphorylation of the proteins (Figure 31B, Figure 32B). This data indicate that C75-mediated blockade of FASN reduces the activity of the PI3K cascade even though C75 is not that effective in inhibiting protein phosphorylation as compared to the specific PI3K inhibitor LY294002. In contrast, our results demonstrate that inactivation of AKT signaling by LY294002

or C75 concurrently slightly activates ERK1/2 in A2780. Moreover, C75 seems to decrease the total protein level of all signal proteins analyzed, whereas LY294002 does not down-regulate or even elevates signal protein expression (Figure 32A).

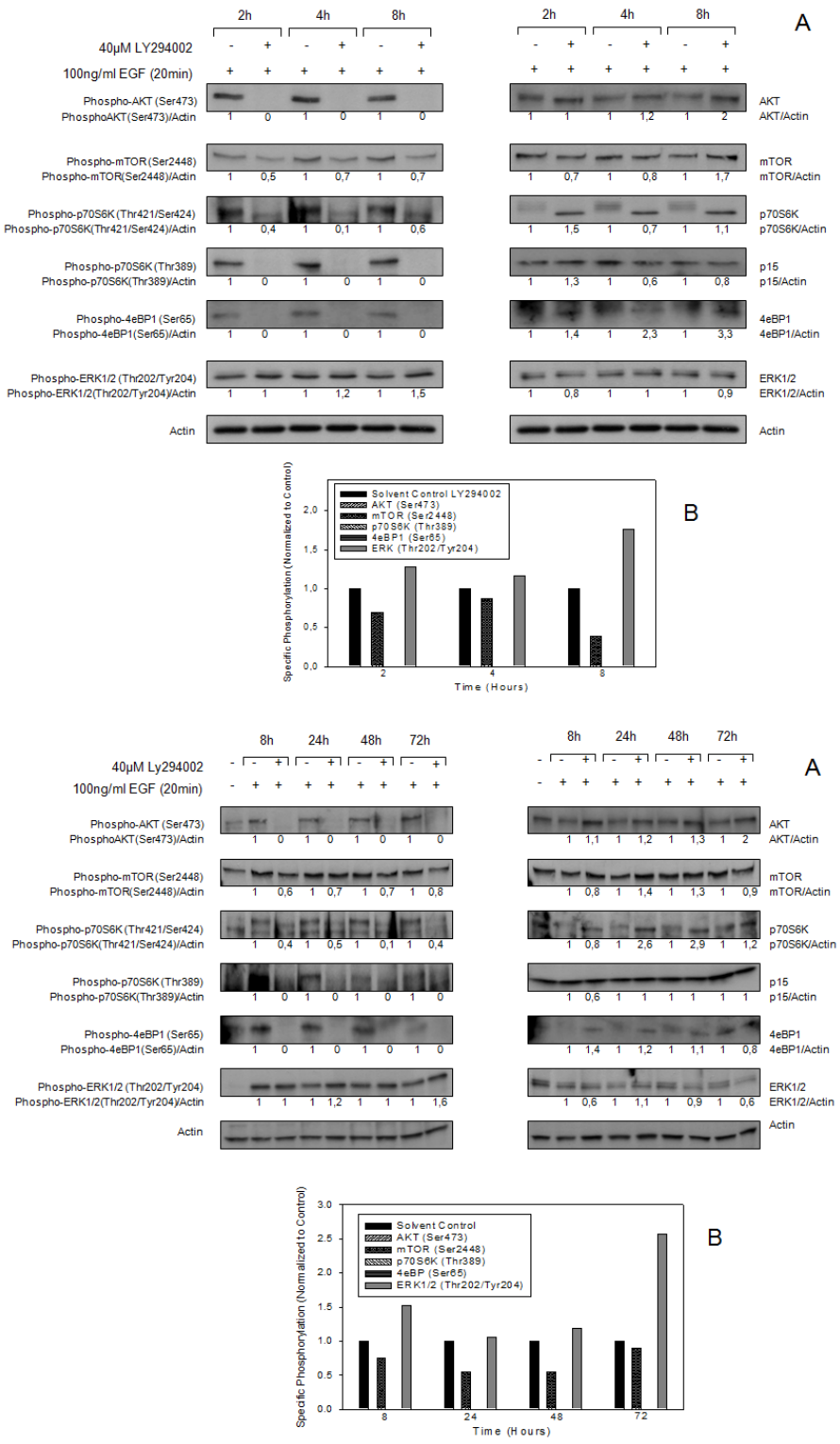

Figure 32: PI3K inhibition by LY294002 is more effective in blocking the PI3K pathway than FASN inhibition.

A, A2780 cells were treated with vehicle (0,1% DMSO) or LY294002 (40µM) for the indicated times. Except from one untreated sample in Figure 32, all cells were stimulated for 20 minutes with 100ng/ml EGF. Cell lysates were collected as described in Materials and Methods for immunoblot analysis with specific antibodies for AKT, phospho-AKT (Ser473), mTOR, phospho-mTOR(Ser2448), p70S6K, phospho-p70S6K (Thr389 or Thr421/Ser424), $p15^{INK4b}$, 4eBP1, phospho-4eBP1 (Ser65), ERK1/2, phospho-ERK1/2 (Thr202/Tyr204), and ß-actin. Experiments were quantified using Herolab Software by measuring the optical density of the band specific for the respective protein of interest relative to that of ß-actin. Values of treated samples were then related to those of solvent control samples. B, specific phosphorylation level of each protein was quantified using the Herolab Software by relating the phospho-protein/ß-actin ratio to the corresponding protein/ß-actin ratio. The resulting value for the solvent control was arbitrarily set at 1 for each time point and the value for the corresponding C75-treated cells was related to it.

3.3.2 Reduction of protein expression levels caused by FASN inhibition appears not to be due to translation inhibition by dephosphorylated 4eBP1

C75-mediated blockade of 4eBP1 phosphorylation (Figure 31B) results in enhanced binding of 4eBP1 to eIF4E thus preventing eIF4E from binding to eIF4F complex and supporting protein translation. This might explain our observation that the steady-state levels of all signaling proteins were reduced by C75 in A2780 cells.

In contrast to many of the PI3K downstream proteins analyzed in this study, the protein level of ß-actin which is transcribed from a “strong” mRNA and is therefore known to be insensitive to alterations of eIF4E availability (Graff et al., 2008), did not decrease. However, AKT and p70S6K decreased before the blocking activity through dephosphorylated 4eBP1 has been established (Figure 31, earlier time points). Therefore, downregulation of signaling proteins can only partially be explained by 4eBP1 bindings of eIF4E. Moreover, if C75-mediated blockade of 4eBP1 phosphoylation would be responsible for a translational blockade of the analyzed proteins, the LY294002-induced complete inhibition of

4eBP1 phosphorylation would have led to the disappearance or at least to a marked decrease of these proteins as well. However, this is not the case (Figure 32). Therefore, we can exclude that C75-mediated prevention of 4eBP1 phosphorylation and thus the consequent decreased eIF4F complex formation and protein translation is the cause for protein level reduction of AKT, mTOR, p70S6K, 4eBP1, $p15^{INK4b}$ and ERK1/2 in A2780.

3.3.3 Reduction of protein expression caused by FASN inhibition appears to be due to enhanced protein degradation

To further elucidate the possible mechanism of C75-dependent reduction of signal protein expression we performed western blot analyzes on samples that have been pretreated with cycloheximide (15µg/ml), a potent translation inhibitor, and C75 (7µg/ml) seperately or in combination. The half-life (IT50) of each PI3K/AKT signaling protein analyzed was reduced significantly by C75 (Figure 33) indicating that FASN inhibition by C75 causes enhanced protein degradation. Cycloheximide single treatment (15µg/ml) downregulates AKT protein level in A2780 with an IT50 of 48 hours. This time indicates the normal degradation time of 50% of this protein without being newly synthesized. Co-exposure of the cells to cyclohehimide and C75 decreased the IT50 for AKT protein to 19 hours (Figure 33, B). Similar effects were seen for all analyzed proteins of the PI3K/AKT cascade (Figure 33). However, the greatest C75-mediated degradation effect was seen for p15. With cycloheximide alone the IT50 of $p15^{INK4b}$ was 57 hours. This value was shortened by coexposure to C75 as low as 18 hours. Our data thus suggest that C75 elevates $p15^{INK4b}$ protein degradation, whereas it concurrently stimulates $p15^{INK4b}$ mRNA expression.

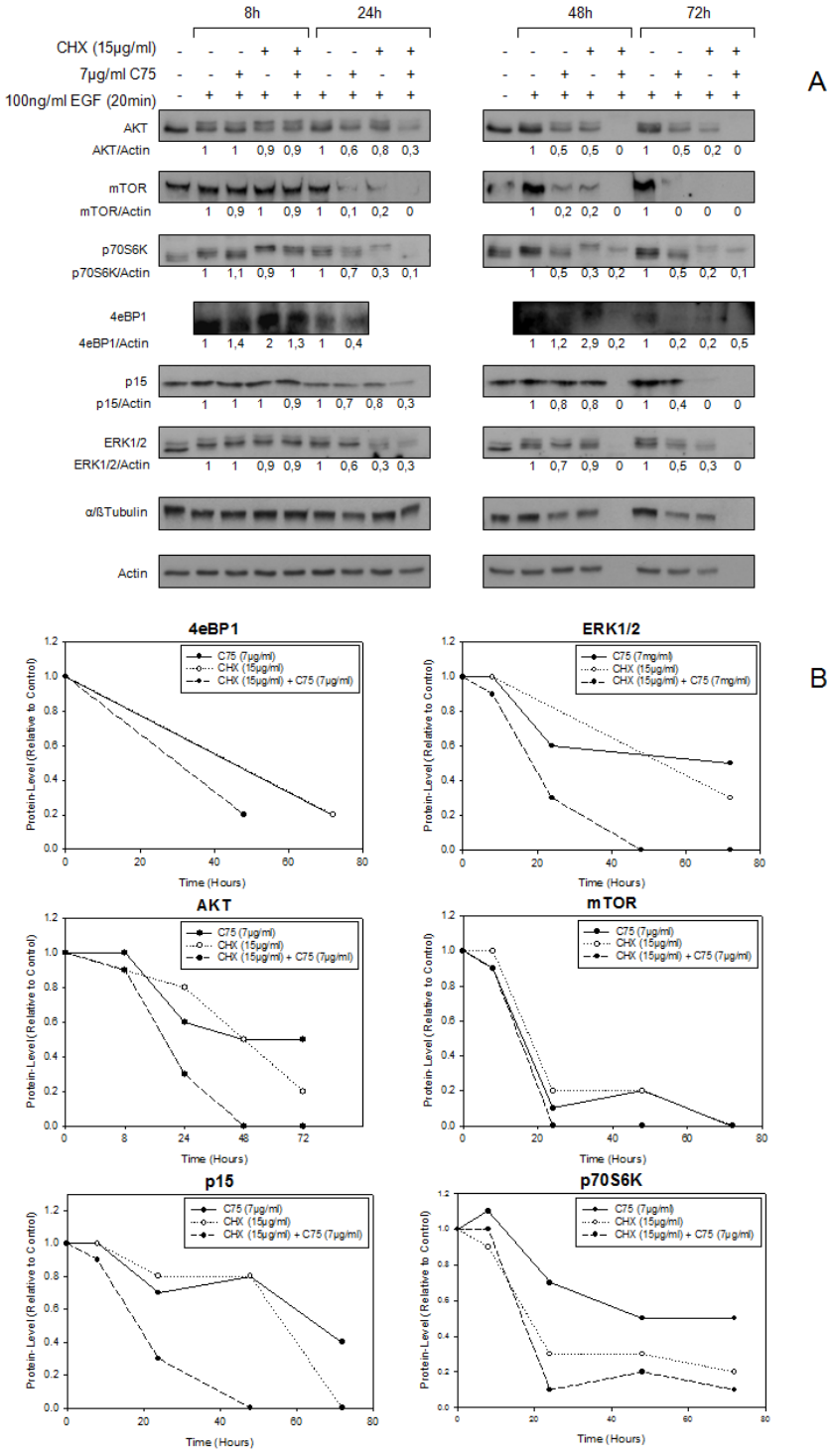

Figure 33: FASN inhibition enhances protein degradation.

A, A2780 cells were treated with vehicle, C75 (7µg/ml), cycloheximide (15µg/ml), or with C75 combined with cycloheximide for the indicated times. Except from one untreated

sample, all cells were stimulated for 20 minutes with 100ng/ml. Cell lysates were collected as described in Materials and Methods for immunoblot analysis with antibodies specific for AKT, mTOR, p70S6K, $p15^{INK4b}$, 4eBP1, ERK1/2, ß-actin and α/ß-tubulin. B, Experiments were quantified by relating the optical density of the band of the protein of interest to that of ß-actin. For each time point the resulting ratios of the sample treated with cycloheximide and C75 seperately or in combination were related to the vehicle control, which was arbitrarily set at 1.

3.3.4 Reduction of protein expression caused by FASN inhibition appears to be due to enhanced proteasomal protein degradation

After having demonstrated that FASN inhibition by C75 augments protein degradation of AKT, mTOR, p70S6K, 4eBP1, $p15^{INK4b}$ and ERK1/2, we then asked whether this might correlate with altered function of the proteasome. Therefore, A2780 cells were treated with 7µg/ml C75 for the indicated periods of time followed by immunoblot analysis of ubiquitin-modified proteins. As expected, FASN inhibition induced accumulation of ubiquitinated proteins (Figure 34A, C). In contrast, inhibition of PI3K rather decreased protein ubiquitination than increasing it (Figure 34B, C). This correlates with slightly enhanced protein levels of several PI3K signaling proteins as demonstrated in Figure 32A. Most importantly, the time-courses of C75-induced protein ubiquitination and C75-mediated reduction of signal protein and $p15^{INK4b}$ protein expression closely conform to each other (Figure 31, Figure 34, C) supporting the hypothesis that FASN activity is involved in the functionality of the proteasomal pathway via a molecular crosstalk between FASN and proteasome pathways.

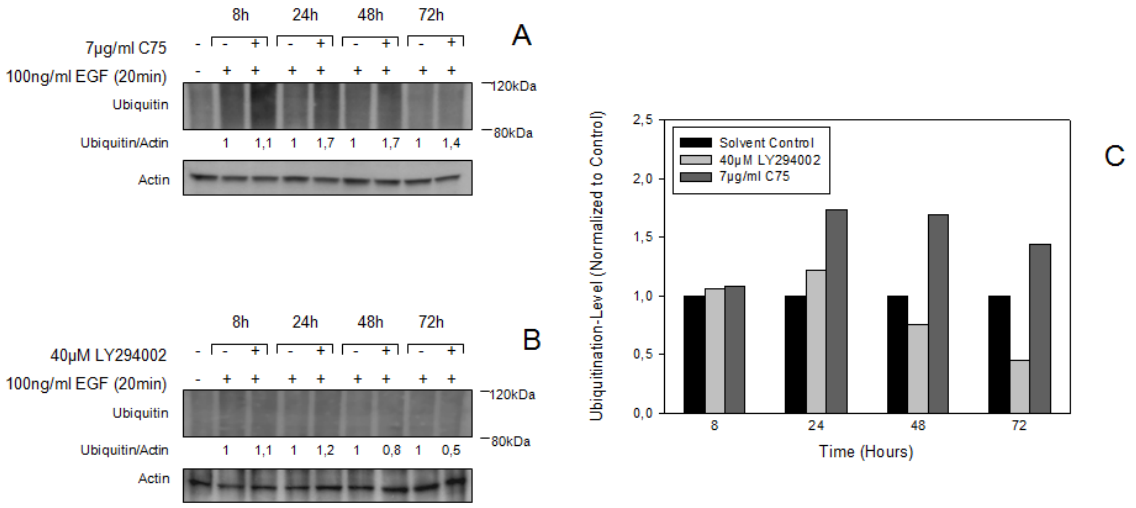

Figure 34: Fatty acid synthase and proteasome pathways crosstalk with each other.
A, A2780 cells were treated with C75 (7µg/ml) or B, LY294002 (40µM) in the presence of DMSO (0,0389% final concentration in C75-treated cells and 0,1% final concentration in LY294002 treated cells) or with the adequate solvent control for 8, 24, 48, 72 hours. Except from one untreated sample, all cells were stimulated for 20 minutes with 100ng/ml EGF. Cell lysates were collected as described in Materials and Methods for immunoblot analysis with antibodies specific for ubiquitin and ß-actin. C, Experiments were quantified by using Herolab Software measuring the optical density of each lane relative to the of ß-actin band. Values of treated samples were then related to those of solvent control samples, which have been arbitrarily set at 1 for each individual time point.

3.4 Changes in gene expression resulting from inhibition of FASN

For gene analysis we used an mRNA array of A2780 FASN-overexpressing ovarian cancer cells. Cells were incubated with 7µg/ml C75 or solvent (0,0389% DMSO) for 48 hours before total mRNA was isolated. The mRNA gene expression array was executed and analyzed by “Kompetenzzentrum für Fluoreszente Bioanalytik in Heidelberg” based on standardized and evaluated procedures. Genes, which have been modified by C75 at least more than 1,3-fold or less than 0,7-fold related to the solvent control are designated as up- or

downregulated, respectively. Only a short abstract of array-data are shown in Table 22.

Inhibition of FASN affected genes that regulate a variety of biological processes including cell proliferation, transcription, apoptosis and degradation are presented. We found, that blockade of FASN enhanced the expression of several anti-proliferative genes such as CDKN1A (p21) and TP53 (p53) (Table 22) or inhibited proliferation-promoting genes coding for various cyclins (CCNA2, CCNB1, CCND2, CCND1, CCNF) (Table 22) and cyclin-dependent kinases (CDK2, CDK10) (Table 22). This coincided with upregulation of several apoptosis-enhancing genes such as FAS, some caspase-encoding genes (CASP4, CASP8), DAPK1, BAX, the cell surface apoptosis genes ANXA1 and ANXA4 and the death receptors TNFRSF10B (TNF-related apoptosis-inducing ligand (TRAIL) receptor) and TNFRSF10D (Table 22). Moreover, our results demonstrate that the inhibition of FASN enhances CPT1, a key enzyme in fatty acid ß-oxidation whose increased expression implicates accumulation of pro-apoptotic signaling molecule ceramide (Table 22). However, compared to our Real Time PCR data the increased expression of CDH1 and CDKN2B could not be confirmed by this array (Figure 19, Figure 21, Table 22). In three independent biological experiments with C75 treated A2780 cells we showed a significant 5,9-fold increase of mRNA expression of DAP kinase by Real Time PCR whereas this array only showed an impaired effect of C75 on DAP kinase gene expression of 1,4-fold augmentation after 48 hours of treatment (Figure 22, Table 22). Correspondingly, stimulation of SOD2 could not be shown that strongly by the mRNA array analysis (1,2-fold) than by Real Time PCR (2,0-fold) after 48 hours of C75 treatment (Figure 24, Table 22). Strong enhancement in gene expression of apoptosis-associated FAS was achieved by FASN inhibition in both gene expression assays (Figure 23, Table 22).

Another effect of FASN inhibition is the regulation of enzymes involved in protein ubiquitination. We found that 48 hours incubation with C75 altered not only the expression of several E2 ubiquitin conjugating enzymes (UBE2Q1, UBE2D1) but

also the expression of the cysteine protease ATG4A, whose activity is induced by reactive oxygen species (ROS; especially via H2O2) and is responsible for autophagosomal protein degradation in the cell (Shouval et al., 2007). Moreover, the gene expression of PSMC4 and PMSC6 (26S proteasome subunits) were also enhanced by FASN inhibition (Table 22). These results confirm posttranslational effects in ovarian tumor cells caused by FASN blockade, which is in accordance with our data shown above (Figure 33, Figure 34).

Abrogation of FASN leads to widespread changes in metabolism. In A2780 lipogenesis is affected by FASN inhibition caused by C75. After 48 hours of treatment with C75 malonyl-CoA accumulation in the cell possibly leads to modulation of ACACA, ACSL1, ACLY and FASN (Table 22). Besides changes in fatty acid metabolism, C75 modulates genes extending to pathways other than fatty acid metabolism. Inhibition of FASN impaired both the glycolysis and the gluconeogenesis, which could be shown by downregulation of LDHC, HK2 and PDK1 (Table 22). This suggests that inhibition of FASN may restrict the ability of tumor cells to produce the energy necessary to proliferate.

While the transcription of PI3K cascade signaling molecules (AKT1, AKT2, AKT3, FRAP1, RPS6KB1, EIF4EBP1) was slightly impaired and gene expression of mTOR-inhibitor (TSC1) was slightly enhanced, our data show a compensatory upregulation of MAP kinase survival pathways (MAPK11, MAPKAP1) (Table 22). Similar compensatory effects were already shown above on protein level in C75-treated A2780, when the specific phosphorylation levels of AKT, mTOR and p70S6K were reduced while the specific phosphorylation level of ERK1/2 was enhanced after 48 hours incubation (Figure 31B).

FASN inhibition also affects transcription. Some modulations in expression of transcription factors are shown in Table 22. In A2780 cells, JUNB is upregulated after 48 hours of incubation with C75, but its translation is reported to be controlled via mTOR (Vesely et al., 2009). Gene expression of FOXO3 which is known to be involved in apoptosis induction or cell-cycle arrest by transcription of related genes (Katayama et al., 2008) is also enhanced by FASN inhibition

(Table 22). Blocking of FASN also results in modulation of epigenetic active enzymes. In contrast to real time PCR, this array did not show an increase in HDAC2 and DNMT3a gene transcription (Figure 26, Figure 28, Table 22) after 48 hours of incubation with C75. However, similar results in real time PCR and array analysis were obtained after 48 hours of incubation concerning the downregulation of DNMT1 and DNMT3b (Figure 25, Figure 27, Table 22). In conclusion, this short abstract of array data (Table 22) provides only a small insight into the comprehensive database of genomic changes that occur in response to FASN inhibition. Nevertheless, these array data confirm that FASN is central not only for tumor cell metabolism, but also for tumor cell signaling.

Protein	Symbol	Gene Classication - Description	Fold change
Tumor Suppressor Genes			
not significantly changed			
p18	CDKN2C	Cyclin-dependent kinase inhibitor 2C	**0.84**
p16	CDKN2A	Cyclin-dependent kinase inhibitor 2A	**0.93**
E-Cadherin	CDH1	Cadherin 1, E-cadherin	**1.01**
p27	CDKN1B	Cyclin-dependent kinase inhibitor 1B	**1.06**
p15	CDKN2B	Cyclin-dependent kinase inhibitor 2B	**1.20**
PTEN	PTEN	Phosphatase and tensin homolog	**1.25**
p19	CDKN2D	Cyclin-dependent kinase inhibitor 2D	**1.26**
p57	CDKN1C	Cyclin-dependent kinase inhibitor 1C	**1.28**
upregulated			
DAP kinase	DAPK1	Death-associated protein kinase 1	**1.41**
p53	TP53	Tumor protein p53	**1.60**
MDM2	MDM2	Mdm2 p53 binding protein homolog	**3.23**
p53INP1	TP53INP1	Tumor protein p53 inducible nuclear protein 1	**3.51**

Protein	Symbol	Gene Classication - Description	Fold change
p53IP3	TP53I3	Tumor protein p53 inducible protein 3	**4.37**
p21	CDKN1A	Cyclin-dependent kinase inhibitor 1A	**6.18**
Proliferation/Cell Cycle			
not significantly changed			
CCND2	CCND2	Cyclin D2	**0.73**
CCND1	CCND1	Cyclin D1	**0.76**
CCNE2	CCNE2	Cyclin E2	**0.76**
CDK9	CDK9	Cyclin-dependent kinase 9	**0.81**
CDK4	CDK4	Cyclin-dependent kinase 4	**0.82**
CDK3	CDK3	Cyclin-dependent kinase 3	**0.92**
CDK5	CDK5	Cyclin-dependent kinase 5	**0.95**
CDK7	CDK7	Cyclin-dependent kinase 7	**1.22**
CDK8	CDK8	Cyclin-dependent kinase 8	**1.26**
CDK6	CDK6	Cyclin-dependent kinase 6	**1.32**
downregulated			
CDK2	CDK2	Cyclin-dependent kinase 2	**0.68**
CDK10	CDK10	Cyclin-dependent kinase 10	**0.63**
BRCA1	BRCA1	Breast cancer 1, early onset	**0.55**
SKP2	SKP2	S-phase kinase-associated protein 2 (p45)	**0.50**
CCNF	CCNF	Cyclin F	**0.37**
CDC2	CDC2	Cell division cycle 2, G1 to S and G2 to M	**0.34**
CCNA2	CCNA2	Cyclin A2	**0.33**
CCNB1	CCNB1	Cyclin B1	**0.30**
CDCA2	CDCA2	Cell division cycle associated 2	**0.25**
Signaling Molecules			
not significantly changed			
EGFR	EGFR	Epidermal growth factor receptor	**1.03**
ERBB2	ERBB2	v-erb-b2 erythroblastic leukemia viral oncogene homolog 2	**0.95**

Protein	Symbol	Gene Classication - Description	Fold change
ERBB3	ERBB3	v-erb-b2 erythroblastic leukemia viral oncogene homolog 3 (avian)	**1.00**
ERBB4	ERBB4	v-erb-a erythroblastic leukemia viral oncogene homolog 4 (avian)	**0.79**
AKT1	AKT1	v-akt murine thymoma viral oncogene homolog 1	**0.73**
AKT2	AKT2	v-akt murine thymoma viral oncogene homolog 2	**0.79**
AKT3	AKT3	v-akt murine thymoma viral oncogene homolog 3 (protein kinase B, gamma)	**0.77**
mTOR	FRAP1	FK506 binding protein 12-rapamycin associated protein 1	**0.78**
TSC1	TSC1	Tuberous sclerosis 1	**1.21**
TSC2	TSC2	Tuberous sclerosis 2	**1.07**
p70S6K	RPS6KB1	Ribosomal protein S6 kinase, 70kDa, polypeptide 1	**0.83**
p70S6K	RPS6KB2	Ribosomal protein S6 kinase, 70kDa, polypeptide 2	**0.98**
MAPK1	MAPK1	Mitogen-activated protein kinase 1	**1.00**
BRAF	BRAF	v-raf murine sarcoma viral oncogene homolog B1	**1.29**
ARAF	ARAF	v-raf murine sarcoma 3611 viral oncogene homolog	**0.76**
RAF1	RAF1	v-raf-1 murine leukemia viral oncogene homolog 1	**0.92**
upregulated			
MAPKAP1	MAPKAP1	Mitogen-activated protein kinase associated protein 1	**1.41**
MAPK11	MAPK11	Mitogen-activated protein kinase 11	**1.54**
downregulated			
eIF4eBP1	EIF4EBP1	Eukaryotic translation initiation factor 4E binding protein 1	**0.57**
Protein Degradation			
upregulated			
26S proteasome	PSMC6	Proteasome (prosome, macropain) 26S subunit, ATPase, 6	**1.31**
UBE2D1	UBE2D1	Ubiquitin-conjugating enzyme E2D 1 (UBC4/5 homolog, yeast)	**1.40**
26S proteasome	PSMC4	Proteasome (prosome, macropain) 26S subunit, ATPase, 4	**1.47**
UBE2Q1	UBE2Q1	Ubiquitin-conjugating enzyme E2Q family member 1	**1.65**
ATG4A	ATG4A	ATG4 autophagy related 4 homolog A (S. cerevisiae)	**2.10**
MDM2	MDM2	Mdm2 p53 binding protein homolog (mouse)	**3.23**

Protein	Symbol	Gene Classication - Description	Fold change
downregulated			
UBE2S	UBE2S	Ubiquitin-conjugating enzyme E2S	**0.51**
UBE2S	UBE2S	OK/SW-cl.73 mRNA for ubiquitin carrier protein, complete cds.	**0.51**
UBE2T	UBE2T	Ubiquitin-conjugating enzyme E2T (putative)	**0.40**
UBE2C	UBE2C	Ubiquitin-conjugating enzyme E2C	**0.34**
Apoptosis			
not significantly changed			
Caspase 2	CASP2	Caspase 2, apoptosis-related cysteine peptidase	**0.75**
BNIP3	BNIP3	BCL2/adenovirus E1B 19kDa interacting protein 3, nuclear gene encoding mitoch. Protein	**0.78**
Caspase 7	CASP7	Caspase 7, apoptosis-related cysteine peptidase	**0.89**
Caspase 3	CASP3	Caspase 3, apoptosis-related cysteine peptidase	**1.06**
DDIT4	DDIT4	DNA-damage-inducible transcript 4	**1.11**
Caspase 1	CASP1	Caspase 1, apoptosis-related cysteine peptidase (interleukin 1, beta, convertase)	**1.16**
Caspase 5	CASP5	Caspase 5, apoptosis-related cysteine peptidase	**1.28**
Caspase 6	CASP6	Caspase 6, apoptosis-related cysteine peptidase	**1.28**
upregulated			
DAP kinase	DAPK1	Death-associated protein kinase 1	**1.41**
Caspase 4	CASP4	Caspase 4, apoptosis-related cysteine peptidase	**1.52**
BAX	BAX	BCL2-associated X protein	**1.62**
Caspase 8	CASP8	Caspase 8, apoptosis-related cysteine peptidase	**1.79**
ANXA1	ANXA1	Homo sapiens annexin A1	**1.86**
AVEN	AVEN	Apoptosis, caspase activation inhibitor	**2.00**
TNFRSF10D	TNFRSF10D	Homo sapiens tumor necrosis factor receptor superfamily, member 10d	**2.41**
GADD45B	GADD45B	Growth arrest and DNA-damage-inducible, beta	**2.55**
TNFRSF10B	TNFRSF10B	Homo sapiens tumor necrosis factor receptor superfamily, member 10b	**2.62**
GADD45A	GADD45A	Growth arrest and DNA-damage-inducible, alpha	**2.81**
FAS	FAS	Fas (TNF receptor superfamily, member 6)	**4.03**
ANXA4	ANXA4	Homo sapiens annexin A4	**7.45**

Protein	Symbol	Gene Classication - Description	Fold change
Epigenetically active enzymes			
not significantly changed			
HDAC2	HDAC2	Histone deacetylase 2	**0.82**
DNMT3A	DNMT3A	DNA (cytosine-5-)-methyltransferase 3 alpha	**0.86**
downregulated			
DNMT1	DNMT1	DNA (cytosine-5-)-methyltransferase 1	**0.57**
DNMT3B	DNMT3B	DNA (cytosine-5-)-methyltransferase 3 beta	**0.55**
Metabolism			
not significantly changed			
LDHA	LDHA	Lactate dehydrogenase A	**0.74**
NOX4	NOX4	NADPH oxidase 4	**0.75**
HIF1A	HIF1A	Hypoxia-inducible factor 1, alpha subunit (basic helix-loop-helix TF)	**0.77**
Catalase	CAT	Catalase	**0.85**
Lyase	ACLY	ATP citrate lyase	**0.87**
LDHB	LDHB	Lactate dehydrogenase B	**0.94**
HIF3A	HIF3A	Hypoxia inducible factor 3, alpha subunit	**1.03**
NOX1	NOX1	NADPH oxidase 1	**1.10**
MnSOD	SOD2	Superoxide dismutase 2, mitochondrial, nuclear gene encoding mitoch. protein	**1.15**
NOX3	NOX3	NADPH oxidase 3	**1.18**
CPT1	CPT1B	Carnitine palmitoyltransferase 1B (muscle) , nuclear gene encoding mitoch. protein	**1.26**
HIF1AN	HIF1AN	Hypoxia-inducible factor 1, alpha subunit inhibitor	**1.28**
upregulated			
CPT1C	CPT1C	Carnitine palmitoyltransferase 1C	**1.50**
ACSL1	ACSL1	Acyl-CoA synthetase long-chain family member 1	**2.11**
CPT1A	CPT1A	Carnitine palmitoyltransferase 1A (liver), nuclear gene encoding mitoch. protein	**3.90**

Protein	Symbol	Gene Classication - Description	Fold change
downregulated			
LDHC	LDHC	Lactate dehydrogenase C	**0.64**
ACACA	ACACA	Acetyl-Coenzyme A carboxylase alpha	**0.59**
FASN	FASN	Fatty acid synthase	**0.54**
Lyase	CLYBL	Citrate lyase beta like	**0.43**
Hexokinase	HK2	Hexokinase 2	**0.38**
PDK1	PDK1	Pyruvate dehydrogenase kinase, isozyme 1, nuclear gene encoding mitoch. protein	**0.21**
Transcription			
upregulated			
ATF4	ATF4	Activating transcription factor 4 (tax-responsive enhancer element B67)	**1.33**
FOXO3	FOXO3	Forkhead box O3	**1.54**
JUNB	JUNB	Jun B proto-oncogene (JUNB), mRNA.	**2.06**
downregulated			
SREBF1	SREBF1	Sterol regulatory element binding transcription factor 1	**0.44**
E2F8	E2F8	E2F transcription factor 8	**0.36**
Housekeeping Genes			
not significantly changed			
GAPDH	GAPDH	Glyceraldehyde-3-phosphate dehydrogenase	**0.98**
ACTB	ACTB	Actin, beta	**0.80**

Table 22: mRNA gene expression array

was executed and analyzed by "Kompetenzzentrum für Fluoreszente Bioanalytik in Heidelberg". Cells were incubated with 7µg/ml C75 or solvent (0,0389% DMSO) for 48 hours before total mRNA was isolated. Genes which have been modified by C75 at least more than 1,3-fold or less than 0,7-fold related to the solvent control are designated as up- or downregulated, respectively. Only a short abstract of array-data are shown in Table 22.

4 Discussion

Unscheduled proliferation in tumor cells frequently results as a consequence of hyperactivation of cell-cycle regulating cyclin-dependent kinases (Cdks) through amplification or mutation or through overexpression of cyclins and, more frequently, inactivation of Cdk inhibitors (Malumbres et al., 2001). In fact, inactivation of Cdk inhibitors is a frequent oncogenic alteration in several tumor types and both $p15^{INK4b}$ and $p16^{INK4a}$ proteins are inhibitors of Cdks that prevent the cell from going through the G1-S phase transition. Therefore, inactivation of $p15^{INK4b}$ and $p16^{INK4a}$ is thought to be an important step in cancer development (Herman et al., 1996). It is well documented that a proportion of ovarian carcinomas harbor $p15^{INK4b}$ methylation (≤33%) or $p16^{INK4a}$ methylation (≤19%) and that CpG island methylation is associated with transcriptional silencing of the tumor suppressor genes (Liu et al., 2, 2005; Rojas et al., 2009; Katsaros et al., 2004; Tam et al., 2007). In our experiments, in FASN inhibited A2780 cells enhanced expression of $p15^{INK4b}$ is more pronounced at the mRNA than at the protein level and actually cannot have further implication on the cell cycle as the protein level of $p15^{INK4b}$ is even reduced in C75 treated A2780 (Figure 19, Figure 31A). A $p15^{INK4b}$ hypermethylated phenotype in ovarian cancer has often been reported (Collins et al., 2006; Liu et al., 1, 2005) but we could not show this methylation status for the promoter gene of $p15^{INK4b}$ in the cell line A2780 (Figure 29). It is reported that inhibition of PI3K by LY294002 leads to G1 arrest in human ovarian cancer cells through $p16^{INK4a}$ regulation by PI3K/AKT/mTOR/p70S6K signaling (Gao et al., 2004). However, in A2780 cells mRNA transcription of $p16^{INK4a}$ was neither stimulated by C75 nor by LY294002 treatment which suggests that the cyclin dependent kinase inhibitor $p16^{INK4a}$ is not responsible for cell cycle blockade in G1, neither. In colon carcinoma and hepatocellular carcinoma cells FASN blockade causes inhibition of DNA replication by blockade of the cell cycle in G1 (Li et al., 2001; Gao et al., 2006).

However, our data suggest that in A2780 ovarian carcinoma cells this C75-induced cell-cycle arrest is caused through various molecular mechanisms that may involve other cyclin dependent kinase inhibitors than $p15^{INK4b}$ or $p16^{INK4a}$. Interestingly, due to C75 treatment we found a significant augmentation of p21 (CDKN1A) expression in A2780 (Table 22). This cyclin dependent kinase inhibitor is known to block cyclin A (CCNA) and cyclin-depedent kinase 2 (CDK2), which are proliferation promoting factors that are also transcriptionally downregulated by FASN inhibition in A2780 cells (Table 22). Maybe massive augmentation of p21 could also be responsible for cell-cycle arrest caused by FASN inhibition in A2780 tumor cells. Moreover, p21 has been shown to play a major role in inducing p53-dependent G1 cell-cycle arrest following DNA damage resulting in Cdk inactivation (Malubres et al., 2003). Notably, in A2780 tumor cells FASN inhibition caused by C75 increased p53 gene expression, which also indicates blockade of S-phase entry by p21 in these cells. Furthermore, it has been reported that in normal cells retinoblastoma (Rb) proteins repress the transcription of genes required for DNA replication or mitosis through sequestering of E2F transcription factors and therefore maintain cells in a quiescent state (Attwool et al., 2004). Upon stimuli, cyclins are normally activated and induce cyclin-depedent kinases Cdk4 and Cdk6. Cyclin D-Cdk4/6 complexes then phosphorylate and inactivate Rb protein, allowing the expression of E2F target genes triggering massive transcription of genes required for DNA replication and mitosis (Malumbres et al., 2001). Interestingly, in our experiments FASN inhibition massively impairs mRNA expression of E2F8 transcription factor, even though the cells have been stimulated with 100ng/ml EGF for 20minutes before lysis and mRNA isolation (Table 22). Maybe this E2F transcriptional downregulation could also account for the possible cell-cycle arrest caused by FASN inhibition in A2780 carcinoma cells. Additionally, FOXO3 (Forkhead box O) transcription factor mRNA expression was enhanced by C75 treatment in A2780 (Table 22). FOXOs are direct targets of AKT phosphorylation and are negatively regulated by AKT (Brunet et al., 1999 C). AKT-dependent

phosphorylation of FOXOs results in their cytoplasmatic localization and inability to exhibit their gene transcriptional activity. FOXOs are reported to be involved in apoptosis induction or cell-cycle arrest by transcription of related genes (Medema et al., 2000). Our results suggest that augmentation in FOXO3 gene expression (Table 22) and reduced AKT activity (Figure 31B) both caused by FASN inhibition could also be associated with potential cell-cycle arrest in A2780 tumor cells. Besides possible C75-induced cell-cycle arrest in tumor cells abrogation of FASN also leads to widespread changes in metabolism, which often induces apoptosis in these cells (Bandyopadhyay et al., 2006). FASN inhibition causes accumulation of its substrate malonyl-CoA. The activity of carnitine palmitoyltransferase 1 (CPT1), which regulates ß-oxidation of fatty acids is blocked by malonyl-CoA. Hence, inhibited CPT1 induces sphingolipid ceramide accumulation, which then provokes ceramide-mediated mitochondrial apoptotic pathway induction as the enhanced transcription of DAP kinase mRNA in our results approves (Figure 22, Table 22) (Bandyopadhyay et al., 2006). Moreover, our mRNA array data of C75 treated A2780 show an increase in mRNA expression level of CPT1 (Table 22), which confirms this effect too (Menendez et al., 2007). Furthermore, CPT1 was co-immunoprecipitated with BCL-2 suggesting a physical association between CPT1 and the mitochondrial apoptotic apparatus (Paumen et al., 1997). In our experiments the increased mRNA levels of TNF-α-associated FAS, TNFRSF10B and TNFRSF10D (Figure 23, Table 22) suggest that FASN blockade in A2780 ovarian carcinoma cells also elevates TNF-α-associated apoptosis. Similar effects caused by FASN inhibition were reported in breast cancer cells (Bandyopadhyay et al., 2006). Additionally, our mRNA array data of C75 treated A2780 cells show an increase in transcription of p53 gene initiating growth arrest or enhanced apoptosis (Table 22). FASN is not only important for phospholipid synthesis of the outer cell membrane but also for inner membranes such as the endoplasmatic reticulum (ER) membrane. Furthermore, FASN activity drives phospholipid synthesis, which primarily occurs in the ER (Swinnen et al., 2003). Because of the direct

connection between FASN activity and phospholipid synthesis, FASN blockade results in ER stress response in a variety of tumor cells, but not in normal cells (Little et al., 2007). Indeed, FASN inhibition has even been shown to cooperate with ER stress inducer to induce cell death by increased unfolded protein response (UPR) signaling (Little et al., 2008). Accordingly, our array data show an augmentation of ATF4 and GADD45A and GADD45B mRNA expression, which are canonical markers of the endoplasmatic reticulum (ER) stress response in tumor cells caused by FASN blockade. For instance, it is known that ATF4 acts to protect the cells from ER-generated reactive oxygen species (Little et al., 2007) indicating that ER-stress could also play a role in programmed cell death induced by FASN inhibition in A2780 cells. All these data suggest that FASN inhibition in tumor cells enhances programmed cell-death via several pathways. In this work we could confirm TNFα-associated, nuclear, ER- and mitochondrial stress induced apoptosis in FASN inhibited A2780 ovarian cancer cells. Besides the already discussed apoptotic effects of FASN inhibition, FASN blockade entails accumulation of NADPH that activates NADPH-oxidase (NOX) thus causing formation of reactive oxygen species (ROS), which in turn stimulates the detoxification activity of MnSOD (Menendez et al., 2007). MnSOD catalyzes the reaction of O_2 to H_2O_2, which is then catalyzed to H_2O and O_2 by catalase. While we could show an increase of mRNA level of the antioxidant enzyme MnSOD caused by FASN blockade (Figure 24, Table 22) in both Real Time PCR and micro array experiments, we could not show any augmentation of catalase in our mRNA array of C75 treated A2780 (Table 22). Hence, there is the possibility that H_2O_2 is not finally cleaned up in the cells after C75 treatment has induced oxidative stress in the cells. However, a conclusive molecular explanation of the anti-proliferative and death promoting effects of FASN-inhibitors is still missing. Moreover, recent findings suggest that ROS production can lead to modulation of methylation of the CDH1 gene promoter (Lim et al., 2008).

It is shown that in a proportion of ovarian carcinomas aberrant promoter methylation of CDH1 gene (≤42%) is detected and that methylation status of CDH1 is closely associated with the decrease of E-Cadherin protein expression (Yuecheng et al., 2006). Interestingly, in A2780 cells C75 and LY294002 increase E-Cadherin mRNA expression level in Real Time PCR indicating that both compounds can modulate the adhesion specificity and maybe can improve targeting invasion and metastases in ovarian carcinoma (Yuecheng et al., 2006). If demethylating effects of C75 or LY294002 result in enhanced CDH1 mRNA expression in A2780 cells remains unclear.

Several types of tumors, including ovarian cancer, are known to have a hypermethylation phenotype (Esteller et al., 2001; Strathdee et al., 2001). Especially, DAP kinase methylation is observed in 67% of patients with malignant ovarian carcinomas (Collins et al., 2006). Our results also show a hypermethylated status in the DAP kinase gene in solvent treated A2780 cells. After C75 treatment, the level of methylated DNA in the DAP kinase gene was decreased (Figure 30). Therefore, we hypothesize that the upregulation of DAP kinase mRNA expression level by FASN blockade, which could be shown by both Real Time PCR and array (Figure 22, Table 22), is caused by demethylating effects of C75 targeting DAP kinase gene. Until now the relationship between the FASN biochemical pathway and the epigenetic regulation of tumor suppressor genes has been completely unexplored. The present study is the first report about epigenetic effects caused by FASN inhibition in ovarian carcinoma cells. Accordingly, we investigated whether modulation of gene expression levels of epigenetic active enzymes might also occur by blocking of FASN. Unlike DNMT3a, which was increased in its mRNA level (Figure 26), DNMT3b and DNMT1 mRNA transcription levels were shown to be decreased by C75-caused FASN inhibition by both Real Time PCR and array (Figure 25, Figure 27, Table 22). This downregulation of DNMTs suggests a transcription-activating effect on the genome and would correlate with the increased DAP kinase gene demethylation and the increased mRNA expression

if its gene after FASN blockade in A2780 cells. Interestingly, in our experiments gene expression of HDAC2 could not be impaired by C75 treatment but was even shown to be enhanced by Real Time PCR analysis (Figure 28). It is well known that epigenetic transcriptional gene silencing is characterized by a hypermethylated and hypoacetylated phenotype (Esteller et al., 2007). Thus, on the one hand our results indicate a transcriptional activation by downregulation of DNMTs (DNMT1, DNMT3b) mRNA levels but on the other hand our results suggest a transcriptional silencing by augmentation of HDAC2 mRNA expression level. Moreover, our mRNA array data of C75 treated A2780 show an increase in mRNA expression level of CPT1 (Table 22). Recently, a new role of CPT1 in histonic acetylation levels of tumors and cancer development was proposed, because CPT1 proteins and HDAC1 were co-immunoprecipitated in nuclear extracts from neoplastic MCF-7 cells (Mazzarelli et al., 2007). In this paper the authors identified a new role of CPT1 in addition to the physiological role in the transport of long-chain fatty acids into mitochondria and showed that CPT1 plays a role in histone acetylation status of tumor cells (Mazzarelli et al., 2007). Maybe in A2780 the C75-enhanced CPT1 also builds complexes with C75-induced HDACs leading to their nuclear import and genome hypoacetylation in these cells. Furthermore, our array data of C75 treated A2780 suggest, that citrate lyase (CLYBL), which converts glucose-derived citrate into acetyl-CoA is markedly decreased (Table 22). As citrate lyase is required for histone acetylation (Wellen et al., 2009) this effect of FASN inhibition could also result in a hypoacetylated phenotype in A2780 cells. In A2780 tumor cells the increase in HDAC2 and CPT1 mRNA expression levels and the decrease of citrate lyase gene expression level could support deacetylating effects caused by FASN inhibition. Accordingly, upregulation of DNMT3a gene expression level by FASN blocking could be a further response to the transcriptional silencing action of C75 in A2780 carcinoma cells. However, our array data also show a downregulation of acetyl-CoA carboxylase (ACACA) mRNA level and a significant augmentation of acetyl-CoA synthetase gene expression due to FASN inhibition (Table 22),

which indicates accumulation of acetyl-CoA in C75-treated A2780 cells. Therefore, we hypothesize that the increased HDAC2 transcription could also be a counteraction against accumulated acetyl-CoA in A2780 cells caused by FASN blockade. In general, the entire epigenetic machinery targets not only specifically to tumor suppressor genes and the modulation of DNMTs or HDACs mRNA expression levels gives us just very indecisive information about their epigenetic activities (Esteller et al., 2007). Nevertheless, this study is the first report about epigenetic effects caused by FASN inhibition in ovarian carcinoma cells and it argues for epigenetic mechanism of action of the FASN blocking drug C75 – although it is likely that many effects are the consequence of secondary mechanisms.

Phosphatidylinositol 3-kinase (PI3K) activity in ovarian cancer cells is well known to be required for the cell proliferation and G1 cell cycle progression. Recent studies indicate that the gene encoding the catalytic subunit of PI3K is amplified in ≤40% of primary ovarian carcinoma cells as well as in several ovarian epithelial cancer cell lines (Gao et al., 2004; Katayama et al., 2008). Modulation of the PI3K/AKT signaling pathway by FASN Inhibition in ovarian carcinoma cell lines has already been observed (Grunt et al., 2009; Wang et al., 2005). Of note, phospholipid endproducts of FASN action are incorporated into cell membranes and form lipid rafts, which accommodate ErbB receptors. Inhibition of FASN decreases these lipid rafts and impedes recruitment and phosphorylation of downstream mediators such as AKT (Grunt et al., 2009). Interestingly, another recent report suggests that ROS evokes an AKT conformational change by forming intramolecular disulfide bonds, which results in disruption of AKT-HSP90 binding and enhancement of AKT-PP2A interaction and dephosphorylation at Ser 473 (Cao et al., 2009). In our experiments we obtained reduction of total protein expression levels (Figure 31A) and impaired phosphorylation levels of AKT, mTOR, p70S6K, p15 and 4eBP1 (Figure 31B) through treatment of the A2780 cells with the FASN inhibiting drug C75. Interestingly, C75 inhibits AKT, mTOR, p70S6K and 4eBP1 phosphorylation caused by EGF stimulation

(100ng/ml) and simultaneously decreases their total protein levels. In contrast, phospho-ERK1/2 levels increase slightly upon C75 treatment in A2780, even though total ERK1/2 protein expression also slightly declines at later time points of exposure (Figure 31A, B). Enhancement of ERK1/2 phosphorylation is also observed in LY294002 treated A2780 ovarian cancer cells (Figure 32A, B). Unlike FASN inhibition by C75, the PI3K inhibitor LY294002 does not remarkably lower the total protein levels of several proteins involved in PI3K/AKT signaling. These data indicate that C75-mediated blockade of FASN reduces the activity of the PI3K cascade and concurrently slightly activates ERK1/2 in A2780, which supports the findings that phospho-AKT negatively regulates the MAPK cascade e.g. by curbing Raf-1 function (Hennessy et al., 2005) or by the proximal mTOR activator Rheb that has been implicated in the direct interaction and inhibition of B-Raf and Raf1 (Karbowniczek et al., 2006). In our experiments C75 seems to decrease the total protein level of all analyzed signal proteins of the PI3K cascade, while LY294002 rather leaves the total protein levels unchanged or even augments the total protein levels of the PI3K cascade molecules. A recent study in breast cancer indicates that FASN inhibition enhances DDIT4 (DNA damage inducible transcript 4), a stress response gene that negatively regulates mTOR pathway, which controls protein biosynthesis through activation of translation initiation factor eIF4E and induces caspase-8-mediated tumor cell apoptosis (Knowles et al., 2008). In our mRNA array data we could not obtain a significant increase of DDIT4 gene expression but caspase-8 gene expression level was enhanced (Table 22). Another study suggests that FASN inhibition causes ER stress and activates unfolded protein response in tumor cells (Little et al., 2007). Interestingly, the authors could show that several indicators of ER stress and inhibition of protein synthesis were detected before caspase 3 and PARP cleavage, the hallmarks of apoptosis (Little et al., 2007). Maybe FASN inhibition leads to apoptosis and protein degradation through ER stress and unfold protein response in A2780 cells, too.

Under normal cellular conditions, eIF4F translation complex assembly is limited as eIF4E is sequestered from eIF4G by binding to eIF4eBP1 (4eBP1). Stimulation of the PI3K/AKT/mTOR signaling then normally leads to 4eBP1 phosphorylation, dislodging 4eBP1 from eIF4E and enabling assembly of the eIF4F complex (Graff et al., 2008). However, we could exclude that the dephosphorylation of 4eBP1 and therefore the decreased eIF4F complex formation and translation is the reason for protein level reduction of AKT, mTOR, p70S6K, 4eBP1 and ERK1/2 by FASN inhibition in A2780 because incubation with LY294002 totally abrogates phosphorylation of 4eBP1 without affecting protein levels of these proteins (Figure 32A, B). Therefore, we assume that translation inhibition by unphosphorylated 4eBP1 does not influence translation of the analyzed proteins. We then investigated whether proteasomal degradation is responsible for decrease in protein levels. Enhanced degradation was obtained in all analyzed proteins caused by C75 while translation was inhibited by Cycloheximide. Especially, the strong degradation of $p15^{INK4b}$ protein lets us hypothesize that this post-translational modification caused by C75 compensates the high increase in mRNA transcription of this gene. Our results show that increased post-translational ubiquitination could be the reason for enhanced protein degradation (Figure 34). Ubiquitination is an important regulatory post-translational modification of lysine residues. Polyubiquitination targets proteins for degradation via the 26S proteasomal pathway. The multienzyme complexes, which mediate protein ubiquitination consist of activating (E1), conjugating (E2), and ligating (E3) enzymes (Gwalter et al., 2008). However, ubiquitination-associated enzymes target their client proteins in a quite non-specific way and up to date only one deubiquitinating enzyme has been matched to a specific substrate. This is ubiquitin-specific protease 2a (USP2a), which interacts with and stabilizes FASN (Graner et al., 2004). Interestingly, a genome-wide analysis of changes in MDA-MB-435 tumor cells caused by FASN knockdown, revealed significant effects of FASN inhibition on enhanced protein ubiquitination (Knowles et al., 2007). Moreover, it has already been reported that the cellular

levels of several members of the serine/threonine protein kinases A, G and C (AGC kinases) are controlled by polyubiquitination through mechanisms, which are independent on activation state or kinase activity (Bogusz et al., 2006). In particular, they could show that the protein levels of serum- and glucocorticoid-induced kinase 1 (SGK1) and ribosomal protein S6 kinase (S6K) are regulated by ubiquitination, which controls their steady-state levels (Brickley et al., 2002; Wang et al., 2008). One study even suggests that ubiquitin ligases Roc1 and MDM2 specifically interact with and induce the ubiquitination of S6K (Gwalter et al., 2008). Thus, these studies show that several signaling pathways can be regulated by steady-state levels of their signaling proteins next to activation by phosphorylation. Even so, a number of studies support a model, whereby activation of kinases triggers their own degradation via the ubiquitin-proteasome pathway to prevent accumulation of activated kinases in the cells (Lu et al., 1998). Our results show highest degradation of all analyzed protein after longer times of exposure to C75. This coincides with the highest ubiquitination status and minimal phosphorylation status of proteins after longer time of treatment with the FASN inhibitor C75 (Figure 31, Figure 34). Theses findings indicate that in A2780 ovarian cancer cells decrease in protein levels of AKT, mTOR, p70S6K, $p15^{INK4b}$ and 4eBP1 is caused by FASN inhibition due to their enhanced ubiquitination and proteasomal degradation and independent of their phosphorylation. Moreover, in our array data we could show a significant increase in MDM2 gene expression level indicating that this ubiquitin ligase could also be associated with enhanced degradation caused by C75 treatment. In absence of phosphorylation, AKT becomes protected by a molecular chaperone, the heat shock protein 90 (Hsp90), from ubiquitination-mediated proteasome degradation (Facchinetti et al., 2008). Maybe a combination of C75 and the Hsp90 inhibitor 17-AAG would abrogate AKT activation even more effectively and potentiate PI3K blockade in ovarian cancer cells. This idea could be a new approach to dispose oncogenic AKT activation in tumor cells. Collectively, these data show that FASN activity is involved in the functionality of the proteasomal

pathway and that there consists a crosstalk between FASN and proteasome pathways. This is an important issue on which further investigations should be focused. In our mRNA array data we further found that FASN inhibition increases the mRNA expression level of ATG4A, which encodes a cysteine protease that is ROS, especially H_2O_2, induced and functions to target proteins for degradation by autophagosomal degradation (Shouval et al., 2007). As we could already show a possible accumulation of H_2O_2 in C75-treated A2780 cells (Table 22) this indicates that maybe other degradation pathways are also influenced by FASN inhibition in A2780 cells.

In summary, this is the first report about the epigenetic modulating action of the FASN inhibitor C75. In this work we further pointed out several effects caused by FASN blocking. We could show and confirm anti-proliferative and apoptotic-inducing effects – among others - induced by demethylation activity, and enhanced ubiquitin-mediated degradation of several protein members of the PI3K cascade.

References

Adams, J. (2003). The development of proteasome inhibitors as anticancer drugs Cancer Cell 5, 417-421.

Adams, R.L. (1995). Eukaryotic DNA methyltransferases--structure and function. Bioessays 17 (2), 139-145.

Alò, P.L., Visca, P., Framarino ,M.L., Botti, C., Monaco, S., Sebastiani, V., Serpieri, D.E., Di Tondo, U. (2000). Immunohistochemical study of fatty acid synthase in ovarian neoplasms. Oncol. Rep. 7 (6), 1383-1388.

American Cancer Society Inc. (2009): Ovarian Cancer. Atlanta (USA). Online source – website last visited on 25.07.2009: http://www.cancer.org/docroot/CRI/CRI_2x.asp?sitearea=&dt=33

Attwooll, C., Deschi, E.L., and Helin, K. (2004). The E2F family: specific functions and overlapping interests. The EMBO Journal 23, 4709–4716.

Bandyopadhyay, S., Zhan, R., Wang, Y., Pai, S.K., Hirota, S., Hosobe, S., Takano, Y., Saito, K., Furuta, E., Iiizumi, M., Mohinta,S., Watabe,M., Chalfant, C., and Watabe, K. (2006). Mechanism of Apoptosis Induced by the Inhibition of Fatty Acid Synthase in Breast Cancer Cells. Cancer Res. 66: (11), 5934-5940.

Bentebibel, A., Sebastia´n, D., Herrero L., Lo´pez-Vin˜as, L., Serra, D., Asins, G., Go´mez-Puertas, P., and Hegardt, F.G. (2006). Novel Effects of C75 on Carnitine Palmitoyltransferase I Activity and Palmitate Oxidation. Biochemistry 45 (14), 4339.

Bentebibel, A., Sebastia´n, D., Herrero, L., Lo´pez-Vin˜as, E., Serra, D., Asins, G., Go´mez-Puertas, P., and Hegardt, F.G. (2006). Novel Effect of C75 on Carnitine Palmitoyltransferase I Activity and Palmitate Oxidation. Biochemistry 45 (14), 4339-4350.

Berchuck, A., Kohler, M.F., Marks, J.R., Wiseman, R., Boyd, J., Bast, R.C. Jr. (1994). The p53 tumor suppressor gene frequently is altered in gynecologic cancers. Am. J. Obstet. Gynecol. 170 (1), 246-252.

Bijman, M.N., van Berkel, M.P., Kok, M., Janmaat, M.L., Boven, E. (2009). Inhibition of functional HER family members increases the sensitivity to docetaxel in human ovarian cancer cell lines. Anticancer Drugs. 20 (6), 450-460.

Birch, D.E., et al. (1996). Simplified hot start PCR. Nature 381, 445-446.

Bogusz, A.M., Brickley, D.R., Pew, T., and Conzen, S.D. (2006). A novel N-terminal hydrophobic motif mediates constitutive degradation of serum- and glucocorticoidinduced kinase-1 by the ubiquitin–proteasome pathway. FEBS Journal 273, 2913–2928.

Brewer, M.A., Johnson, .K, Follen, M., Gershenson, D., Bast, R. Jr. (2003). Prevention of ovarian cancer: intraepithelial neoplasia. Clin Cancer Res. 9 (1), 20-30.

Brickley, D.R., Mikosz, C.A., Hagan, C.R., Conzen, S.D. (2002). Ubiquitin modification of serum and glucocorticoid-induced protein kinase-1 (SGK-1). J. Biol. Chem. 277 (45), 43064-43070.

Brunet, A., Bonni,A., Zigmond, M.J., Lin, M.Z., Juo,P., Hu, L.S., Anderson, M.J., Arden, K.C., Blenis, J., and Greenberg, M.E. (1999). Akt Promotes Cell Survival

by Phosphorylating and Inhibiting a Forkhead Transcription Factor. Cell 96, 857–868.

Brusselmans, K., Vrolix, R., Verhoeven, G., and Swinnen, J.V. (2005). Induction of Cancer Cell Apoptosis by Flavonoids Is Associated with Their Ability to Inhibit Fatty Acid Synthase Activity. The Journal of Biological Chemistry 280 (7/18), 5636–5645.

Cannistra, S.A. (2004). Cancer of the Ovary. M.D. N Engl J Med. 351, 2519-29.

Cao, J., Xu, D., Wang, D., Wu, R., Zhang, L., Zhu, H., He, Q., Yang, B. (2009). ROS-driven Akt dephosphorylation at Ser-473 is involved in 4-HPR-mediated apoptosis in NB4 cells. Free Radical Biology & Medicine, Article in Press.

Carracedo, A., Ma, L., Teruya-Feldstein, J., Rojo, F., Salmena, L., Alimonti, A., Egia, A., Sasaki, A.T, Kozma, S.C., Papa, A., Nardella, C., Cantley, L.C., Baselga,J., and Pandolfi, P.P. (2008). Inhibition of mTORC1 leads to MAPK pathway activation through a PI3K-dependent feedback loop in human cancer. The Journal of Clinical Investigation 118 (9), 3065-3074

Citri, A., and Yarden, Y. (2006). EGF–ERBB signalling: towards the systems level. Nature Reviews| Molecular Cell Biology 7, 505-516.

Collins, Y., Dicioccio, R., Keitz, B., Lele, S. and Odinsi, K. (2006). Methylation of death-associated protein kinase in ovarian carcinomas. Int J Gynecol Cancer 16 (Suppl. 1), 195–199.

Costello, J.F., and Plass, C. (2001). Methylation matters. J Med Genet 38, 285–303.

Darcy, KM., Brady, W.E., McBroom, J.W., Bell, J.G., Young, R.C., McGuire, W.P., Linnoila, R.I., Hendricks, D., Bonome, T., Farley, J.H. (2008). Associations between p53 overexpression and multiple measures of clinical outcome in high-risk, early stage or suboptimally-resected, advanced stage epithelial ovarian cancers: A Gynecologic Oncology Group study. Gynecologic Oncology 111, 487–495.

Datta, S.R., Brunet, A., and Greenberg, M.E. (1999). Cellular survival: a play in three Akts. Genes Dev. 13, 2905-2927.

Easton, J.B., and Houghton, P.J. (2006). mTOR and cancer therapy. Oncogene Review 25, 6436–6446.

Espada, J., Ballestar, E., Fraga, M.F. Villar-Garea, A., Juarranz, A., Stockert, J.C., Robertson, K.D., Fuks, F., and Esteller, M. (2004). Human DNA Methyltransferase 1 Is Required for Maintenance of the Histone H3 Modification Pattern. The Journal of Biological Chemistry 279 (35/27), 37175–37184.

Esteller Manel (2007). Epigenetic gene silencing in cancer: the DNA hypermethylome. Human Molecular Genetics 16, R50–R59.

Facchinetti, V., Ouyang, W., Wei, H., Soto, N., Lazorchak, A., Gould, C., Lowry, C., Newton, A.C., Mao, Y., Miao, R.Q., Sessa, W.C., Qin, J., Zhang, P., Su, B., Jacinto, E. (2008). The mammalian target of rapamycin complex 2 controls folding and stability of Akt and protein kinase C. EMBO J. 27 (14), 1932-1943.

Furuta, E., Pai, S.K., Zhan, R., Bandyopadhyay, S., Watabe, M., Mo, Y., Hirota, S., Hosobe, S., Tsukada, T., Miura, K., Kamada, S., Saito, K., Iiizumi, M., Liu, W., Ericsson, J., and Watabe, K. (2008). Fatty Acid Synthase Gene Is Up-

regulated by Hypoxia via Activation of Akt and Sterol Regulatory Element Binding Protein-1. Cancer Res 68 (4), 1003-1011.

Gansler, T.S., Hardman, W., Hunt, D.A., Schaffel, S., Hennigar, R.A. (1997). Increased expression of fatty acid synthase (OA-519) in ovarian neoplasms predicts shorter survival. Hum. Pathol. 28(6), 686-692.

Gao, N., Flynn, D.C., Zhang, Z., Zhong, X., Walker, V., Liu, K.J., Shi, X., and Jiang, B. (2004). G1 cell cycle progression and the expression of G1 cyclins are regulated by PI3K/AKT/mTOR/p70S6K1 signaling in human ovarian cancer cells. Am J Physiol Cell Physiol 287, C281–C291.

Gao, Y., Lin, L., Zhu, C., Chen, Y., Hou, Y., Ding, J. (2006). Growth Arrest Induced by C75, A Fatty Acid Synthase Inhibitor, was Partially Modulated by p38 MAPK but Not by p53 In Human Hepatocellular Carcinoma. Cancer Biology & Therapy 5 (8), 978-985.

Graff, J.R., Konicek, B.W., Carter, J.H., and Marcusson, E.G. (2008). Targeting the Eukaryotic Translation Initiation Factor 4E for Cancer Therapy. Cancer Res 68 (3), 631-634

Graner, E., Tang, D., Rossi, S., Baron, A., Migita, T., Weinstein, L.J., Lechpammer, M., Huesken, D., Zimmermann, D., Signoretti, S., and Massimo Loda, M. (2004). The isopeptidase USP2a regulates the stability of fatty acid synthase in prostate cancer. Cancer Cell 5, 253-261.

Grunt, T.W., Wagner, R., Grusch, M., Berger, W., Singer, C.F., Marian, B., Zielinski, C.C., and Ruth Lupu, R. (2009). Interaction between fatty acid synthase- and ErbB-systems in ovarian cancer cells. Biochem. Biophys. Res. Comm. 385 (3), 454 – 459.

Gwalter, J., Wang, M.L., Gout, I. (2009). The ubiquitination of ribosomal S6 kinases is independent from the mitogen-induced phosphorylation/activation of the kinase. The International Journal of Biochemistry & Cell Biology 41, 828–833.

Harbour, J.W., and Dean. D.C. (2000). The Rb/E2F pathway: expanding roles and emerging paradigms. Genes Dev. 14, 2393-2409.

Heinonen, H., Nieminen, A., Saarela, M., Kallioniemi, A., Klefström, J., Hautaniemi, S., and Monni, O. (2008). Deciphering downstream gene targets of PI3K/mTOR/p70S6K pathway in breast cancer. BMC Genomics 9 (348), 1471-2164.

Hennan, J.G., Jen, J., Merlo, A., and Baylin, S.B. (1996). Hypermethylation-associated Inactivation Indicates a Tumor Suppressor Role for P15INK4B1. Cancer Research 56, 722-727.

Hennessy, B.T., Smith, D.L., Ram, P.T., Lu, Y., and Mills, G.B. (1996). Exploiting the PI3K/AKT Pathway for Cancer Drug Discovery. Nature Reviews/Drug Discovery 4, 988 -1004.

House, M.G., Guo, M.Z., Iacobuzio-Donahue, C., and Herman, J.G. (2003). Molecular progression of promoter methylation in intraductal papillary mucinous neoplasms (IPMN) of the pancreas. Carcinogenesis 24 (2), 193–198.

Huang, J., and Manning, B.D. (2009). A complex interplay between Akt, TSC2 and the two mTOR complexes. Biochem. Soc. Trans. 37, 217–222.

Jin Sungkwan, H., Lee, H., Woo, S., Seo, S., Choe, T., Yoo, D., Lee, S., Um, H., Lee, S.J., Park, M., Kim, J., Hong, S., Rhee, C., Park, I. (2007). Hypoxic

condition- and high cell density-induced expression of Redd1 is regulated by activation of hypoxia-inducible factor-1α and Sp1 through the phosphatidylinositol 3-kinase/Akt signaling pathway. Cellular Signalling 19, 1393–1403.

Karbowniczek, M., Robertson, G.P., and Henske, E.P. (2006). Rheb Inhibits C-Raf Activity and B-Raf/C-Raf Heterodimerization. The Journal of Biological Chemistry 281 (35), 25447–25456.

Katayama, K., Nakamura, A., Sugimoto, Y., Tsuruo, T., and Fujita, N. (2008). FOXO transcription factor-dependent p15INK4b and p19INK4d expression. Oncogene 27, 1677–1686.

Katsaros, D., Cho, W., Singal, R., Fracchioli, S., Rigault de la Longrais, I.A., Arisio, R., Massobrio, M., Smith, M., Zheng, W., Glass, J., Yu,H. (2004). Methylation of tumor suppressor gene p16 and prognosis of epithelial ovarian cancer. Gynecologic Oncology 94, 685–692.

Kelland, L.R. (2005). Emerging drugs for ovarian cancer. Expert Opin. Emerg. Drugs. 10 (2), 413-424.

Kim, W.Y., and Sharpless, N.E. (2006). The Regulation of INK4/ARF in Cancer and Aging. Cell 127, 265-275.

Knowles, L. M., and Smith, J.W. (2007). Genome-wide changes accompanying knockdown of fatty acid synthase in breast cancer. BMC Genomics 8, 168 181.

Knowles, L.M., Axelrod, F., Browne, C.D., and Smith, J.W. (2004). A Fatty Acid Synthase Blockade Induces Tumor Cell-cycle Arrest by Down-regulating Skp2. The Journal of Biological Chemistry 279 (29), 30540–30545.

Knowles, L.M., Yang, C., Osterman, A., and Smith, J.W. (2008). Inhibition of Fatty-acid Synthase Induces Caspase-8-mediated Tumor Cell Apoptosis by Up-regulating DDIT4. The Journal of Biological Chemistry 283 (46), 31378–31384.

Lassus, H., Leminen, A., Vayrynen, A., Cheng, G., Gustafsson, J., Isola, J., and Butzowa, R. (2004). ERBB2 amplification is superior to protein expression status in predicting patient outcome in serous ovarian carcinoma. Gynecologic Oncology 92, 31–39.

Lassus, H., Sihto, H., Leminen, A., Joensuu, H., Isola, J., Nupponen, N.N., Butzow, R. (2006). Gene amplification, mutation, and protein expression of EGFR and mutations of ERBB2 in serous ovarian carcinoma. J Mol Med 84, 671–681.

Li, J., Gorospe, M., Chrest, F.J., Kumaravel, T.S., Evans, M.K., Han, W.F., and Pizer, E.S. (2001). Pharmacological Inhibition of Fatty Acid Synthase Activity Produces Both Cytostatic and Cytotoxic Effects Modulated by p53. Cancer Research 61, 1493–1499.

Lim, S., GU, J., Kim, M.S., Soo Kim, H., Park, Y.N., Keun Park, C., Cho, J.W., Min Park, Y., and Jung, G. (2008). Epigenetic Changes Induced by Reactive Oxygen Species in Hepatocellular Carcinoma: Methylation of the E-cadherin Promoter. Gastroenterology 135, 2128–2140.

Little, J.L., Wheeler, F.B., Fels, D.R., Koumenis, C., and Kridel, S.J. (2007). Inhibition of Fatty Acid Synthase Induces Endoplasmic Reticulum Stress in Tumor Cells. Cancer Res. 67 (3), 1262-1269.

Little, J.L., Wheeler, F.B., Koumenis, C., and Kridel; S.J. (2008). Disruption of crosstalk between the fatty acid synthesis and proteasome pathways enhances

unfolded protein response signaling and cell death. Mol. Cancer Ther. 7, 3816-3824.

Liu, W., 1, Innocenti, F., Wu, M.H., Desai, A.A., Dolan, M.E., Cook, E.H., and Ratain, M.R. (2005). A Functional Common Polymorphism in a Sp1 Recognition Site of the Epidermal Growth Factor Receptor Gene Promoter. Cancer Res. 65 (1), 46-53.

Liu, Z., 2, Wang, L.E., Wang, L., Lu, K.H., Mills, G.B., Bondy, M.L., and Qingyi Wei, Q. (2005). Methylation and Messenger RNAExpression of p15INK4b but Not p16INK4a Are Independent Risk Factors for Ovarian Cancer. Clin. Cancer Res. 11 (13), 4968-4976.

Lu, Z., Liu, D., Hornia, A., Devonish, W., Pagano, M., and Foster; D.A. (1998). Activation of Protein Kinase C Triggers Its Ubiquitination and Degradation. Molecular and Cellular Biology 18 (2), 839–845.

Lupu, R., Menendez, J.A. (2006). Pharmacological inhibitors of Fatty Acid Synthase (FASN)--catalyzed endogenous fatty acid biogenesis: a new family of anti-cancer agents? Curr. Pharm. Biotechnol. 7 (6), 483-93. Review

Malumbres, M., and Barbacid, M. (2001). To Cycle or Not to Cycle: A Critical Decision in Cancer. Nature/Reviews/Cancer 1, 222-231.

Malumbres, M., Carnero, A. (2003). Cell cycle deregulation: a common motif in cancer. Prog. Cell Cycle Res. 5, 5-18 Review.

Manning, B.D., Tee, A.R., Logsdon, M.N., Blenis, J., and Cantley, L.C. (2002). Identification of the Tuberous Sclerosis Complex-2 Tumor Suppressor Gene

Product Tuberin as a Target of the Phosphoinositide 3-Kinase/Akt Pathway. Molecular Cell 10, 151–162.

Mazzarelli, P., Pucci, S., Bonanno, E., Sesti; F., Calvani, M., Spagnoli, L.G. (2007). Carnitine Palmitoyltransferase I in Human Carcinomas Novel Role in Histone Deacetylation? Cancer Biology and Therapy 6 (10), 1606-1613.

Medema, R.H., Kops, G.J.P.L., Bos, J.L., and Burgering, B.M.T. (2000). AFX-like Forkhead transcription factorsmediate cell-cycle regulation by Ras and PKB through p27kip1. Nature 404, 782-787.

Menendez, J.A., and Lupu, R. (2007). Fatty acid synthase and the lipogenic phenotype in cancer pathogenesis. Nature Reviews 7, 763-777.

Menendez, J.A., 1, Lupu, R. (2005). RNA interference-mediated silencing of the p53 tumor-suppressor protein drastically increases apoptosis after inhibition of endogenous fatty acid metabolism in breast cancer cells. Int. J. Mol. Med. 15 (1), 33-40.

Menendez, J.A., 2, Vellon, L., and Lupu, R. (2005). Orlistat: From Antiobesity Drug to Anticancer Agent in Her-2/neu (erbB-2)-Overexpressing Gastrointestinal Tumors?, Society for Experimental Biology and Medicine 230, 151-154.

Menendez, J.A., 3, Vellon, L., and Lupu, R. (2005). Targeting fatty acid synthase-driven lipid rafts: a novel strategy to overcome trastuzumab resistance in breast cancer cells. Medical Hypotheses 64, 997–1001.

Menendez, J.A., 4, Mehmi, I., Atlas, E., Colomer, R., Lupu, R. (2004). Novel signaling molecules implicated in tumor-associated fatty acid synthase-dependent breast cancer cell proliferation and survival: Role of exogenous

dietary fatty acids, p53-p21WAF1/CIP1, ERK1/2 MAPK, p27KIP1, BRCA1, and NF-kappaB. Int. J. Oncol. 24 (3), 591-608.

Menendez, J.A., 5, Vellon, L., Mehmi, I., Oza, B.P., Ropero, S., Colomer, R., and Lupu, R. (2004). Inhibition of fatty acid synthase (FAS) suppresses HER2_neu (erbB-2) oncogene overexpression in cancer cells. PNAS, 101 (29), 10715–10720.

Meng, Q., Xia, C., Fang, J., Rojanasakul, Y., Jiang, B. (2006). Role of PI3K and AKT specific isoforms in ovarian cancer cell migration, invasion and proliferation through the p70S6K1 pathway. Cellular Signalling 18, 2262–2271.

Nagy, P., Vereb, G., Sebestyén, Z., Horváth, G., Lockett, S.J., Damjanovich, S., Park, J.W., Jovin, T.M., and Szöllo, J. (2002). Lipid rafts and the local density of ErbB proteins influence the biological role of homo- and heteroassociations of ErbB2. Journal of Cell Science 115 (22), 4251-4262.

Nave, B.T., Ouwens, D.M., Withers, D.J., Alessi, D.R., and Shepherd, P.R.(1999). Mammalian target of rapamycin is a direct target for protein kinase B: identification of a convergence point for opposing effects of insulin and amino-acid deficiency on protein translation. Biochem. J. 344, 427-431.

Obrig, T.G., Culp, W.J., McKeehan, W.L., and Hardesty, B. (1971). The Mechanism by which Cycloheximide and Related Glutarimide Antibiotics Inhibit Peptide Synthesis on Reticulocyte Ribosomes. The Journal of Biological Chemistry 246 (1), 174-181.

Olayioye, M.A., Neve, R.M., Lane, H.A., Hynes, N.E. (2000). The ErbB signalling network: receptor heterodimerization in development and cancer. The EMBO Journal 19 (13), 3159-3167.

Oncologychannel (2007): FIGO System & TNM System. Northampton (USA). Online source – website last visited on 25.07.2009: http://www.oncologychannel.com/ovariancancer/figo-system-tnm-system.shtml

Paumen, M.B., Ishida, Y., Han, H., Muramatsu, M., Eguchi, Y. Tsujimoto, Y., and Honjo, T. (1997). Direct Interaction of the Mitochondrial Membrane Protein Carnitine Palmitoyltransferase I with Bcl-2. Biochemical and Biophysical Research Communications 231, 523–525.

Pizer, E.S., Thupari, J., Han, W.F., Pinn, M.L., Chrest, F.J., Frehywot,G.L., Townsend, C.A., and Kuhajda, F.P. (2000). Malonyl-Coenzyme-A Is a Potential Mediator of Cytotoxicity Induced by Fatty-Acid Synthase Inhibition in Human Breast Cancer Cells and Xenografts. Cancer Research 60, 213–218.

Pizer, E.S., Wood, F.D., Heine, H.S., Romantsev,F.E., Pasternack, G.R., and Kuhajda, F.P. (1996). Inhibition of Fatty Acid Synthesis Delays Disease Progression in a Xenograft Model of Ovarian Cancer Cancer Research 56, 1189-1193.

Price, A.C., Choi, K., Heath, R.J., Li, Z., White, S.W., and Rock, C.O. (2001). Inhibition of b-Ketoacyl-Acyl Carrier Protein Synthases by Thiolactomycin and Cerulenin – Structure and Mechanim. The Journal of Biological Chemistry 276 (9), 6551–6559.

Pullen, N., Thomas, G. (1997). The modular phosphorylation and activation of p70s6k. FEBS Letters 410, 78-82.

Rathi, A., Virmani, A.K., Schorge, J.O., Elias, K.J., Maruyama, R., Minna, J.D., Mok, S.C., Girard, L., Fishman, D.A., and Gazdar, A.F. (2002). Methylation

Profiles of Sporadic Ovarian Tumors and nonmalignant Ovaries from High-Risk Women. Clinical Cancer Research 8, 3324–3331.

Reibenwein, J., Krainer, M. (2008). Targeting signaling pathways in ovarian cancer. Expert Opin.Ther. Targets 12 (3), 353-365.

Rendina, A.R., and Cheng, D. (2005). Characterization of the inactivation of rat fatty acid synthase by C75: inhibition of partial reactions and protection by substrates. Biochem. J. 388, 895–903.

Roder, K., Wolf, S.S., Larkin, K.J., Schweizer, M. (1999). Interaction between the two ubiquitously expressed transcription factors NF-Y and Sp1. Gene 234, 61–69.

Rodríguez-González, A., Ramírez de Molina, A., Bañez-Coronel, M., Megias, D., Lacal, J.C. (2005). Inhibition of choline kinase renders a highly selective cytotoxic effect in tumour cells through a mitochondrial independent mechanism. Int. J. Oncol. 26 (4), 999-1008.

Sarbassov, D.D., Ali, S.M., Sengupta, S., Sheen, J., Hsu, P.P., Bagley, A.F. Markhard, A.L., and Sabatini, D.M. (2006). Prolonged Rapamycin Treatment Inhibits mTORC2 Assembly and Akt/PKB. Molecular Cell 22, 159–168.

Scherz-Shouval, R., Shvets, E., Fass, E., Shorer, H., Gil, L., and Elazar, Z. (2007). Reactive oxygen species are essential for autophagy and specifically regulate the activity of Atg4. The EMBO Journal 26, 1749–1760.

Shayesteh, L., Lu, Y., Kuo, W., Baldocchi, R., Godfrey, T., Collins, C., Pinkel, D., Powell, B., Mills, G.B., and Gray, J.W. (1999). PIK3CA is implicated as an oncogene in ovarian cancer. Nature Genetics 21, 99-102.

Stephens, L., Anderson, K., Stokoe, D., Erdjument-Bromage, H., Painter, G.F., Holmes, A.B., Gaffney, P.R.J., Reese, C.B., McCormick, F., Tempst, P., Coadwell, J., Hawkins, P.T. (1998). Protein Kinase B Kinases That Mediate Phosphatidylinositol 3,4,5-Trisphosphate– Dependent Activation of Protein Kinase B. Science 279, 710-714.

Stirzaker, C., Millar, D.S., Paul, C.L., Warnecke, P.M., Harrison, J., Vincent, P.C. Frommer, M., and Clark, S.J. (1997). Extensive DNA Methylation Spanning the Rb Promoter in Retinoblastoma Tumors. Cancer Research 57, 2229-2237.

Strathdee, G., Appleton, K., Illand, M., Millan, D.W.M., Sargent, J., Paul, J., and Brown, R. (2001). Primary Ovarian Carcinomas Display Multiple Methylator Phenotypes Involving Known Tumor Suppressor Genes. American Journal of Pathology 158 (3), 1121-1127.

Swinnen, J.V., Van Veldhoven, P.P., Timmermans, L., De Schrijver, E., Brusselmans, K., Vanderhoydonc, F., Van de Sande, T., Heemers, H., Heyns, W., and Verhoevena, G. (2003). Fatty acid synthase drives the synthesis of phospholipids partitioning into detergent-resistant membrane microdomains. Biochemical and Biophysical Research Communications 302, 898–903.

Tam, K.F., Liu, V. W. S., Liu, S. S., Tsang, P. C. K., Cheung, A. N. Y., Yip, A. M. W., Ngan H. Y. S. (2007). Methylation profile in benign, borderline and malignant ovarian tumors. J. Cancer Res. Clin. Oncol. 133, 331–341.

Thupari, J.N., Pinn, M.L., and Kuhajda, F.P. (2001). Fatty Acid Synthase Inhibition in Human Breast Cancer Cells Leads to Malonyl-CoA-Induced Inhibition of Fatty Acid Oxidation and Cytotoxicity. Biochemical and Biophysical Research Communications 285, 217–223.

Wakil, S.J., and Chirala, S.S. (2004). Structure and Function of Animal Fatty Acid Synthase. Lipids 39 (11), 1045-1053.

Wang, H.Q., Altomare, D.A., Skele, K.L., Poulikakos, P.I., Kuhajda, F.P., Di Cristofano, A., and Testa, J.R. (2005). Positive feedback regulation between AKT activation and fatty acid synthase expression in ovarian carcinoma cells. Oncogene 24, 3574–3582.

Wang, M., Panasyuk, G., Gwalter, J., Nemazanyy, I., Fenton, T., Filonenko, V., Gout, I. (2008). Regulation of ribosomal protein S6 kinases by ubiquitination. Biochemical and Biophysical Research Communications 369, 382–387.

Wang, X., Lin, J., Chen, Y., Zhong, W., Zhao, G., Liu, ., Li, S., Wang, L., Li, S. (2009). Novel fatty acid synthase (FAS) inhibitors: Design, synthesis, biological evaluation, and molecular docking studies. Bioorganic & Medicinal Chemistry 17, 1898–1904.

Wellen, K.E., Hatzivassiliou, G., Sachdeva, U.M., Bui, T.V., Cross, J.R., Thompson, C.B. (2009). ATP-Citrate Lyase Links Cellular Metabolism to Histone Acetylation. Science 324, 1076-1080.

Wong, Y.F., Chung, T.K.H., Cheung, T.H., Nobori, T., Yim, S.F., Lai, K.W.H, Yu, A.I., Diccianni, M.B., Li, T.Z., Chang, A.M.Z. (1997). p16INK4 and p15INK4B Alterations in Primary Gynecologic Malignancy. Gynecologic Oncology 65, 319–324.

Yuecheng; Y., Hongmei, L., Xiaoyan, X. (2006). Clinical evaluation of E-cadherin expression and its regulation mechanism in epithelial ovarian cancer. Clin. Exp. Metastasis 23, 65–74.

Zipper, H., Brunner, H., Bernhagen, J., and Vitzthum, F. (2004). Investigations on DNA intercalation and surface binding by SYBR Green I, its structure determination and methodological implications. Nucleic Acids Research 32 (12), e103, 1-10

Curriculum Vitae

Familienname:	Tomek
Vorname:	Katharina
Geburtsdatum:	22. September 1980
Geburtsort:	Hainburg/Donau
Nationalität:	Österreich
Familienstand:	ledig

Schulbildung:

1995 – 1999	Oberstufenrealgymnasium Wr. Neustadt
1999 – 2002	**Akademie für den Med. Techn. Laboratoriumsdienst**
2002 - 2009	Universität Wien, Studienrichtung: **Molekularbiologie**

Berufserfahrung/Praktika während des Studiums:

Feb.03 -März 06:	Inst. für Onkologie, Innere Med. I, AKH-Wien Prof. Thomas W. Grunt, Signaling Networks Program
Juli-August 2007:	Max F. Perutz Laboratories, University of Vienna Prof. Baccarini, „Function of MAPK-Pathway in Differentiation Process in Keratinozytes"
Sept. 2007:	Department of Medical Biochemistry, Division of Molecular Genetics, Medizinische Universität Prof. Schneider, „Microglial Clusterin may be the missing link between LR11 and ß-Amyloid in Alzheimer disease prevention"
März-April 2008:	Institute of Molecular Cell Biology, University of Vienna Prof. Wiche, „Phosphorylation of Plec1f may result in Disassembly of Focal Adhesions"
Seit August 2008:	Diplomarbeit am Inst. für Onkologie, Innere Med. I, AKH-Wien Prof. Thomas W. Grunt, „Effects of Fatty Acid Synthase Inhibitor C75 in Ovarian Cancer"

Sprachkenntnisse: Deutsch (Muttersprache), Englisch (fließend)

EDV-Kenntnisse: Microsoft Office Produkte, diverse Bild-Auswertungsprogramme

Kontakt: E-mail: katharina_tomek@gmx.at

Publikationen:

1. GRUNT, T.W., PUCKMAIER, K., TOMEK, K., KAINZ, B., GAIGER, A., : An EGFR inhibitor induces RAR-beta expression in breast and ovarian cancer cells. Proc. AACR, Anaheim, CA, 46, Abstr.# 1513, 2005

2. GRUNT, T.W., TOMEK, K., PUCKMAIER, K., KAINZ, B., GAIGER, A., ZIELINSKI, C.C., The Epidermal Growth Faktor-Receptor Inhibitor PD 153035 Upregulates Retinoic Acid Receptor-beta by Epigenetic Mechanisms. Proc. AACR, Washington, DC, 47, Abstr.# 1248, 2006

3. GRUNT, T.W., TOMEK, K., WAGNER, R., PUCKMAIER, K., KAINZ, B., RUENZLER, D., GAIGER, A., KOEHLER, G., ZIELINSKI, C.C., : Effects of Epidermal Growth Factor-Receptor Inhibitors that are not Mediated by Blockade of ErbB Pathways. 14th International Conference of the International Society of Differentiation (ISD), Oct 7-11, 2006, Innsbruck, Austria; Differentiation, 74, 460, Abstr.# 040, 2006

4. GRUNT, T.W., WAGNER, R., TOMEK, K., PUCKMAIER, K., ZIELINSKI, C.C.: The Epidermal Growth Factor-Receptor Inhibitor PD153035 Induces Retinoic Acid Receptor-beta by Intercalation into DNA. 14th International Conference of the International Society of Differentiation (ISD), Oct 7-11, 2006, Innsbruck, Austria; Differentiation, 74, 467, Abstr.# P64, 2006.

5. GRUNT, T.W., WAGNER, R., TOMEK, K., PUCKMAIER, K., ZIELINSKI, C.C.: There is more to some EGF receptor inhibitors – PD153035 reveals triple action: EGF receptor inhibition, DNA – intercalation, RAR-beta induction. Proc. AACR, Los Angeles, CA, submitted, 2007-02-27